AN ABSTRACT OF THE THESIS OF

Kendall Lyman Carder (Name) for the Doctor of Philosophy (Degree)

in Oceanography (Major) presented on Sept. 30, 1969 (Date)

Title: PARTICLES IN THE EASTERN PACIFIC OCEAN: THEIR DISTRIBUTION AND EFFECT UPON OPTICAL PARAMETERS

Abstract approved: Redacted for Privacy

The distribution of particles in the Eastern Pacific Ocean was investigated from 2 January to 14 February, 1969 on the YALOC-69 cruise of Oregon State University. The size distributions were well fitted by the two-parameter Weibull distribution function, with a predominant number of them nearly exponential in distributional shape. Although particles smaller in diameter than 1μ could not be measured, extrapolation of the Weibull distribution into the small particle range indicated the median particle diameter was smaller than 1μ.

Measurements of light scattering were taken simultaneously with the particle size determinations. A linear relationship between the total particulate surface area and the volume scattering function, $\beta(45^{\circ})$ was indicated, as well as between $\beta(45^{\circ})/\beta(135^{\circ})$ and the mean particle diameter of distributions sharing a common shape

parameter. Five different characteristic distributional shapes were found which typified all but a few of the distributions. No direct relationship was found between the distributional shapes and the water types encountered on the cruise. The first-order exponential shapes of the size distributions suggest that a detrital decay mechanism of the larger particles (i. e. phytoplankton) could be a dominant factor in determining the small particle end of oceanic particle distributions.

Particles in the Eastern Pacific Ocean: Their Distribution and Effect Upon Optical Parameters

by

Kendall Lyman Carder

A THESIS

submitted to

Oregon State University

in partial fulfillment of
the requirements for the
degree of

Doctor of Philosophy

June 1970

APPROVED:

Redacted for Privacy

Assistant Professor of Department of Oceanography
in charge of major

Redacted for Privacy

Head of Department of Oceanography

Redacted for Privacy

Dean of Graduate School

Date thesis is presented September 30, 1969

Typed by Barbara Eby for Kendall L. Carder

ACKNOWLEDGEMENT

The author would like to express a deep sense of gratitude to Dr. George F. Beardsley, his thesis advisor, for his indispensable support and guidance in this investigation. He is indebted to Dr. Ha Song Pak, who provided and reduced the light scattering measurements, and to Dr. David R. Thomas for his constructive advice on statistics.

This investigation was supported by the Office of Naval Research, Grant No. 1286(10).

TABLE OF CONTENTS

LIST OF FIGURES

LIST OF TABLES

PARTICLES IN THE EASTERN PACIFIC OCEAN: THEIR DISTRIBUTION AND EFFECT UPON OPTICAL PARAMETERS

I. INTRODUCTION

Problem

The scattering of light by suspended material in sea water is a recognized method of identifying and tracing water masses. Its utility has been proven even without a thorough knowledge of the relationships between the size distributions of particles and the resultant scatter of light. This dissertation will study several aspects of these relations.

The distribution of particle sizes is of interest in the study of light scattering, particle settling velocities, sedimentology, surface area adsorption, and detrital decomposition. Rapid methods of determining the mean particle diameter, the total particulate surface area, and the total concentration of particles in a sample of sea water would be welcomed by investigators working in these and many other fields. This dissertation will suggest and test various optical techniques for the measurement of each of these particle sample characteristics when a wide range of particle sizes (oceanic samples) is involved.

Mie (1908) applied electro-magnetic field theory to the study of the scattering of a plane, monochromatic light wave by a dielectric sphere. He showed that the scattered light field depends upon the diameter of the sphere, its index of refraction, and the wavelength of the incident light, assuming that the scattered wavelength is the same as that of the incident light. Any variations of these parameters will most definitely have an effect upon the scattered light field. Assuming that the spherical particles are separated by at least three times their radii, the scattered light field from a system of particles is the sum of the scattered fields due to each of the individual particles. If the characteristics of each particle is known, the light field from a system of them is theoretically predictable.

A theoretical analysis of the scattered light field in order to ascertain the individual particle characteristics is not possible at the present time. The infinite possibilities of particle size, shape, and index of refraction make rigorous Mie theory intractable. Shapes can vary from the approximately spherical form of an Isochrysis galbana (algal) cell to flat, disk-like diatoms, to long, chain-forming diatoms. Sand, clay, and silt add to the complexity. Sizes of suspended material range upwards from those of bacteria and detritus (diameter $< 1\mu$) to those of large phytoplankton (diameter $< 20\mu$), while indices of refraction remain for the most part within the range 1.05 to 1.25. Only by a great deal of simplification can even a few

mean characteristics of the total population be estimated from optical scattering data.

The shapes of oceanic particles are generally assumed to approximate that of a sphere due to their random orientations. Hodkinson (1963) showed that nonabsorbing, nonspherical particles should produce the same diffraction patterns as spherical ones of the same cross-sectional area. Since opaque particles produce the same diffraction patterns as transparent ones of the same cross-sectional area, forward light scattering in sea water is dominated by diffraction. This means that diffraction plays a large role in the scattering of light, for scattering in the near-forward direction contributes most heavily to the total scattering in sea water according to Jerlov (1968). For these reasons, partical shape and index of refraction are believed to play roles secondary to that played by particle size in the scattering of light in the ocean.

Jerlov (1968) states, "Particle size is the major parameter in scattering". The problem remains, though, to determine what the distributions of particle sizes are in the oceans in order to relate the effects of distributional variations to the accompanying optical measurements.

Several investigators have made particle size determinations using instrumentation of various types, but no large scale oceanic particle analysis has been made. Part of the reason for this is that

the traditional particle sizing instrument is the microscope. To count the numbers of various sized particles at sea microscopically is slow, laborious, and quite frankly nauseous in rough weather. Filtering methods for small particles are impracticle because filters tend to remove particles smaller in size than their pore size due to the generally nonspherical shape of the particles. For these reasons, a search was attempted to find an instrument that could be readily adapted to ship-board use and rapid enough to operate to make a large scale particle analysis of the oceans feasible.

The Coulter Counter (see Appendix for a description) was originally designed to count blood cells, but it has been recently used in the laboratory to count phytoplankton. Sheldon and Parsons (1967) measured particle sizes in bay waters during a phytoplankton bloom (population explosion), but their study consisted of primarily large particle (diameter $> 3\mu$) measurements. The microscopic sizing technique has been compared to that of the Coulter Counter by Mulligan and Kingsbury (1968), and they found that for small particles it is inferior in accuracy to the Coulter Counter. Certainly the Coulter Counter is much faster to operate, but its objection is that particles and organisms cannot be visually identified by this method. Nevertheless, the Coulter Counter appears to be a very useful instrument for the rapid generation of particle size distributions at

the numerous stations and depths involved in an oceanic particle size analysis survey.

Thus, to best attack the problem of understanding the effects of particle size distributional variations upon the scattering of light by the particulates in sea water, simultaneous optical and particle size determinations were deemed necessary. In addition, the development of optical techniques for the rapid estimation of mean particle sizes and other particle sample distribution characteristics by a comparison of the scatterers and the scattering would supplement the particle analysis measurements by allowing an optical estimation of these characteristics to be made for those depths for which no particle analyses could be made.

The following sub-section outlines in more detail the specific questions to be studied and presented in this dissertation.

Synopsis of Dissertation Problem

The purpose of this dissertation is to investigate several questions. These are treated quite generally in this section, with a more rigorous development to follow in the Background section. In order for the reader to quickly scan the individual problems as well as the integrated study, these questions are presented in outline form as follows:

Questions:

1. What are the particle size distributions in various regions of the ocean?
   a. What are the derived particle distribution characteristics?
      1. Size distribution (relative frequency polygon)
      2. Expected or mean particle diameter
      3. Expected or mean particle surface area
      4. Expected or mean particle volume
      5. Total particle volume
      6. Total particle surface area
      7. Effective optical area
   b. Can the cumulative and relative frequency polygons of the particle samples be conveniently approximated by Weibull or gamma cumulative distribution and probability density functions respectively?
2. What are the inherent optical properties of the sea water samples in the oceanic regions of study? (definitions of the inherent optical properties are found in Section II under Scattering Theory)
   a. Beam transmittance
   b. Volume scattering function $\beta(\theta)$ for $\theta = 45^{o}$, 90^{o} and 135^{o}

c. Total scattering coefficient

d. Total attenuation coefficient

3. How well can the particle distribution characteristics be determined from the inherent optical properties?

a. Which characteristics and properties are involved?

1. Total particle surface area vs. $\beta(45^{o})$

2. Mean particle diameter vs. $\beta(45^{o})$

3. (Mean particle surface area)$^{1/2}$ vs. $\beta(45^{o})/\beta(135^{o})$

4. $\beta(45^{o})$ vs. the number of particles N

b. Where can these relationships be used with best accuracy?

1. Optical approximations of particle distribution characteristics

a. Regional limitations due to variations of particle size distribution

b. Regional limitations due to variations of distribution characteristics

2. Optical approximations of particle distribution characteristics, used for interpolation between the depths at which particle distribution measurements were taken

4. How well can water masses and currents be characterized by their particle size distributions?
    a. By direct determination of distributions or by distribution characteristics
    b. By optical estimators of distribution characteristics

With this general synopsis of the problems to be studied in this research program as a guide, each of the outline questions will be developed and answered. Partial answers already exist to some of these questions. They are discussed in the following section and expanded throughout the remainder of the dissertation.

II. BACKGROUND

Introduction

There seems to be a great amount of confusion as to what the particle sizes are in the oceans. Much of this variation in reported sizes is probably due to special and temporal differences between measurements. Burt (1955) estimated the predominance of small (diameter $< 1\mu$) particles due to the selective attenuance of Chesapeake Bay waters. Sasaki et. al. (1962) suggest that deep water particles are also small by a comparison of their light scattering data with Mie theory. Kullenberg (1969) has theoretically determined an average particle size of about 4μ from the near-forward light scattering field at mid-depths in the Baltic. Hinzpeter (1962) found by the dispersion of the volume scattering function in the Baltic that small particles were dominant there. These optical estimates of particle sizes tell nothing about the size distribution of the particles, only the average sized particle that effectively scatters light.

In most microscopic work of particle sizing the oceans, only particles of size larger than 2μ have been studied. The works of Lisitsyn (1961) and Ochakovsky (1966) seem more complete, and their results are summarized by Table 2.1. This table points to the predominance of small particles in the regions examined. Ochakovsky's data indicates that most of the particles fall within

the 1 to 25μ range, while Lisitsyn's shows a predominance of particles smaller in diameter than 1μ, the lower limit of Ochakovsky's measurements. The large numbers of small particles presented in Table 2.1 suggests that there is a high proportion of detritus present in the samples, since most phytoplankton and zooplankton are larger in diameter than 3μ in the Equatorial Pacific according to Eppley (1967). As detritus is a decay or decomposition process derivative, one might expect an exponential distribution of particle sizes once the sizes were below those of actively growing organisms.

Since a knowledge of the particle size distributions in the ocean is essential to any theoretical prediction of or empirical determination of the scattered light field therein, it is appropriate that a study of these distributions be a prelude to the discussion of the light scattering due to these particles.

Table 2.1. Size distribution of particles in the sea (after Jerlov, 1968).

Table 2.1a. Size distribution of particles (% total particle number) in the sea (Lisitsyn, 1961).

Region	Depth (m)	Concentration (mg/l)	Fractions μ					
			>100	100-50	50-10	10-5	5-1	<1
West Pacific	5-7	0.279	0.33	---	11.67	1.81	2.89	83.23
	100	0.800	0.20	0.20	2.80	3.09	2.83	90.86

Table 2.1b. Size distribution of particles (relative number) in the sea (Ochakovsky, 1966a).

Region	b m^{-1}	Fractions μ					
		>50	50-25	25-10	10-5	5-2.5	2.5-1
Mediterranean	0.10	3.5	10.4	40.7	23.6	56.5	480
	0.15	2.8	14.3	56.1	31.5	81.0	326
	0.20	1.8	10.3	41.4	28.3	57.5	890

Particle Analyses

For grouped data in the form of a cumulative frequency distribution such as shown in Figure 2. 1, one can determine all of the derived distribution characteristics listed in Question 1a. Expressions for each of these are developed in this section. For this dissertation it was not possible to count particles smaller in size than 1. 13μ, so the derived sample characteristics are actually from a conditional distribution. The development of expressions for these characteristics is unchanged, however.

Figure 2. 1. Cumulative frequency distribution of particle diameters.

Let D_i be the diameter of the i^{th} incremental diameter, and N_i be the number of particles greater in size than the i^{th} diameter. Then the cumulative frequency distribution can be expressed as

$$N(D_i) = N_1 - N_i, \quad (\text{for } i=1, 2, \ldots, n) \tag{2.1}$$

or the cumulative probability distribution as

$$F(D_i) = 1 - \frac{N_i}{N_1} \tag{2.2}$$

Here N_1 is the number of particles of diameter larger than D_1.

The frequency density function can be written as

$$\eta(D_i') = N_i - N_{i+1}, \quad (\text{for } i=1, 2, \ldots, n-1) \tag{2.3}$$

or the relative frequency density function as

$$f(D_1') = \frac{N_i - N_{i+1}}{N_1} \Big/ (D_{i+1} - D_i), \quad (\text{for } i=1, 2, \ldots, n-1), \tag{2.4}$$

Here, D_i can best be associated with $f(D_i)$ if D_i is actually the incremental center, D_i', or

$$D_1' = \frac{D_i + D_{i+1}}{2}, \tag{2.5}$$

and $(D_{i+1} - D_i)$ is the diameter incremental width.

The expected particle diameter $\bar{D}$ can be written as

$$\bar{D} = \sum_{i=1}^{n=1} \frac{(N_i - N_{i+1})}{N_1} (D_1') \tag{2.6}$$

and the expected particle surface area $\overline{S}$ as

$$\overline{S} = \pi \sum_{i=1}^{n-1} \frac{(N_i - N_{i+1})}{N_1} (D_i')^2 . \tag{2.7}$$

The expected particle volume $\overline{V}$ is expressed as

$$\overline{V} = \frac{\pi}{6} \sum_{i=1}^{n-1} \frac{(N_i - N_{i+1})}{N_1} (D_i')^3 , \tag{2.8}$$

Of course the total particle surface area Σs and total particle volume ΣV are simply $\overline{S}$ and $\overline{D}$ respectively without the denominators. Dividing ΣV by the volume of the water Vw containing it, one can determine the particle concentration Cp:

$$Cp = \Sigma V / Vw \tag{2.9}$$

An optical function which is very important in scattering problems is the efficiency factor or the effective area coefficient $K(D_i)$. For a polydisperse system of particles, we shall define

$$E.O.A. = \sum_{i=1}^{n-1} K(D_i) (N_i - N_{i+1}) (D_i')^2 \tag{2.10}$$

as the effective optical area. $K(D_i)$ is discussed more specifically below.

In order to estimate the lower diameter limit D* below which E. O. A. changes very little, it is assumed that the particle diameter probability density function is exponential. For large particles, $K(D_i)$ is essentially a constant "2" according to Burt (1955), but

it decreases to zero as the diameter decreases. Therefore, a conservative estimate of the error ϵ involved in neglecting particles of diameter smaller than 1μ can be found by setting $K(D_i) = 2$, and $D^* = 1\mu$.

$$(2.11) \quad \epsilon = \frac{2\int_0^{x'} x^2 e^{-x} dx}{2\int_0^{\infty} x^2 e^{-x} dx} = \frac{\left[-x^2 e^{-x} - 2 e^{-x}(x+1) \right]_0^{x'}}{\left[-x^2 e^{-x} - 2 e^{-x}(x+1) \right]_0^{\infty}}$$

$$\epsilon = \frac{-e^{-x'}(x^{2'} + 2x' + 2) + 2}{2}$$

Now if $x = D/b$ where b is the scale parameter, this becomes

$$(2.12) \qquad \epsilon = \frac{1}{b} \; \frac{-e^{-D^*}(D^{2*} + 2D^* + 2) + 2}{2},$$

If $D^* = 1$,

$$\epsilon = \frac{2 - 1.84}{2b} = \frac{.16}{2b} = \frac{.08}{b}$$

If $b = 1$, the maximum error is $< 8\%$. If $b = 2$, it is $< 4\%$. In either case, the neglecting of particles smaller than 1μ in diameter is essentially negligible for the E.O.A. This agrees with Jerlov (1968) when he determined the dominant scattering cross-section of the particles listed in Table 2.1 to be due to particles larger than 2μ in diameter.

Since the number of particles in each of the oceanic samples considered was quite large (about 1000), the particle distribution

characteristics such as the mean and variance are good estimates for the corresponding parameters of the total particle population within a given homogeneous volume of water. For this reason attempts are made later to approximate the general shape of the size distribution of a given particle population by fitting various statistical cumulative distribution functions to the sample data. These c. d. f.'s indicate the number of parameters needed to describe the population size distribution and the number of statistics ($\overline{D}$, $\overline{S}$, ...) or sample characteristics needed to describe the sample particle size distribution. If only two statistics are needed to characterize the size distribution of a particle sample then only a listing of $\overline{D}$ and $\overline{S}$ is needed in a data report, and the report is much more compact and meaningful.

The distribution of particle sizes plays a very important role in the scattering of light. Several theoretical and empirical relationships between particle size and light scattering have been determined by earlier investigators, but before these can be discussed, some light scattering properties must be defined and light scattering theory developed.

Light Scattering Theory

The inherent optical properties of sea water are those properties which are independent of the incident irradiance field of

light. These properties are the volume scattering function, the total scattering coefficient, the absorption coefficient, and the attenuation coefficient, all defined below.

When a beam of light is transmitted through sea water, the light is attenuated by absorption and scattering, both by the water itself and the suspended particles within. The intensity of the light propagated through a water path of x meters is

$$N = N_0 e^{-(a+b)x} \tag{2.13}$$

where N_0 is the radiance (flux/ster.-m^2.) at $x = 0$, "a" is the absorption coefficient, and "b" is the scattering coefficient. The sum of "a" and "b" is the attenuation coefficient "c".

In this study the primary interest is in the light scattering, so attention is immediately focused on an expression for the determination of the radiant intensity $I(\theta)$ (watt/ster.) at some angle θ with respect to the direction of the incident beam propagation. This is demonstrated in Figure 2.2. Then

$$I(\theta) = E V \beta(\theta) \tag{2.14}$$

where E is the irradiance incident upon a volume V defined by the intersection of the light beam and the solid angle of acceptance of the detector. $\beta(\theta)$ is the volume scattering function. Figure 2.3 shows a typical oceanic curve of the volume scattering function and one for pure water. Notice the near-forward angular dominance of

the oceanic curve as compared to the symmetrical shape of the curve for pure water, having only scatterers of molecular size. This indicates the particle size dependency of the volume scattering function for sea water.

If the volume scattering function is integrated over 4π steradians, the resulting expression defines the total scattering coefficient:

$$b = 2\pi \int_0^{\pi} \beta(\theta) \sin\theta \, d\theta. \tag{2.15}$$

According to Jerlov (1953), there is a linear relationship between the total scattering function "b" and $\beta(45^{\circ})$. Diermendjan (1963) supports this premise with theoretical proof. So, the total scattering function can be expressed as

$$b \doteq K\beta(45^{\circ}), \qquad \text{where } K \doteq 10. \tag{2.16}$$

From Mie theory for N spheres of diameter D per unit volume, the total scattering has been shown by Jerlov (1968) to be

$$b \doteq (\pi/4)\, k\, ND^2, \tag{2.17}$$

where "k" is the efficiency factor or effective area coefficient. Combining Equations 2.16 and 2.17 allows $\beta(45^{\circ})$ to be written as

$$\beta(45^{\circ}) \doteq K_1 ND_1^2 \tag{2.18}$$

where $K_1 = \frac{\pi}{4}\frac{k}{K}$. For a polydisperse system of particles Equation 2.18 can be written as

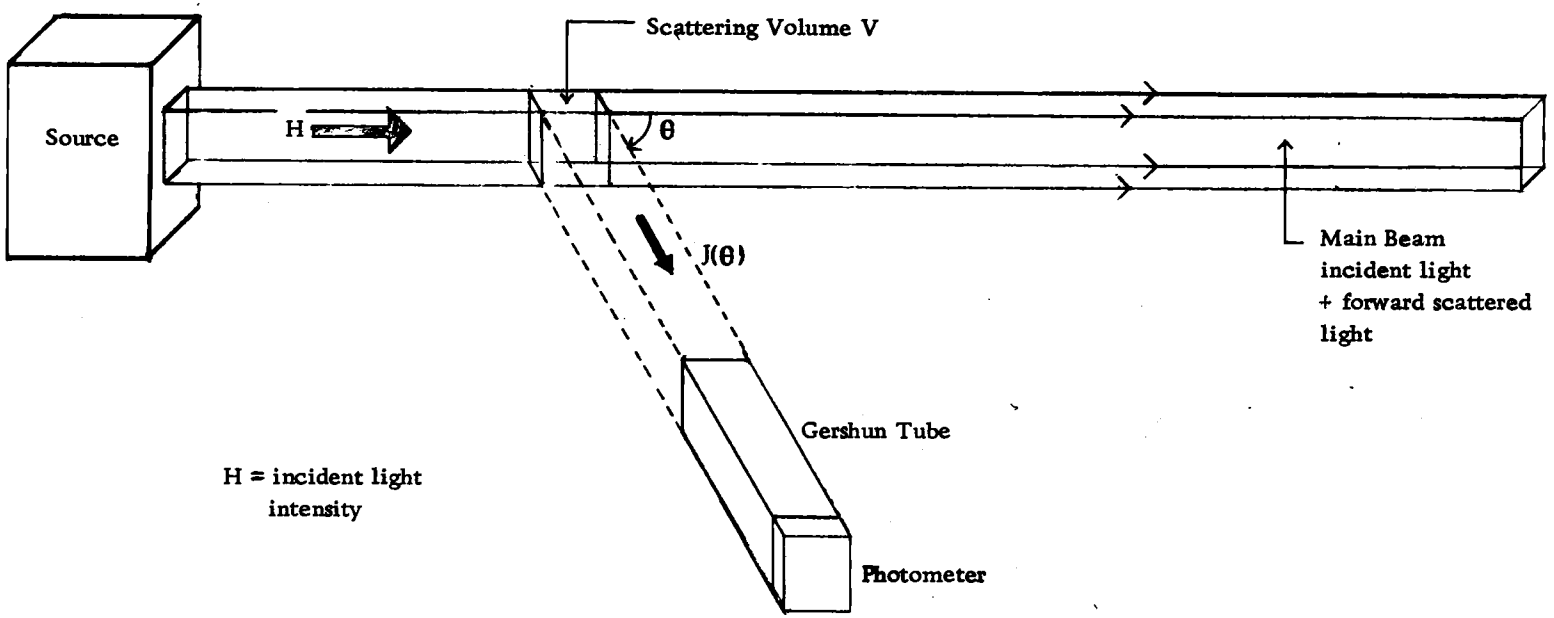

Figure 2.2. The Standard Nephalometer

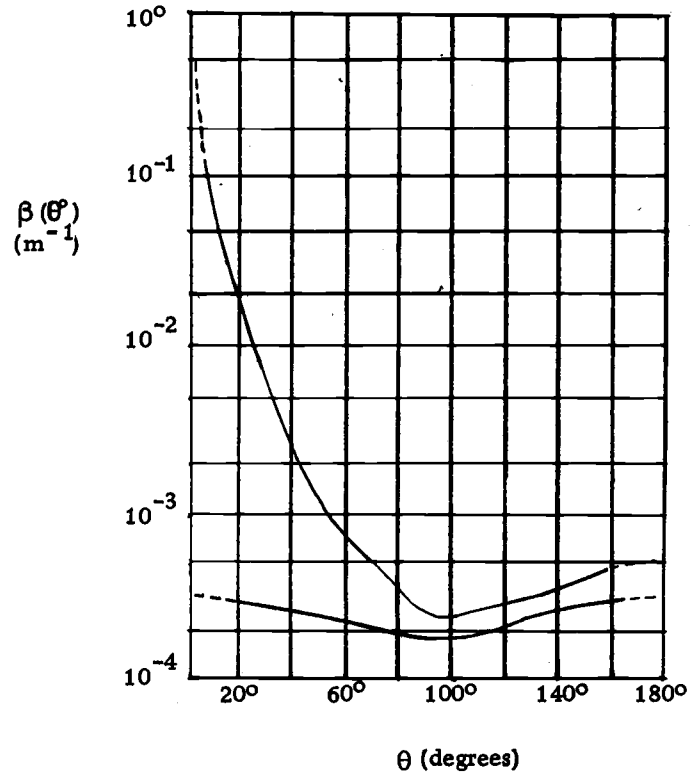

Figure 2.3. Comparison between the scattering function (in absolute units) for ocean water (upper curve) and that for pure water (lower curve). [from Jerlov (1961), page 15]

$$(2.19) \qquad \beta(45^{\circ}) \doteq K_1 \sum_{i=1}^{n-1} (N_i - N_{i+1})(D'_1)^2.$$

Here, K_1 is treated as a constant since for large particles ($D > 1\mu$), $k \doteq 2$ accoring to Van de Hulst (1957). Jerlov and Kullenberg (1953) substantiated this for minerogenic particles as did Jerlov (1955) for calcareous suspensions.

$\beta(45^{\circ})$ then is an optical parameter representing the total surface area of the scattering particles. Dividing Equation 2.19 by the total number of particles gives the mean or expected value of the particle surface area. Or,

$$(2.20) \qquad \overline{S} = \beta(45^{\circ})/K_1 \sum_{i=1}^{n-1} (N_i - N_{i+1}) = \sum_{i=1}^{n-1} (N_i - N_{i+1})(D_i)^2 / \sum_{i=1}^{n-1} (N_i - N_{i+1}).$$

An optical technique for the determination of the mean particle size invokes the use of a scattering ratio:

$$(2.23) \qquad R = \beta(45^{\circ})/\beta(135^{\circ})$$

Figure 2.4 after Ashley and Cobb (1958) demonstrates the role played by particle size as a scattering parameter. The large particles scatter predominately in the forward direction, resulting in a much larger scattering ratio R than has the small particle scattering. The distribution of particle sizes over a wide range greatly complicates the problem, though. In addition to the

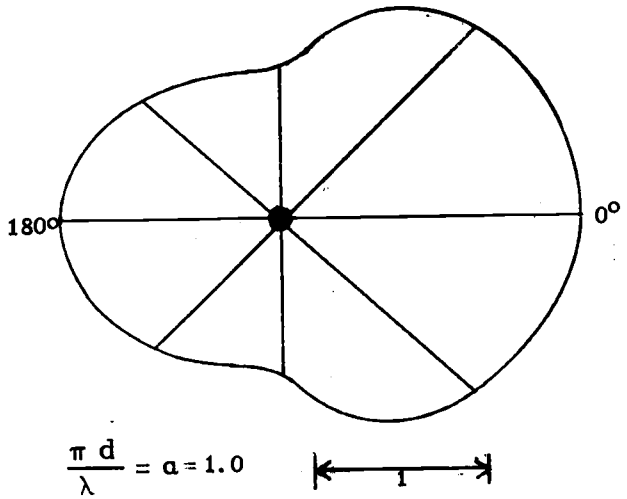

Rayleigh - like scattering

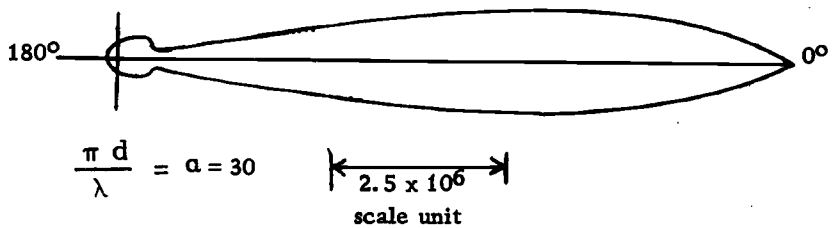

Mie scattering

Figure 2.4. Polar plots of total scattered light intensity, $\left[\frac{i_1 + i_2}{2}\right]$, for single particles (m=1.20) illuminated by unpolarized light [from Ashley and Cobb, 1958, page 267].

determination of the role that the scattering parameters play in the behavior of R, one must learn the distribution of these parameters and their range of variation. In view of the complexity of this situation, data was taken with the hope that nature would simplify the problem into an empirically tractable representation of the size dependency of R, at least in some oceanic areas. Since both $\beta(45^{o})$ and $\beta(135^{o})$ are directly dependent upon the total number of particles, it is suggested that R is independent of the particle concentration. For a polydisperse system of particles, a distributional effect $f(N_i)$ would occur which hopefully would remain consistent enough in a given region to allow R to be useful in determining the mean particle diameter emperically. Thus,

$$\bar{D} = kf(N_i)\, g(R) \tag{2.24}$$

where k is a constant, and g(R) is an empirical function of R.

With the development of the above theory, a study of the optical and particle measurements and their interrelationships can be made. The descriptions of the instruments and the data reduction techniques involved with each are found in Appendices A and B. The program used in the data acquisition of this dissertation is discussed next.

III. EXPERIMENTAL PROGRAM

Since very little is known about the size distribution of particles or their spatial distribution in the oceans it would be extremely informative to obtain this information over a wide range of oceanic regions. Simultaneous optical data for comparison would be an added bonus. There are always ship time, bunk space, or track plan limitations in any survey type investigation, so an opportunity to participate in the YALOC-69 cruise to the Galopagos region of the Pacific provided an excellent chance to encounter numberous different oceanic regions.

Figure 3.1 shows a station plan for the overall cruise, while Figure 3.2 details that of the Galopagos Islands region. The cruise track covered areas from the winter coastal conditions off Oregon and California to the summer waters off Peru. Water types from the East North Pacific Central and Pacific Subaractic to the Pacific Equatorial were encountered along with the crossing of a variety of different currents.

Since the number of samples processed by an individual is limited by the cruising time between stations, certain compromises between distributional resolution and the number of samples processed had to be made. Four depths were chosen as the minimum number allowable from which to draw samples and still cover the

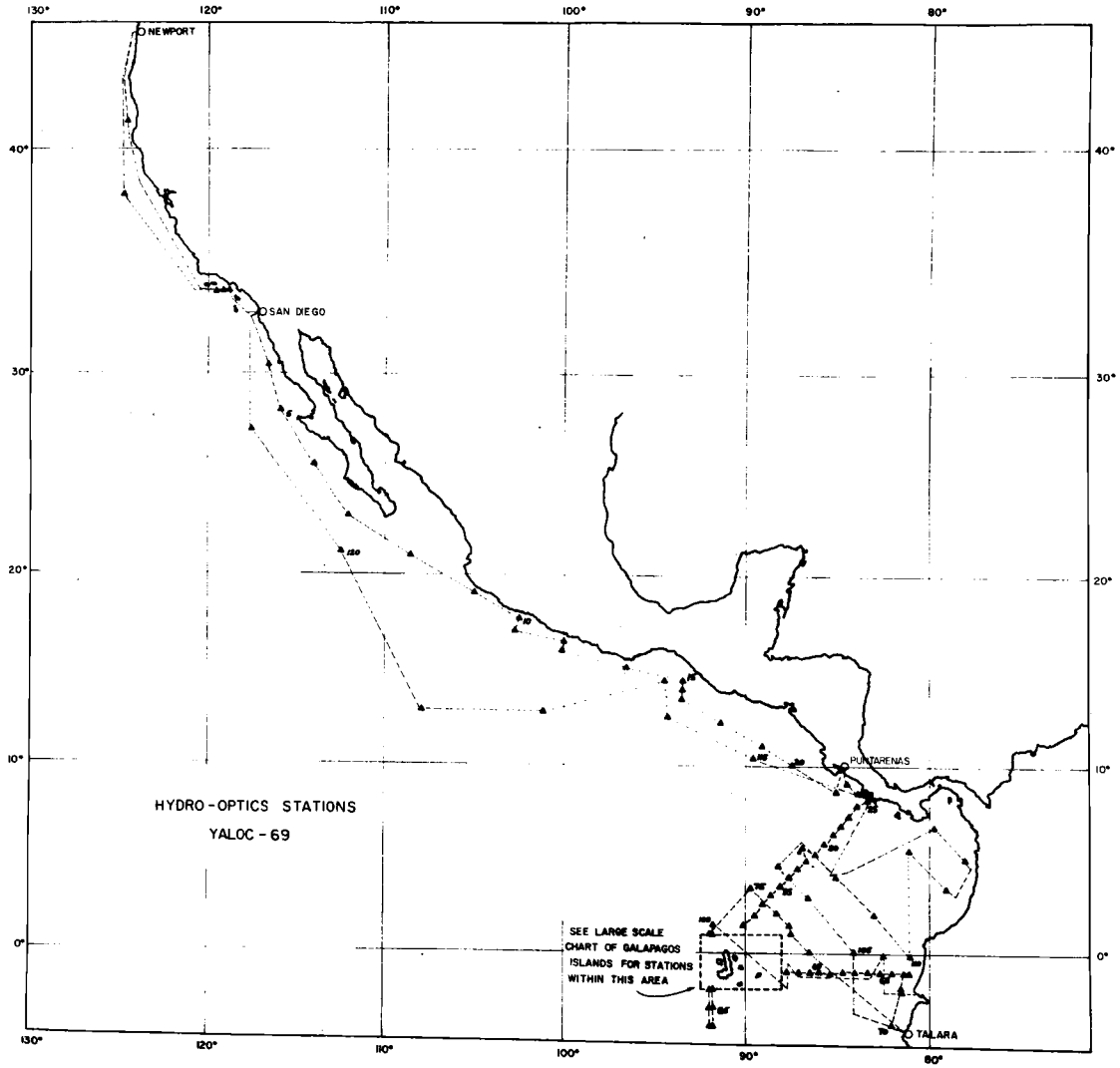

Figure 3.1. Cruise track: YALOC-69.

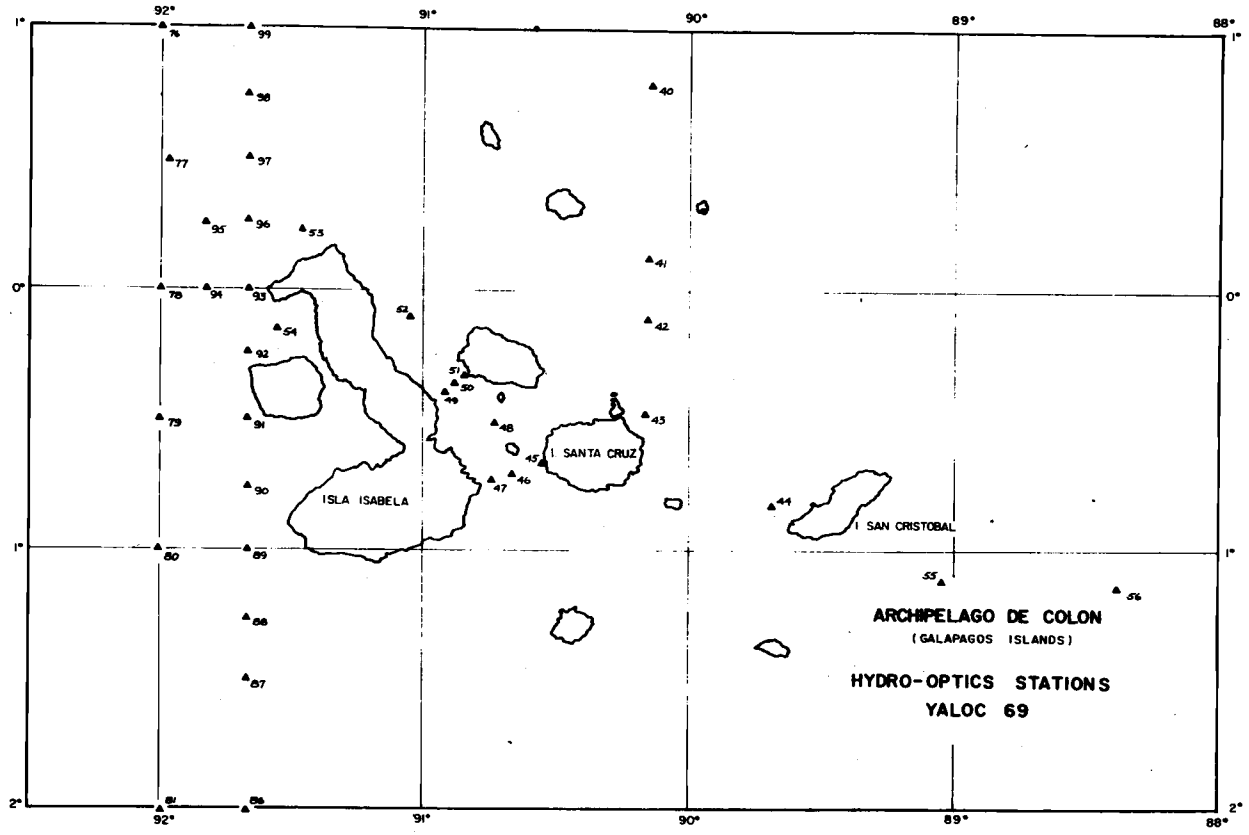

Figure 3.2. Galapagos Island stations: YALOC-69.

water column with any degree of adequacy. Particles smaller in diameter than 1μ were neglected for two reasons: Equation 2.12 indicated that these particles can be neglected with small error in the E.O.A., and measurements of particles much smaller than 1μ involve excessive electrical noise (using a 100μ orifice) on the Coulter Counter. With these two stipulations in mind, particle distribution resolution became the foremost consideration in the utilization of the remaining station time. Since the resolution is highly dependent upon the distributional shape and the shape could only be determined after a sample was measured, a certain amount of trial and error was involved. This manifests itself in the early data tables where at first a variety of different diameter spacings appear. At station YPT-32, adequate electrical noise shieldings of the Coulter Counter was obtained to allow the counts to be taken at a minimum diameter size of 1.13μ rather than the earlier setting of 1.75μ Throughout the rest of the cruise, distributional resolution is superior to the earlier stages so the consequential increased attention focused upon stations YPT-32 through YPT-69 is for this reason.

Three replicates of N_i were taken at each D_i for variance estimates and increased accuracy. Sudden line voltage surges and infrequent orifice clogging affect the particle counts, and although most of then were detected, the selection of the median of the three

replicates essentially eliminated the effects of inaccurate counts due to these error sources. Throughout the data, then, the value listed will be of the median of the three replicates.

The depths chosen most frequently to represent the particle content of the water column were 0m, the pycnocline depth, 100m, and 1000m. In order to determine the bottle spacing for any given hydro cast, it was extremely helpful to know in advance what the depths of the maximum turbidity and the thermocline were. For these purposes a transmissometer and a bathythermograph were employed prior to the hydro cast. The first gave a trace of the relative transmittance (transmitted radiant flux/incident radiant flux) versus depth, while the second recorded the temperature as a function of depth. An effort was made to place at least one bottle in the maximum turdidity layer which generally occurred at the top of the thermocline. Some typical transmissometer and bathythermograph curves are shown in Figure 3.3 taken at station YNS-13.

Plastic N.I.O. bottles were used throughout the cruise to collect water samples for optical, chemical, and particle size analyses. Standard reversing thermometers accompanied these bottles for "in situ" depth and temperature measurements. The salinity of the water samples was measured by an inductive salinometer, while the Winkler method was used for oxygen determinations.

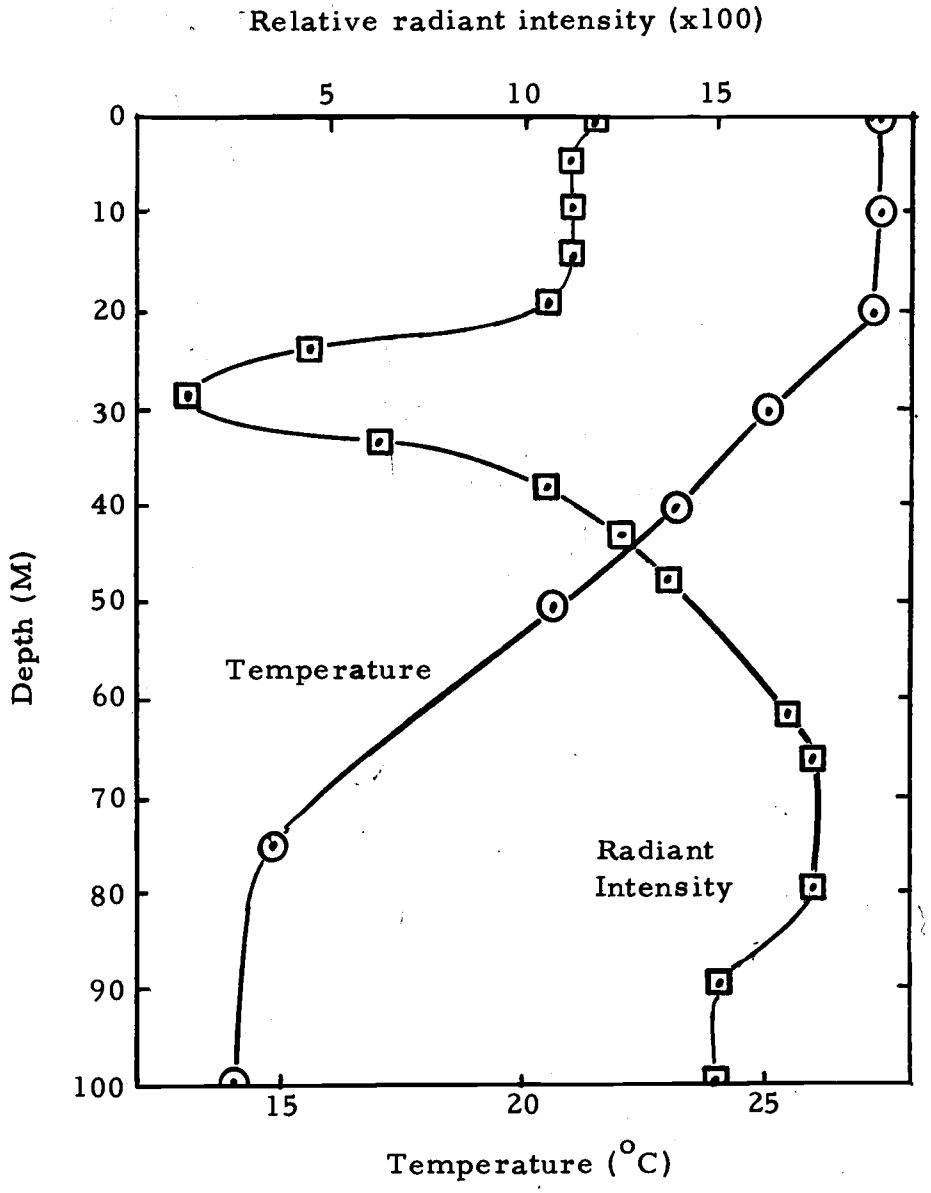

Figure 3.3. B-T and transmissometer traces for YNS-13.

Particle and optical analysis methods and a discussion of the Coulter Counter Model A and the Brice-Phoenix Light Scattering photometer are found in Appendices A and B respectively. Also included are calibration and data reduction techniques. Optical measurements were taken on each bottle sample of water.

IV. RESULTS

For the first 23 stations of YALOC-69, a variety of approaches to the problem of best determining the particle content of the ocean were tried. At least one total count N_{10} of the particles was made on most of the bottle samples, and a complete particle size distribution was generated for the surface samples. Distributions were also determined for stations with a strong turbidity maximum at the pycnocline. Beyond station YPT-23, a consistent program measuring size distributions from four depths was undertaken. This decision was based upon preliminary shipboard results and is discussed in more detail below.

Table 4. 1 lists the station, positions, times and epths at which sampling bottles were placed. Salinity, temperature, O_2, and optics measurements were taken at each of these depths; one "x" denotes a particle content count N_{10}, and two "x's" (xx), represents a complete particle size distribution run.

Table 4. 2 lists the particle frequencies N_i of diameter greater than the corresponding diameter D_i for the stations and depths at which complete particle distribution work was performed. Some typical examples of surface particle size distributions are shown by the relative frequency polygons in Figure 4. 1. Included on the graphs

Table 4.1. Station and Measurement Identification

Station	Lat. (N)	Long. (W)	Date	Time (GCT)	Depths (meters)							
YNS-1	41 10.8	124 36.2	1-03-69	1926	0 xx	10 xx	20 x	30 xx	49 x	75 x	99 x	148 x
					199 x	299	400	501	601	802	1001	
YNS-2	33 42	119 32.2	1-05-69	2030	0 xx	10 x	19	29 x	49 x	75 x	98 x	146 x
					198 x	299 x	401 x	500 x	600 x	800 x	887 x	1001 x
					1086 x	1202 x	1488	1689	1789	1839		
YNS-3	33 45.0	118 46.0	1-06-69	0400	0	10	20	30	50	76	100	150
					199	300	400	430	501	581	601	631
					683	734	783	834				
YSP-4	29 23.7	116 33.0	1-08-69	1750	0 xx	10 x	20 x	29 x	30 x	35 xx	40 x	45 x
					50 xx	76 xx	99 x	147	198 x	299	401 x	500
					599 x	80	1001	1201				
YSP-5	28 15.0	115 55.0	1-09-69	0931	0 xx	9 x	20 x	29 x	49 x	75 x	100 x	149 x
					199 x	300	400 x	501	602 x	801	1002 x	1203
YSP-6	25 35.1	114 00.1	1-10-69	0547	0 xx	10 x	19 x	29 x	49 xx	75 x	100 x	101
					106	111	116 x	121	148	199 x	299	400 x
					500	601 x	802	1001 x	1203	1293	1595	2091
					2945	3568	3799	3850				
YSP-7	22 57.0	112 05.0	1-11-69	0928	0 xx	10 x	20 x	29 x	49 x	75 x	100 x	147 x
					198 x	299	399 x	599 x	801	1001 x	1201	
YSP-8	21 00.0	108 32.0	1-12-69	1131	0 xx	10 x	20 x	30 x	49 x	75 x	100 x	148 x
					199 x	299	401 x	602 x	803	1003 x	1204	1496
					1695	1996	2495	2696	2795	2846		
YSP-9	10 05.2	105 00.0	1-13-69	1549	0 xx	9 x	19 x	29 x	48 x	75 x	99 x	147 x
					198 x	298 x	398 x	597	798 x			

Table 4.1 (continued)

Station	Lat. (N)	Long. (W)	Date	Time (GCT)	Depths (meters)							
YSP-10	17 39.9	102 30.0	1-14-69	1122	0 xx	10 x	20 x	25 x	30 x	35 x	40 xx	49 x
					75 x	100 x	150 x	201 x	302	402 x	604 x	807
YSP-11	17 03.8	102 45.5	1-14-69	1892	0 xx	10 x	20 x	30 x	40 x	49 x	76 x	99 x
					147 x	198 x	299	399 x	600 x	801	1001 x	1202
YSP-12	16 30.0	100 00.0	1-15-69	1256	0 xx	10 x	20 x	30 x	40 x	49 x	75 x	99 x
					148 x	199 x	299	400 x	601 x	801	1001 x	1203
YSP-13	16 00.0	100 10.5	1-15-69	1900	0 xx	10 x	20 x	29 x	39 x	48 x	73 x	97 x
					146 x	196 x	295	395 x	592 x	793	989 x	1187
					1227	1526	2016	2525	2926	3328	3428	3476
YSP-14	15 10.1	096 34.9	1-17-69	0001	0 x	10 x	20 x	30 x	40 x	49 x	74 x	98 x
					147 x	197 x	298 x	398 x	598 x	797	997 x	1197
YSP-15	14 28.9	093 25.4	1-17-69	2218	0 xx	9 x	19 xx	29 x	39 x	49 x	76 x	100 x
					148 x	199 x	298	400 x	601 x	801	1000 x	1202
YSP-16	14 02.8	093 29.8	1-18-69	0325	0 x	10 x	20 x	30 x	40	50 x	75 x	99 x
					149 x	198 x	248	300	401 x	600 x	801	1001 x
					1202	1502	2003	2407	2909	3411	3914	4412
					4918	5018	5069					
YSP-17	13 30.0	093 30.3	1-18-69	2200	0 xx	10 x	19 x	29 x	39 x	49 x	74 x	99 x
					147 x	197 x	248	299	403 x	599 x	800	990 x
					1199							
YSP-18	12 18.5	91 20.5	1-19-69	1435	0 xx	10 x	20 x	30 x	40 x	48 x	75 x	98 x
					148 x	199 x	248	298	398 x	597 x	796	994 x
					1194							

Table 4.1 (continued)

Station	Lat. (N)	Long. (W)	Date	Time (GCT)	Depths (meters)							
YSP-19	11 05.5	89 09.5	1-20-69	0747	0 xx	10 x	20 x	30 x	40 x	50 x	75 x	99 x
					149 x	199 x	247	266 x	291 x	300	316 x	341 x
					365 x	400 x	598 x	800	999 x	1199	1221	1620
					2120	2620	3119	3420	3520	3583		
YSP-20	10 06.0	87 28.0	1-20-69	0542	0 xx	10 x	20 x	30 x	40 x	50 x	75 x	99 x
					148 x	198 x	248	300	400 x	600 x	801	1001 x
					1201							
YSP-21	08 40.0	85 00.0	1-22-69	0035	0 xx	10 x	20 x	20 x	40 xx	50 x	76 x	100 x
					149 x	200 x	249	300	401 x	602 x	804	1003 x
					1204							
YPT-22	09 06.4	084 26.2	1-25-69	2226	0 xx	10 x	20 x	30 x	40 x	50 x	75 x	99 x
					146 x	199 x	249	300	400 x	601 x	804	905 x
YPT-23	08 31.1	83 53.0	1-25-69	0503	0 xx	10 x	20 x	30 x	40 x	50 x	75 x	100 x
					150 x	201 x	250					
YPT-24	08 21.2	83 12.5	1-26-69	1040	0	10	20	30	40	50	76	91
YPT-25	08 09.1	83 19.3	1-26-69	1431	0 xx	10	20	30 xx	39	49	74	98 xx
					149	198	249	300	400	601	802	1003 xx
					1189	1203	1489	1587	1688	1737	1763	
YPT-26	07 41.3	83 47.1	1-27-69	0024	0	10	19	29	39	49	73	98
					147	198	247	298	398	598	798	996
					1197	1345						
YPT-27	07 14.5	84 16.0	1-27-69	0645	0 xx	10	20 x	30 xx	49	75	99	148 xx
					199	247	298	398	597	797	994 xx	1143

Table 4.1 (continued)

Station	Lat. (N)	Long. (W)	Date	Time (GCT)	Depths (meters)							
YPT-28	06 45.6	84 44.4	1-27-69	1318	0	10	20	30	40	50	76	99
					149	198	248	299	401	600	800	1007
					1201							
YPT-29	06 18.0	85 12.2	1-27-69	1935	0 xx	10	20	30	40 xx	50	75	100 xx
					149	199	800	403	600	802	1001 xx	1203
					1501	1752						
YPT-30	05 50.0	85 41.0	1-28-69	0256	0	10	20	29	40	50	74	99
					148	198	298	398	598	799	997	1198
					1498	1648						
YPT-31	05 13.2	86 10.0	1-28-69	1805	0 xx	10	20	30	40	50 xx	75	99 xx
					149	198	300	400	600	801	1000 xx	1201
					1412	1476						
YPT-31	04 37.5	86 53.2	1-28-69	1407	0 xx	10	20	30	40	50	76	100
					148	199	300	400	599	650		
YPT-32	04 52.3	86 38.0	1-29-69	0247	0	10	20	30	40	50	74	99
					149	199	248	300	401	600	801	1000
					1101							
YPT-33	04 26.1	87 06.5	1-29-69	0850	0	10	20	30	40	50	74	99
					148	198	299	400	600	801	998	1199
					1401							
YPT-34	03 57.5	87 34.5	1-29-69	1458	0 xx	10	20	30	40 xx	50	75	100 xx
					149	199	299	500	600	803	1003 xx	1204
					1406	1558						

Table 4.1 (continued)

Station	Lat. (N)	Long. (W)	Date	Time (GCT)	Depths (meters)							
YPT-35	3 29.6	88 04.0	1-29-69	2108	1	11	21	31	41	50	76	99
					149	199	298	598	798	997	1196	1495
					1795							
YPT-36	3 02.6	88 33.2	1-30-69	0315	0 xx	10	20	30 xx	40	50	78	100 xx
					149	200	301	402	603	804	1004 xx	1205
					1506							
YPT-37	2 34.0	89 01.1	1-30-69	1038	0 xx	10	20	30	40 xx	50	74	99 xx
					149	199	300	401	604	803	1002 xx	1205
					1505	1807						
YPT-38	2 05.0	89 29.3	1-30-69	1715	0 xx	10	20	30	40 x	49	75	97
					147	197	298	399	600	800	999	1124
					1200	1422	1500	1674	1924	2173	2222	2247
YPT-39	1 28.4	90 08.8	1-30-69	1705	0 xx	10	20	30	40	49 xx	75	99 xx
					147	198	299	400	600	801	1001 xx	1203
					1503	1703						
YPT-40	00 47.0	90 08.9	1-31-69	1125	0 xx	10	20	30	40 xx	49	75	98 xx
					147	198	299	399	600	801	1001 xx	1202
					1502	1803	2002					
YPT-41	00 07.2	90 09.3	1-31-69	1805	0 xx	10	20 xx	30	40	49	75	99 xx
					147	198	298	399	600	800	999 xx	1200
					1499							
	(S)	(W)										
YPT-42	00 07.0	90 09.5	2-1-69	0041	0 xx	10	20	30	40 xx	49	75	99 xx
					148	199	300	401				
YPT-43	00 28.8	90 10.0	2-1-69	0458	0 xx	10	20	30	40 xx	49	75	99 xx
					147	198	299	399	600	801	1000	

Table 4.1. (continued)

Station	Lat. (S)	Long. (W)	Date	Time (GCT)	Depths (meters)							
YPT-44	00 50.4	89 41.2	2-1-69	1213	0 xx	10	20	30	40 xx	49	75	99 xx
					148	199	300	401	480			
YPT-45	00 40.0	90 33.4	2-2-69	0719	0	10	20	30	49	75	99	
YPT-46	00 42.8	90 39.8	2-2-69	0902	0 xx	10	20	30	40	49	75	99
					148	198						
YPT-47	00 44.2	90 44.7	2-2-69	1042	0	10	20	30	40	49		
YPT-48	00 31.0	90 44.1	2-2-69	1319	0	10	15	20	30	40	49	75
					99	148	199	300	401	501		
YPT-49	00 24.0	90 55.4	2-2-69	1533	0	10	20	30	40	49	75	99
YPT-50	00 21.9	90 52.8	2-2-69	1802	0 xx	10	13	20	30	40	49	75
					99	149	189	290	394			
YPT-51	00 20.2	90 51.0	2-2-69	2007	0	10	20	30	40	49	74	98
					146	197	298	398				
YPT-52	00 06.7	91 03.1	2-2-69	2239	0 xx	10	20	30	40 xx	49	75	98 xx
					147	197	298	399	600	800	999 xx	1200
					1500	2000						
YPT-53	00 13.2	91 27.8	2-3-69	0505	0 xx	10	20	30	40 xx	49	75	99 xx
					148	198	299	399	605	801	1000 xx	1201
					1490	2001 xx						
YPT-54	00 09.4	91 33.4	2-3-69	0932	0	10	20	30	40	49	75	99
					147	198	299	399	600	801	1001	1202
					1502	2002						
YPT-55	01 07.4	89 03.0	2-5-69	0851	0 xx	10	20	30	40	49 xx	75	99 xx
					148	199	248					

Table 4.1 (continued)

Station	Lat. (S)	Long. (W)	Date	Time (GCT)	Depths (meters)							
YPT-56	01 08.9	88 23.1	2-5-69	1511	0 xx	10	20	30	40 xx	64	89 xx	137
					187	287	387	586	765	874		
YPT-57	01 07.0	87 43.0	2-5-69	2355	0 xx	10 xx	20	30	40	49 xx	74	98 xx
					197	297	396	595	794	992 xx	1191	
YPT-58	01 07.0	87 02.6	2-6-69	0648	0 xx	10	20	30 xx	34	49	147 xx	198
					298	398	598	798	997 xx	1197	1497	1597
YPT-59	01 07.8	86 24.0	2-6-69	1825	0 xx	10	20 xx	30	40	49	75	98 xx
					147	198	298	398	599	799	998 xx	1198
					1499	1898						
YPT-60	01 07.5	85 56.1	2-7-69	0005	0 xx	10	20	30 xx	40	49	75	99 xx
					147	198	298	398	598	798	995 xx	1197
					1497	1994 xx						
YPT-61	01 09.0	85 20.9	2-7-69	0628	0 xx	10	20 xx	30	40	49	75	98 xx
					147	197	298	398	598	798	997 xx	1147
					1197	1445	1499	1694	1941	2190	2240	2265
YPT-62	01 06.6	84 41.0	2-7-69	1744	0 xx	10	20	30 xx	40	49	75	99 xx
					147	198	299	398	599	800	1000 xx	1200
					1501	1800 xx						
YPT-63	01 01.0	93 58.8	2-8-69	0230	0 xx	10	20 xx	30	40	49	75	98 xx
					147	198	298	398	598	798	997 xx	1197
					1498							
YPT-64	01 06.0	83 18.7	2-8-69	1020	0 xx	10	20	30 xx	40	49	75	99 xx
					147	198	298	398	599	800	999 xx	1199
					1348							

Table 4.1. (continued)

Station	Lat. (S)	Long. (W)	Date	Time (GCT)	Depths (meters)							
YPT-65	01 07.0	82 40.0	2-8-69	1728	0 xx	10	20	30	40 xx	49	75	99 xx
					147	198	299	398	599	799	998 xx	1198
					1298							
YPT-66	01 07.5	82 00.0	2-8-69	2352	0 xx	10	20	30	40	49 xx	75	99
					147	199	298	398	599	800	999	1199
					1399							
YPT-67	01 08.1	81 06.6	2-9-69	0701	0 xx	10	20	30	40	49 xx	75	99
					148	173 xx	199 xx					
YPT-68	01 07.0	81 21.8	2-9-69	1240	0 xx	10	20	30 xx	40	49	75	99 xx
					148	199	300	300	600	801	1002	1201
					1503	1897	2002	2195	2393	2592	2740	2891
YPT-60	01 56.8	81 32.1	2-10-69	0148	0 xx	10	20	30	40	49 xx	75	99 xx
					147	198	298	398	599	800	990	999 xx
					1189	1199	1489	1986	2485	2683	2882	2932
					2957							

Table 4. 2. Cumulative Frequencies of Particle Size

Diameter(μ)		1.14	1.75	3.05	3.84	4.44	4.93	5.40	6.36	7.12	7.76	8.32	8.83	9.28	9.70	10.1	11.7	13.6	15.1	16.4
YNS-1	Om		2001	771	517	345	278	206	145	73										
	10m		2129	825	510	369	257	213	113	82	51									
	30m		1280	408	231	167	126	106	68	47	33									
	125m		613	179	114	73	64													
YNS-2	Om		1211	587	543	427	347	289	173	141	102	83	73	67						
YSP-4	Om		759	282	171	119	82	68	52	33	28	23	20							
	35m		923	274	178	141	111	101	66	55	41	34								
	50m		778	261	129	92	68	60	42	29	29									
	75m		259	94	56	39	32													
YSP-5	Om		1531	430	239	157	109	91	66	49	37	27	19							
YSP-6	Om		894	367	213	155	99	85	45	33	25	17								
	50m		757	265	148	90	70	54	39	22	19	13								
YSP-7	Om		770	279	134	101	69	55	27	26	18	14	12							
YSP-8	Om		529	176	106	77	64	61	34	28	21	18	17							
YSP-9	Om		411	142	86	63	47	47	25	23	16	12	11							
YSP-10	Om		660	230	132	87	64	63	39	27	22	14	9							
	40m		1293	516	317	260	216	170	125	83	70	66	48	42						
YSP-11	Om		454	177	123	94	73	63	39	36	23	20	16							
YSP-12	Om		705	245	145	98	77	59	47	31	29	20	18							
YSP-13	Om		916	265	168	133	105	80	50	36	26	25	23							
YSP-14	Om		973	290	239	155	117	89	55	42	34	25	23	18						
	20m		1629	615	410	350	246	228	122	73	57	54	37	32	26	20				
YSP-15	Om		954	318	214	178	152	140	84	69	60	55	55	52	43	40	33	22	18	9
	20m		1461	621	414	279	213	203	139	105	82	68	52	45	34	30	17	8	6	5
YSP-16	Om		1275	507	198	182	98	78	50	33	26	19	15	12	11	9				
YSP-17	Om		808	274	211	143	111	95	57	45	35	28	24	22	15	15				
YSP-18	Om		868	268	194	146	112	100	65	58	43	37	30	29	21	20	10	5	4	3
YSP-19	Om		1046	349	220	150	101	68	50	33	28	24	16	12	11	9				
YSP-20	Om		1498	722	479	307	190	155	90	74	46	45	30	25	19	15	8	4	2	2
YSP-20	15m		1771	818	619	466	358	355	251	207	155	118	106	76	56	44	27	10	10	9
YSP-21	Om	4276	3041	293	162	94	54	54	35	24	16	11	11	9	6	4				

Table 4.2 (cont.)

Diameter(μ)		1.14	1.75	3.05	3.84	4.44	4.93	5.40	6.36	7.12	7.76	8.32	8.83	9.28	9.70	10.1	11.7	13.6	15.1	16.4
YSP-21	40m		1538	820	649	474	383	313	213	138	99	86	66	55	49	38	22	12	10	6
YPT-22	0m		1237	434	238	145	119	88	71	47	35	32	23	22	18	16	12	11	8	
YPT-23	0m		1004	328	205	142	115	100	75	60	47	42	25	25	19	17				
YPT-25	0m		544	295	172	111	103	73	54	41	37	32	32	32	32	32	32	31	29	21
	30m		660	256	185	151	132	99	58	36	25	16	13	13	8	8				
	100m	206	100	36	17	16	10	10	8											
	1000m	215	111	35	25	16	13	11	8											
YPT-27	0m		748	257	168	118	103	88	55	37	24	24	20	16	13	11	5	5	2	2
	30m		653	245	154	111	87	72	41	31	22	14	11		7	7				
	150m		536	175	129	93	73	49	23	15	10	5	5	3	1	1				
	1000m		303	125	87	74	52	45	23	9	6	5	3	3						
YPT-29	0m		418	158	108	88	70	57	51	38	34	29	23	23	17	10	4			
	40m		1102	326	230	170	126	98	59	39	26	18	14	14	11	10				
	100m		149	47	28	17	17	17	9	7	6									
	1000m		81	22	16	15	8	8	6	4										
YPT-31	0m		578	208	146	96	74	62	29	24	18	17	14	11	11	9				
	50m		871	400	268	173	127	110	75	50	49	37	34	27	25	20	14	8	5	3
	100m		140	51	34	23	23	23	13	12	11	9	8	7	5	3				
	1000m		85	27	14	11	6	6	5	4										
YPT-32	0m	1679	915	378	287	259	211	186	171	144	139	136	127	125	116	109				

Table 4. 2 (cont.)

Diameter (μ)		1.14	1.75	3.05	3.84	4.44	4.93	5.40	6.36	7.12	7.76	8.32	8.83	9.28	9.70	10.1	11.7	13.6	15.1	16.4
YPT-34	0m	685	464	142	75	54	42	41	28	20	19	13	13	10	10	10				
	40m	879	375	124	97	74	55	49	29	28	23	17	14	11	10	9				
	100m	309	151	52	34	21	18	15	10	5	5									
	1000m	147	71	23	14	9	9	9	5	5	5									
YPT-36	0m	1627	828	230	130	82	58	58	31	25	14	12	12	9	5	4				
	30m	2241	1420	631	320	260	196	165	114	74	62	50	44	27	27	21	13	10	6	3
	100m	473	237	72	59	43	31	19	14	8	6	4	4	4						
	1000m	293	167	52	23	20	11	11	6	4	4									
YPT-37	0m	1286	755	237	122	90	69	56	27	21	12	12	6	6	4	3				
	40m	1602	1080	404	231	161	107	92	50	36	28	25	12	12	9	5				
	100m	439	225	89	74	52	41	32	13	9	5									
	1000m	209	128	31	12	5	3													
YPT-38	0m	1309	724	247	147	96	81	55	26	26	18	13	10	9	7	5				
	40m	1780	1032	419	238	152	99	-	-	-	-	-	-	-	-	-				
YPT-39	0m	3692	1683	665	377	237	169	140	81	55	43	29	25	21	15	15	6	6	2	1
	50m	1584	870	416	245	169	111	99	64	40	29	29	16	14	14	8				
	100m	526	237	79	62	30	28	13	9	7										
	1000m	202	96	30	15	11	5													
YPT-40	0m	2291	1477	579	359	230	169	128	87	58	43	43	22	18	12	8				
	40m	1221	640	266	144	103	60	75	32	27	21	16	10	9	8	8				
	100m	364	173	64	44	41	29	28	24	11	4									
	1000m	164	67	23	16	12	6													
YPT-41	0m	2827	1360	454	256	142	116	91	73	55	35	23	20	17	10	9				
	20m	5192	2559	1049	627	384	301	245	169	108	83	58	40	31	27	19	11	3	2	2
	100m	479	218	76	46	31	28	18	13	7	5									
	1000m	212	105	34	15	8	8													
YPT-42	0m	2545	1269	444	193	142	96	63	37	29	17	15	14	7	7	6				
	40m	1116	622	250	164	124	90	73	40	25	16	14	11	10	7	4				
	100m	359	168	69	43	34	20	17	12	10	10									

Table 4.2 (cont.)

Diameter(μ)		1.14	1.75	3.05	3.84	4.44	4.93	5.40	6.36	7.12	7.76	8.32	8.83	9.28	9.70	10.1	11.7	13.6	15.1	16.4
YPT-43	0m	4178	1904	621	392	292	220	183	148	120	114	106	93	85	46	29	31	30		
	20m	1305	762	332	254	167	140	112	80	53	47	35	33	25	24	16	10	4		
	100m	404	213	81	61	47	32	32	23	12	11	7								
YPT-44	0m	2304	974	313	167	117	91	66	47	34	17	17	17	17	13	11	9			
	40m	1230	627	286	154	123	81	45	27	18	15	8								
	100m	362	190	72	44	32	37	17	8	7										
YPT-46	0m	2266	1017	298	155	108	78	64	47	43	31	25	21	20	18	12				
YPT-50	0m	2361	1175	433	248	164	101	98	54	41	29	22	22	16	13	8				
YPT-52	0m	6127	2575	922	561	403	276	216	127	80	54	39	34	22	20	20	9	6	4	3
	40m	3964	1853	750	412	243	160	118	83	44	40	34	24	17	17	12				
	100m	432	205	77	49	41	35	34	21	16	9	9	9	5						
	1000m	214	116	31	28	18	14	8	8	3										
YPT-53	0m	4259	2394	982	693	457	323	261	167	120	90	78	56	40	40	29	19	7	5	5
	40m	947	508	189	125	74	63	50	34	23	17	9	7	7	7	7				
	100m	427	204	62	51	33	26	16	11	11	6									
	1000m	294	169	32	15	11	11	6	6											
	2000m	287	126	33	18	11	11	6	6											
YPT-55	0m	3492	1800	692	257	158	127	114	69	63	47	32	29	21	19	14				
	50m	2045	940	353	211	146	102	89	52	36	31	27	17	17	11	8				
	100m	430	203	67	30	20	16	10	9	8										
YPT-56	0m	2930	1587	594	297	205	138	120	69	63	39	34	23	21	21	13	10	6	4	3
	40m	2047	1053	382	239	165	118	109	57	46	31	30	29	15	11	11				
	90m	692	275	49	28	21	13	10	7	2										
YPT-57	0m	1976	1186	417	287	157	116	89	45	40	31	21	15	14	9					
	10m	2767	1696	628	401	278	179	146	86	53	48	32	28	23	18	15				
	100m	419	200	94	52	41	19	19	15	11	8									
	1000m	213	130	33	25	14	10	11	4	4										
YPT-58	0m	2071	1180	394	168	105	77	61	37	30	22	18	11	10	10	5				
	30m	2428	1383	469	284	205	145	131	77	47	43	39	23	20	19	15	6	5		
	150m	1768	503	47	31	19	15	15	10	5										
	1000m	170	72	29	12	7	7													

Table 4.2 (cont.)

Diameter(μ)		1.14	1.75	3.05	3.84	4.44	4.93	5.40	6.36	7.12	7.76	8.32	8.83	9.28	9.70	10.1	11.7	13.6	15.1	16.4
YPT-59	0m	1857	1031	372	239	157	116	88	61	46	36	23	21	14	10	7				
	20m	3379	1701	600	338	223	162	137	79	57	48	41	31	28	21	13				
	100m	401	188	97	57	31	21	21	14	13	10	10	7							
	1000m	186	87	30	16	12	8													
YPT-60	0m	1928	1058	429	272	174	123	118	73	44	35	27	21	17	11	8				
	30m	3207	1888	806	526	358	220	193	121	80	61	45	34	27	15	15				
	100m	341	206	80	54	39	22	22	13	11	6									
	1000m	167	77	24	11	11	5													
	2000m	185	90	22	12	10	8													
YPT-61	0m	2091	1106	450	242	213	121	94	66	43	32	23	17	14	10	8				
	20m	1963	1291	502	316	190	140	124	90	56	50	34	33	26	19	15				
	100m	226	118	40	29	29	25	18	18	10	9	5								
	1000m	169	77	25	14	9	9													
YPT-62	0m	3152	1562	631	348	229	151	113	89	57	44	36	25	15	15	13				
	30m	2458	1333	562	361	271	211	188	136	91	76	55	47	33	33	25	16	8	4	4
	100m	396	211	83	42	30	24	21	15	11	6	5								
	1000m	200	101	22	16	11	10													
	2000m	173	88	30	13	8	6													
YPT-63	0m	2940	1496	545	329	192	137	107	88	46	36	31	19	17	12	10				
	20m	1116	699	300	218	161	128	128	81	53	44	28	26	20	19	12				
	100m	299	184	64	49	28	23	18	15	11	8									
	1000m	182	84	33	20	12	8													
YPT-64	0m	3632	1735	565	266	178	118	102	46	36	30	27	18	18	11	8				
	30m	1733	981	375	246	203	134	129	99	62	56	50	43	31	27	17				
	100m	339	221	69	36	29	28	18	12	9										
	1000m	171	86	26	16	12	12													
YPT-65	0m	2680	1387	434	229	188	101	79	47	38	32	23	23	18	15	14				
	40m	1435	663	195	124	90	69	65	43	32	23	22	16	15	15	10				
	100m	460	235	68	36	33	21	20	12	10	6									
	1000m	193	90	26	25	8	7													

Table 4.2 (cont.)

Diameter(μ)		1.14	1.75	3.05	3.84	4.44	4.93	5.40	6.36	7.12	7.76	8.32	8.83	9.28	9.70	10.1	11.7	13.6	15.1	16.4
YPT-66	0m	4057	2152	770	594	464	358	307	185	108	80	57	45	38	27	21	13	8	3	3
	50m	1243	471	127	75	62	42	42	37	25	19	17	17	17	14	11				
YPT-67	0m	4933	2797	954	511	372	330	243	155	111	85	70	50	39	39	39	30	20	14	8
	75m	1117	429	124	68	41	33	30	12	9										
	175m	877	452	132	77	59	43	36	21	13	11									
	200m	408	225	71	37	32	29	22	8	8	4									
YPT-68	0m	2370	1139	423	234	163	124	81	51	38	38	30	26	17	17	10				
	30m	1216	675	265	157	109	74	63	36	29	26	18	15	15	10	7				
	100m	275	157	51	32	29	21	19	16	11	6									
YPT-69	0m	4343	2526	1052	686	393	309	227	139	114	86	71	67	52	49	40	20	15	12	5
	50m	794	379	108	62	42	34	29	22	15	10	10	5							
	100m	401	211	67	40	37	24	19	15	10	7									
	1000m	288	160	52	26	17	13	10	10	3										

are the total number of particles counted, N_{10} for stations prior to YPT-32 and N_5 for the later stations. N_5 and N_{10} represent the number of particles larger than threeholds 5 and 10, which correspond to diameters of size 1.13 microns and 1.75 microns respectively (see Appendix A). Each of these curves appears to have a roughly exponential shape. Figure 4.2 shows the relative frequency polygons at four depths per station of four different stations. Again there remains a high degree of similarity in the appearance of the curves, even with depth.

Table 4.3 lists the stations and depths at which the temperature, salinity, dissolved oxygen, N_{10}, N_5, $\overline{D}$, $\overline{S}$, $\beta(45^{\circ})$, and the scattering ratio R are listed. The depths included are only the ones at which complete particle distributions were generated. A complete listing of all hydrographic and optical data taken on YALOC-69 will appear at the end of 1969 in the form of an Oregon State University Department of Oceanography cruise report on YALOC-69. The data appearing in this dissertation is primarily optical-particle interaction oriented.

Because of the general homogeneity of the frequency polygon shapes, N_5 and N_{10} were used as indicators of the relative particle content of the water column. This allowed an easy comparison to be made with $\beta(45^{\circ})$, an optical particle content indicator. Figures 4.3, 4.4, 4.5, and 4.6 denote the relative agreement between $\beta(45^{\circ})$

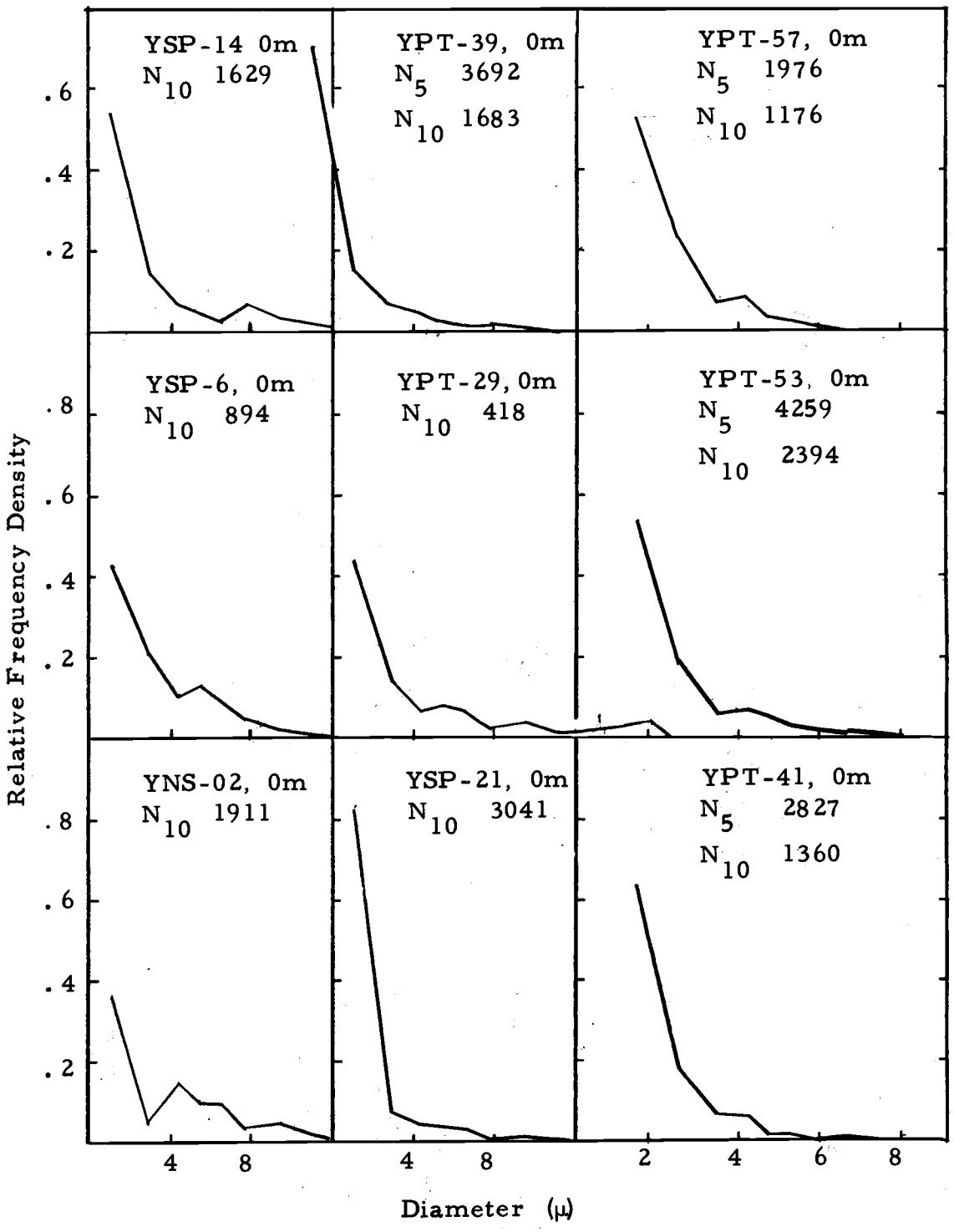

Figure 4.1. Some typical particle frequency densities for surface waters.

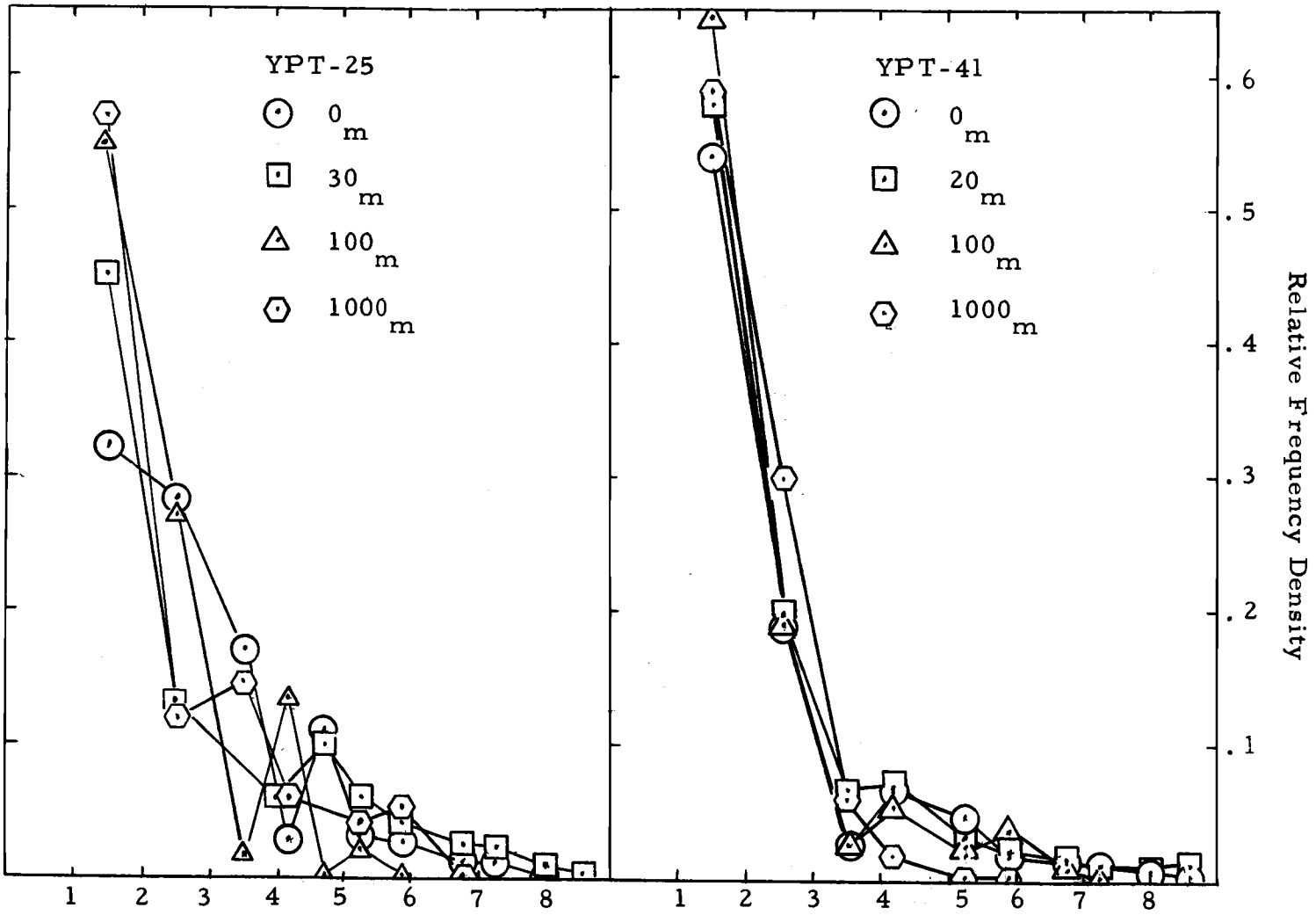

Figure 4. 2. Particle size distribution with depth.

Table 4.3. Particle and hydrographic measurements.

Station	Depth (m)	T(C)	S(‰)	O_2(Ml/l)	N_{10}	N_5	$\bar{D}(\mu)$	$\bar{S}(\mu^2)$	$\beta(45^\circ)\times10^{-2}$ (m^{-1})	$\beta(135^\circ)\times10^{-2}$ (m^{-1})	R
YNS-1	0	10.57	32.910	6.23	2001				2.88	.345	8.35
	10	10.51	32.918	6.14	2129				4.11	.544	7.54
	30	10.71	33.061	6.05	1280				1.57	.252	6.24
	148	9.64	33.717	3.53	613				--	--	--
YNS-2	0	14.06	33.479	6.20	1211				1.25	.246	6.60
YSP-4	0	16.08	33.652	6.11	759				.629	.186	3.38
	35	15.47	33.582	5.78	923				.806	.190	4.25
	50	14.96	33.527	5.65	778				.852	.225	3.78
	76	12.10	33.736	4.89	259				.616	.211	2.93
YSP-5	0	16.84	33.885	5.65	1531				1.46	.240	6.09
YSP-6	0	18.98	34.109	6.03	894				.642	.206	3.12
	49	17.76	33.949	5.36	757				1.08	.251	4.31
YSP-7	0	22.52	34.529	5.10	770				.646	.203	3.18
YSP-8	0	24.85	34.281	4.86	529				.646	.203	3.18
YSP-9	0	27.10	33.983	4.73	411				.559	.199	2.81
YSP-10	0	27.72	33.992	4.85	660				.640	.197	3.25
YSP-11	0	28.69	33.213	4.68	454				.628	.207	3.03
YSP-12	0	27.90	33.676	4.75	705				1.03	.230	4.48
YSP-13	0	28.21	33.728	4.75	916				.719	.202	3.57
YSP-14	0	28.53	33.655	4.81	973				.860	.233	3.70
	20	26.95	33.710	4.41	1629				1.14	.258	4.42
YSP-15	0	28.14	33.184	4.91	954				1.40	.287	4.87
	19	26.56	33.420	5.18	1461				1.55	.274	5.67
YSP-16	0	26.46	33.510	4.95	1275				1.26	.260	4.84
YSP-17	0	27.08	33.474	4.80	808				1.22	.219	5.57
YSP-18	0	27.09	33.350	4.83	868				.934	.214	4.36
YSP-19	0	25.78	33.925	4.60	1046				.756	.234	.323
YSP-20	0	27.25	34.863	4.82	1498				1.01	1.74	5.83
	15	--	--	--	1771				2.75	.346	7.94

Table 4.3. (continued)

Station	Depth (m)	T(C)	S (‰)	O_2(Ml/l)	N_{10}	N_5	$\bar{D}(\mu)$	$\bar{S}(\mu^2)$	$\beta\ (45^\circ)X10^{-2}$ (m^{-1})	$\beta\ (135^\circ)X10^{-2}$ (m^{-1})	R
YSP-21	0	28.79	31.485	4.68	3041	4276			.758	.210	3.62
	40	24.88	33.830	5.02	1538				2.32	.364	6.36
YPT-22	0	29.42	31.046	4.84	1237				.899	.204	4.41
YPT-23	0	29.29	30.719	4.80	1004				.804	.182	4.43
YPT-25	0	29.05	30.693	5.05	544				.873	.227	3.85
	30	26.08	33.209	4.52	660				.787	.221	3.55
	98	14.61	34.924	0.94	100	206			.393	.222	1.77
	1003	4.51	34.584	1.09	111	215			.286	.183	1.56
YPT-27	0	28.75	31.965	4.70	748				.600	.182	3.30
	30	26.53	34.016	4.90	653				.825	.602	13.70
	148	14.11	34.919	0.68	536				.468	.187	2.50
	994	4.51	34.586	0.98	303				.385	.181	2.12
YPT-29	0	28.73	32.686	4.71	418				--	--	--
	40	25.82	33.443	4.71	1102				1.20	.368	3.25
	100	14.82	34.907	0.82	149				.552	.276	2.00
	1001	4.51	34.583	1.11	81				.389	.214	1.82
YPT-31	0	28.09	30.030	4.74	578				.665	.197	3.37
	50	22.15	34.207	3.22	871				.997	.210	4.75
	99	15.01	34.943	1.24	140				.384	.165	2.32
	1000	4.66	34.583	0.98	85				.311	.170	1.83
YPT-32	0	28.46	31.113	4.71	915	1679			.725	.308	2.35
YPT-34	0	27.92	30.594	4.80	464	685			.484	.199	2.43
	40	27.61	32.090	4.91	375	879			.622	.227	2.74
	100	14.94	34.950	--	151	309			.426	.194	2.19
	1003	4.72	34.575	1.41	71	147			.442	.193	2.29
YPT-36	0	28.03	30.598	4.78	828	1627			.576	.266	2.17
	30	25.78	33.504	4.60	1420	2241			1.06	.288	3.67
	100	15.42	35.016	2.25	237	473			.461	.188	2.46
	1004	4.81	34.575	1.35	167	293			.292	.254	1.15

Table 4.3. (continued)

Station	Depth (m)	T(C)	S (‰)	O_2(Ml/l)	N_{10}	N_5	$\bar{D}(\mu)$	$\bar{S}(\mu^2)$	$\beta(45^\circ)X10^{-2}$ (m^{-1})	$\beta(135^\circ)X10^{-2}$ (m^{-1})	R
YPT-37	0	27.82	30.414	4.80	755	1286	2.41	7.61	.637	.208	2.17
	40	22.39	34.231	3.39	1080	1602	2.66	9.4	1.08	.258	3.67
	99	15.27	34.977	1.84	225	429	2.43	8.55	.744	.246	2.46
	1002	4.70	34.571	1.37	128	209	2.25	5.84	.394	.239	1.65
YPT-38	0	27.15	31.137	4.77	724	1309	2.41	7.94	.777	.219	3.55
	40	24.67	33.653	4.79	1032						
YPT-39	0	25.81	33.791	4.87	1683	3692	2.27	7.04			
	49	17.31	35.073	2.97	870	1584	2.59	8.66	.845	.222	3.81
	99	15.43	35.054	2.58	237	526	2.26	6.91	.541	.217	2.49
	1001	4.59	34.574	1.60	96	202	2.17	5.81	.347	.187	1.85
YPT-40	0	24.41	34.252	4.82	1477	2291	2.66	9.59	1.13	.245	4.64
	40	17.42	35.092	2.77	640	1221	2.45	8.52	.695	.200	3.48
	98	15.32	35.059	2.53	173	364	2.41	8.29	.433	.191	2.26
	1001	4.75	34.576	1.45	67	164	2.15	5.97	.391	.213	1.84
YPT-41	0	24.53	34.404	4.99	1360	2827	2.27	7.20	1.06	.238	4.39
	20	22.62	34.744	4.14	2559	5192	2.38	7.85	1.59	.329	5.37
	99	15.68	35.092	2.47	218	479	2.25	6.78	.572	.205	2.79
	999	4.86	34.576	1.47	105	212	2.22	6.12	.327	.188	1.73
YPT-42	0	24.06	34.473	4.77	1269	2545	2.24	6.55	1.11	.251	4.43
	40	16.74	35.045	2.66	622	1116	2.54	8.92	.640	.210	3.05
	99	15.30	35.059	2.55	168	359	2.36	7.72	.501	.198	2.53
YPT-43	0	22.61	34.620	4.37	1904	4178	2.26	7.36	1.17	.241	4.89
	40	18.09	35.004	3.22	762	1305	2.76	11.54	.840	.201	4.18
	99	15.25	35.059	2.96	213	404	2.52	9.06	.437	.186	2.35
YPT-44	0	21.48	34.737	4.08	974	2304	2.16	6.30	.799	.226	3.53
	40	18.33	35.008	2.98	627	1230	2.41	7.70	.838	.224	3.74
	99	15.27	35.064	2.35	190	326	2.39	7.52	.542	.191	2.84
YPT-46	0	24.34	34.409	4.77	1017	2266	2.19	6.58	1.71	.304	5.62

Table 4.3. (continued)

Station	Depth (m)	T(C)	S (‰)	O_2(Ml/l)	N_{10}	N_5	$\bar{D}(\mu)$	$\bar{S}(\mu^2)$	β (45°)X10^{-2} (m^{-1})	β (135°)X10^{-2} (m^{-1})	R
YPT-50	0	24.49	34.420	4.80	1175	2361	2.33	7.38			
YPT-52	0	24.19	34.477	4.94	2575	6127	2.19	6.48			
	40	20.05	34.811	3.85	1853	3964	2.28	6.97	1.05	.227	4.64
	98	15.15	35.030	2.30	206	432	2.42	8.57	.458	.194	2.36
	999	4.83	34.570	1.61	116	214	2.36	7.29	.332	.172	1.92
YPT-53	0	24.43	34.563	5.63	2394	4259	2.58	9.62	1.51	.334	4.53
	40	17.03	35.030	2.89	508	947	2.46	8.47	.585	.183	3.19
	99	15.08	35.062	2.70	204	427	2.28	6.99	.454	.166	2.74
	1000	--	34.565	1.73	169	294	2.19	5.62	.299	.194	1.86
	2001	2.19	34.651	2.58	126	287	2.10	5.59	.384	.202	2.27
YPT-55	0	25.34	34.707	5.00	1800	3492	2.32	7.16	1.36	.271	5.02
	49	18.91	35.018	3.14	940	2045	2.29	7.33	1.16	.260	4.46
	99	15.95	35.092	2.38	203	420	2.22	6.32	.591	.185	3.19
YPT-56	0	24.61	34.490	4.96	1587	2930	2.41	8.03	1.39	.253	5.50
	40	22.58	35.001	4.21	1053	2047	2.40	8.06	.982	.232	4.24
	89	15.88	35.108	2.49	275	692	1.97	4.69	.447	.177	2.52
YPT-57	0	26.84	32.388	4.80	1186	1976	2.51	8.43	1.08	.252	4.49
	10	24.82	33.814	4.91	1696	2767	2.57	8.92	1.56	.268	5.71
	98	15.40	35.089	2.38	200	419	2.39	7.81	.443	.175	2.52
	992	4.63	34.572	1.61	130	213	2.40	7.28	.356	.167	2.14
YPT-58	0	26.95	32.411	4.89	1180	2071	2.36	7.17	.819	.219	3.75
	30	22.97	34.720	4.52	1383	2428	2.47	8.52	1.21	.253	4.77
	147	14.80	35.023	2.22	503	1768	1.78	3.64	.372	.0882	2.22
	997	4.68	34.572	1.50	72	170	2.13	5.63	.318	.161	1.98
YPT-59	0	27.01	32.776	4.79	1031	1857			.825	.201	5.82
	20	22.79	34.528	4.43	1701	3379	1.35	.259	5.19		
	98	14.89	35.026	2.30	188	401			.538	.183	2.94
	998	4.62	34.572	1.54	87	186			.336	.201	1.67

Table 4.3. (continued)

Station	Depth (m)	T(C)	S (‰)	O_2 (ml/l)	N_{10}	N_5	$\bar{D}(\mu)$	$\bar{S}(\mu^2)$	$\beta\ (45^\circ)X10^{-2}$ (m^{-1})	$\beta\ (135^\circ)X10^{-2}$ (m^{-1})	R
YPT-60	0	26.69	32.960	4.90	1058	1928	2.51	8.73	.972	.257	3.79
	30	22.02	34.853	4.31	1888	3207	2.61	9.32	1.26	.288	4.37
	99	15.00	35.035	2.29	206	341	2.58	8.91	.476	.211	2.22
	995	4.74	34.573	1.50	77	167	2.14	5.55	.405	.244	1.66
	1994	2.34	34.640	2.43	90	185	2.14	5.57	.378	.169	2.23
YPT-61	0	26.37	32.935	4.99	1106	2091	2.44	8.18	1.04	.245	4.26
	20	21.98	34.590	4.10	1291	1963	2.70	10.02	1.26	.269	4.68
	98	14.99	35.039	2.15	118	226	2.54	9.57	.368	.172	2.15
	997	4.73	34.578	1.48	77	169	2.16	5.76	.291	.166	1.76
YPT-62	0	26.30	33.715	4.86	1562	3152	2.36	7.59	1.12	.235	4.78
	30	20.02	35.148	3.05	1333	2458	2.61	10.40	1.25	.261	4.79
	99	15.10	35.037	2.21	211	396	2.42	7.93	.414	.181	2.28
	1000	4.67	34.578	1.49	101	200	2.17	5.73	.310	.175	1.77
	1000	2.47	34.644	2.19	88	173	2.22	5.93	.419	.180	1.97
YPT-63	0	25.23	33.370	4.78	1496	2940	2.35	7.46	.731	.238	3.08
	20	21.25	34.999	3.78	699	1116	2.85	11.97	.736	.241	3.05
	98	15.17	35.030	2.18	184	299	2.59	9.08	.433	.198	2.19
	997	4.54	34.570	1.54	84	182	2.22	6.16	.316	.177	1.79
YPT-64	0	25.09	33.804	5.00	1735	3632	2.21	6.36	.923	.232	3.98
	30	19.29	36.127	2.96	981	1733	2.62	10.15	.898	.237	3.79
	99	15.39	35.033	2.19	221	339	2.53	8.26	.369	.175	2.11
	999	4.39	34.580	1.52	86	171	2.24	6.30	.400	.193	2.07
YPT-65	0	25.29	34.047	4.97	1387	2680	2.30	7.08	1.21	.260	4.68
	40	17.78	36.132	2.57	663	1436	2.26	7.33	1.21	.346	3.48
	99	15.93	36.028	2.29	235	460	2.28	6.86	.780	.338	2.31
	998	4.59	34.579	1.51	90	193	2.17	5.79	.327	.184	1.78
YPT-66	0	24.72	34.616	5.16	2152	4057	2.51	9.21	1.33	.258	5.16
	49	17.47	35.062	2.57	471	1243	2.11	6.50	.741	.206	3.60

Table 4.3. (continued)

Station	Depth (m)	T(C)	S (‰)	O_2(Ml/l)	N_{10}	N_5	$\bar{D}(\mu)$	$\bar{S}(\mu^2)$	$\beta\ (45^\circ)X10^{-2}$ (m^{-1})	$\beta\ (135^\circ)X10^{-2}$ (m^{-1})	R
YPT-67	0	23.90	34.616	5.16	2797	4923	2.47	8.85	--	.363	7.80
	75	15.75	35.008	2.19	429	1117	2.04	5.25	.689	.226	3.05
	173	14.62	34.987	1.63	452	877	2.28	6.81	.670	.203	3.31
	199	13.05	34.910	0.76	225	408	2.37	7.33	.448	.185	2.43
YPT-68	0	23.30	34.733	5.12	1139	2370	2.31	7.34	.893	.383	2.33
	30	18.05	34.941	2.47	675	1216	2.49	8.64	.793	.227	3.50
	99	15.14	35.007	1.79	157	275	2.50	8.67	.418	.181	2.31
YPT-69	0	23.73	34.782	5.46	2526	4343	2.59	9.68	2.08	.309	6.73
	49	16.81	34.989	2.19	379	794	2.23	6.61	.683	203	3.37
	99	15.54	35.009	2.02	211	401	2.37	7.54	.442	.188	2.35
	999	4.53	34.574	1.48	160	288	2.34	6.99	.365	.170	2.15

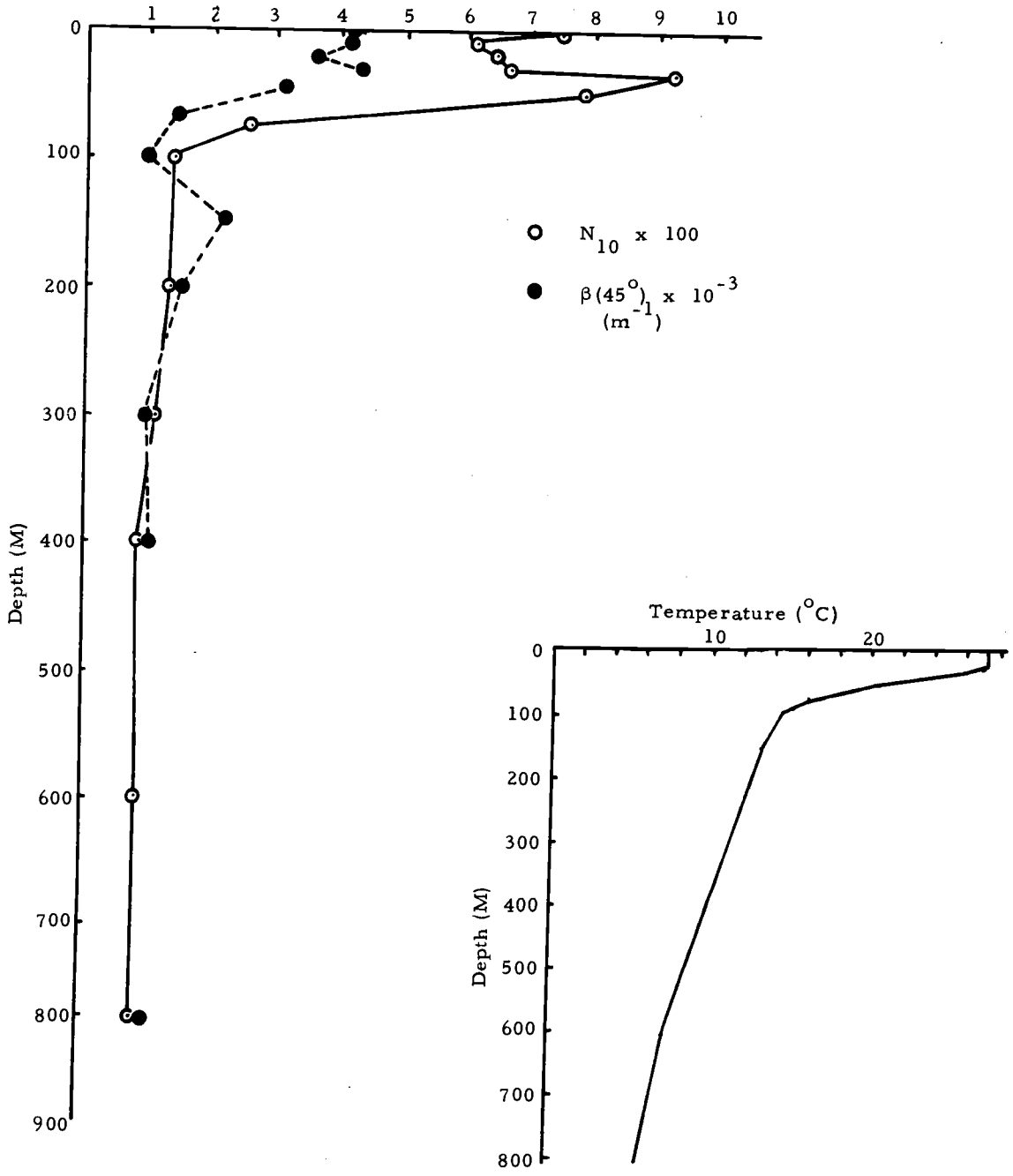

Figure 4.3. Particle number and $\beta(45^{o})$ vs. depth at YSP-4.

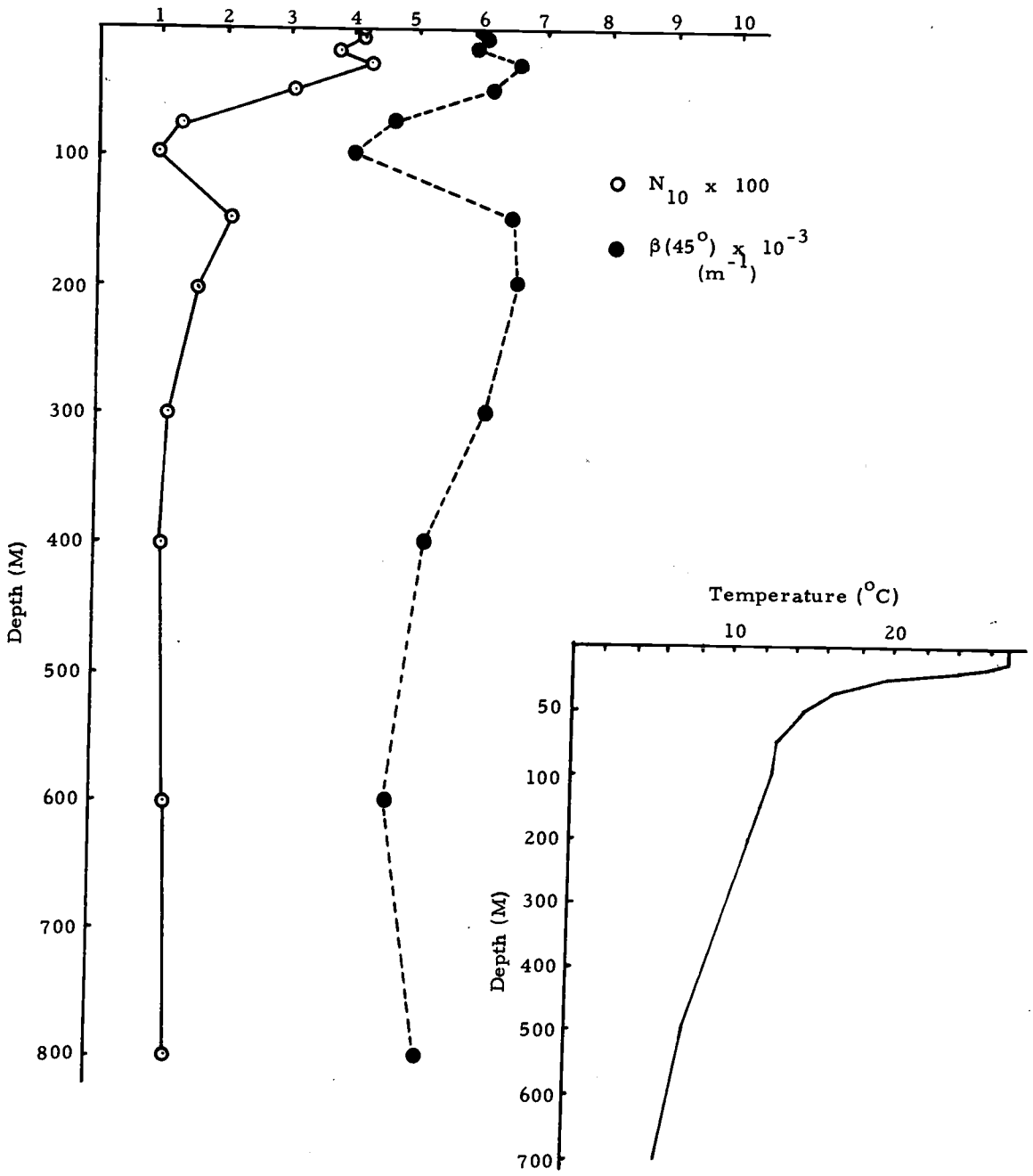

Figure 4. 4. Particle number and $\beta(45^{o})$ vs. depth at YSP-9.

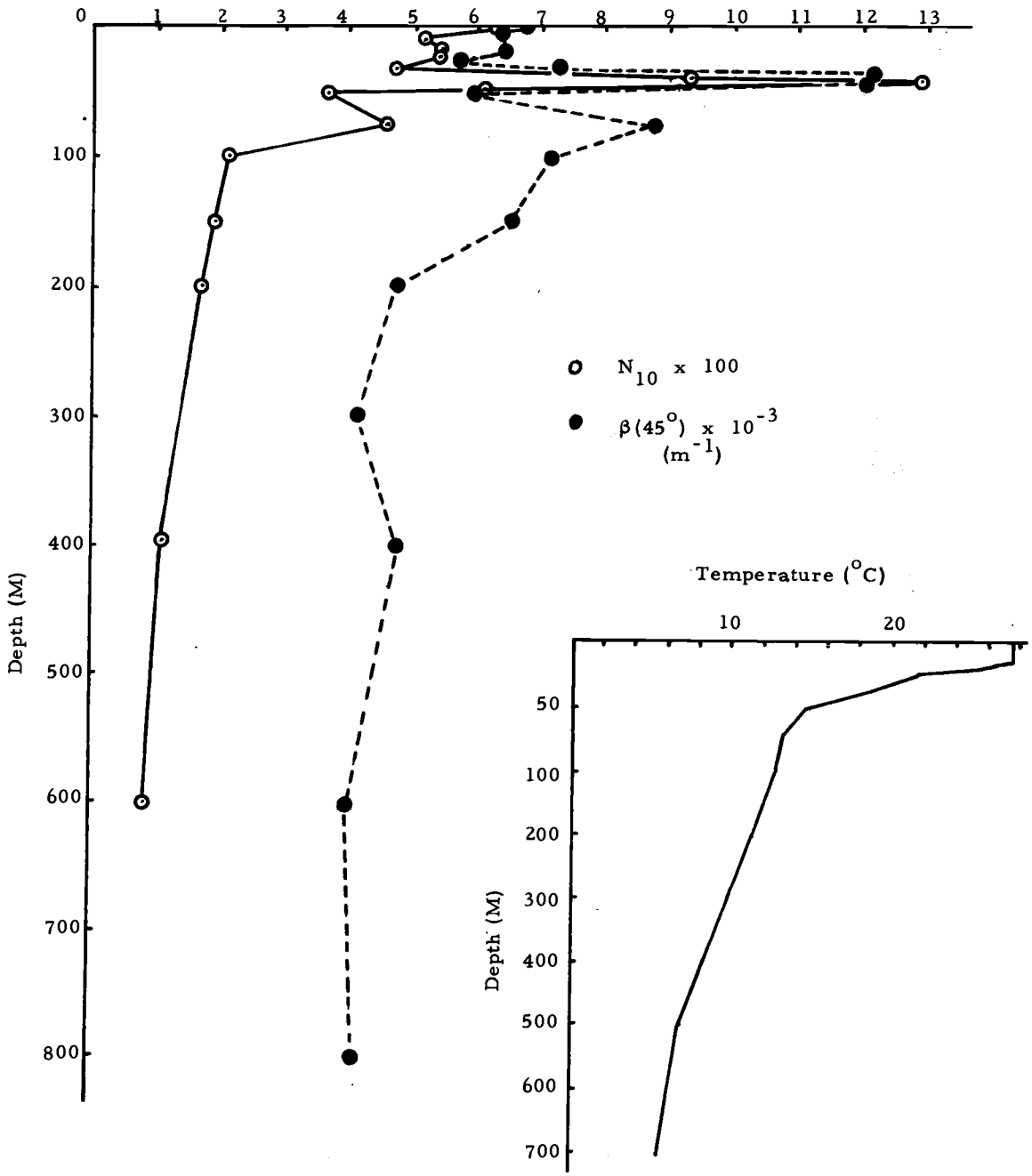

Figure 4.5. Particle number and $\beta(45^{o})$ vs. depth at YSP-10.

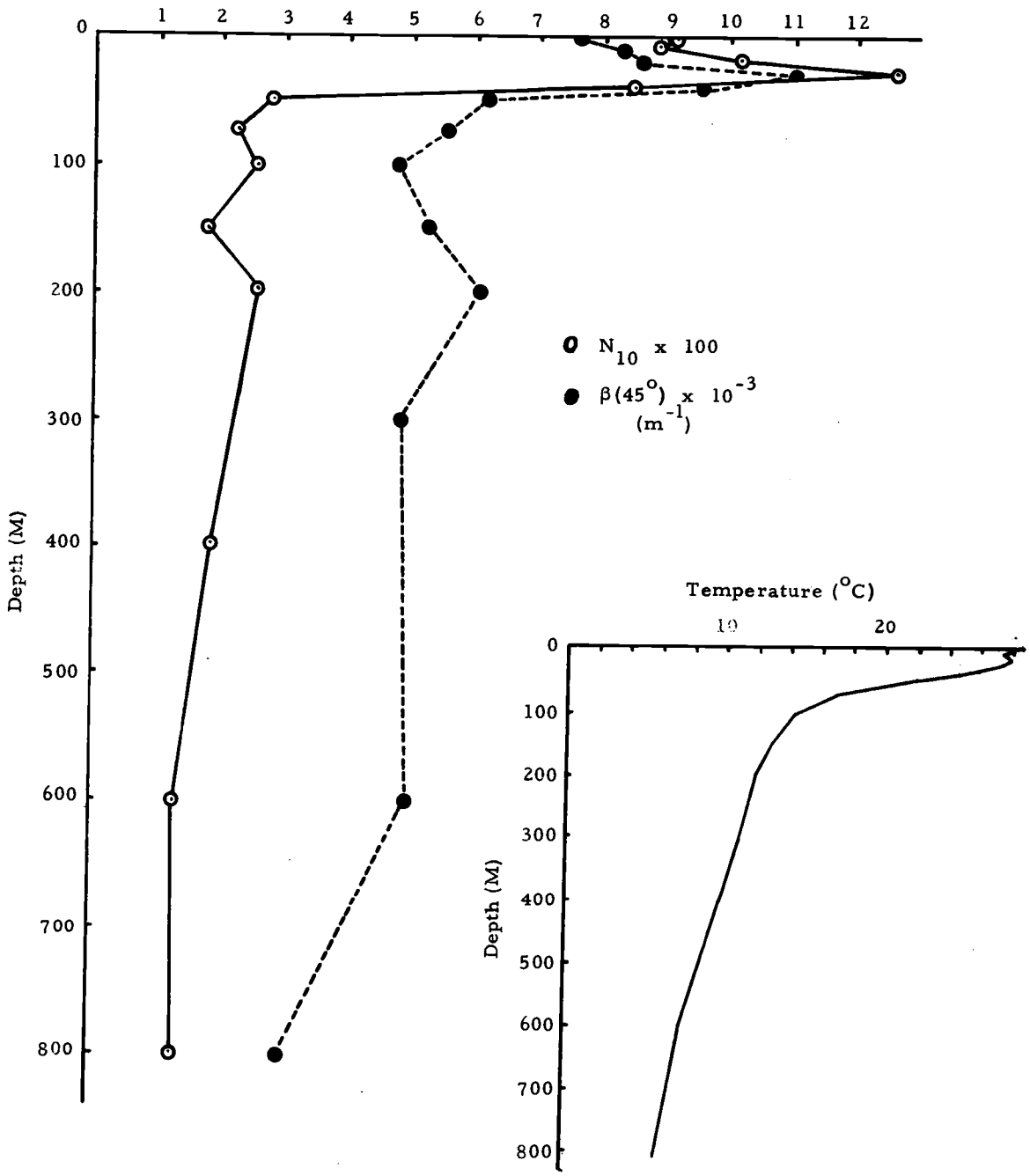

Figure 4.6. Particle number and $\beta(45^{\circ})$ vs. depth at YSP-13.

and N_{10} with depth. The temperature-depth profile insets show the typical trend of turbidity maxima (when they occur), correlating well with the tops of the thermoclines.

Since $\beta(45^{o})$ has been found to agree so well with N_{10} throughout the first 23 stations, it was decided that duplication of effort existed and the station time available could better be used if the Coulter Counter were employed exclusively in the generation of particle size distributions. The Brice-Phoenix scatterometer then became the primary instrument used to measure the particle content throughout the water column. This is quite acceptable in view of $\beta(45^{o})$ being a measure of total particle surface area (Equation 2.19).

As a result of instrumental shuffling, numerous particle size distributions could finally be generated by the Coulter Counter. An effort was made to fit theoretical curves to some of the resultant relative frequency polygons as shown in Figures 4.7 and 4.8. Included on the graphs are shape, scale, and location parameters; α, β, and c respectively for the gamma probability density functions (see Appendix C). The units on the abscissa are the generalized units $r = (x-c)/\beta$. Although the relative frequency polygons of Figure 4.1 will not all be as smoothly fit by the gamma p.d.f., it is apparent that their general shapes are very similar to those of YPT-39 and YPT-41, appearing also in Figures 4.7 and 4.8. The

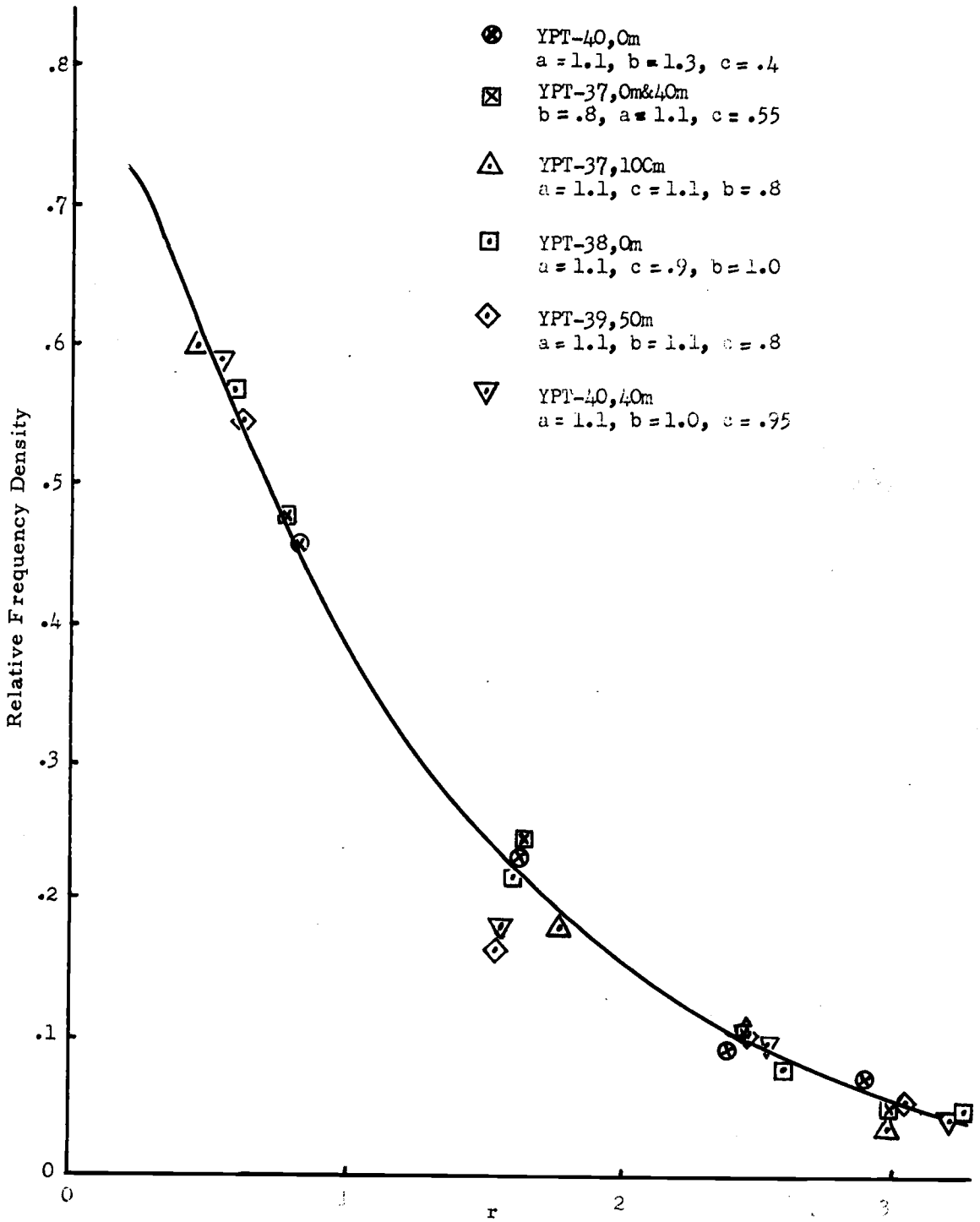

Figure 4.7. The relative frequency density of particle diameters.

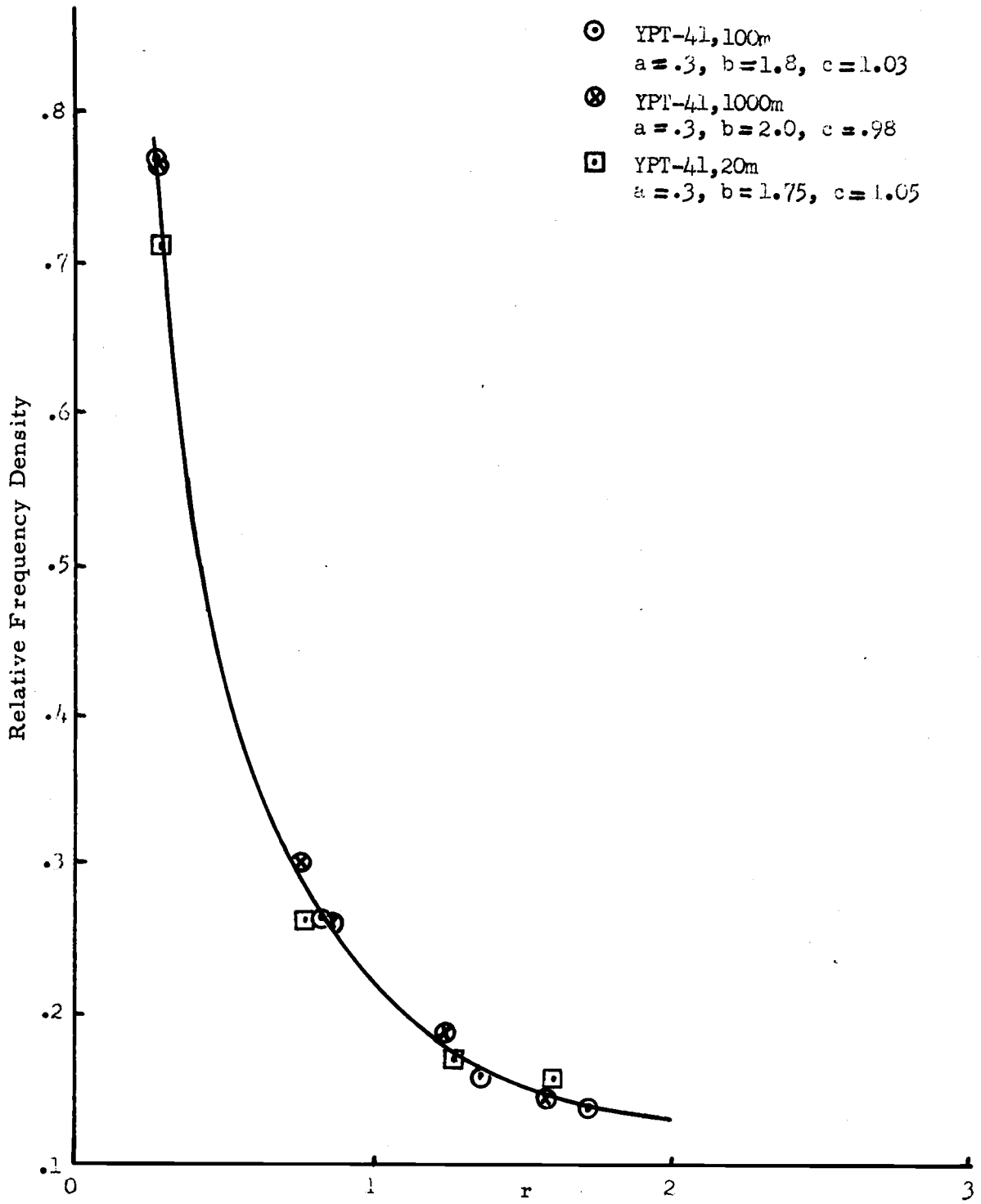

Figure 4.8. The relative frequency density of particle diameters.

difficulty of fitting the gamma p. d. f. to data overtaxes its usefulness (see Appendix C), so another method was used for further work in the analysis section.

Figure 4. 9 shows the particle content N_{10} found at the surface and at the pycnocline depths along the cruise track. Particle content increases markedly in the near-shore regions. Particle content at the pycnocline is generally greater than that at the surface in the more stable subtropical waters, but this trend is reversed in the Galapagos Island region, where the South Equatorial Pacific current averaged about 25 cm/sec. (see Figure 5. 13), increasing turbulent mixing.

Figure 4. 10 shows profiles of the optical parameter $\beta(45^{o})$. It supplements Figures 4. 3 through 4. 6 as an indication of the particle content of the waters sampled in the latter stages of the cruise. Figure 4. 9 shows the accompanying temperature profiles. Again, when turbidity maxima occur, their depths correspond to the upper portions of the thermoclines, where the increase in stability is greatest.

Figure 4. 12 through 4. 16 are temperature-salinity diagrams for stations between YPT-34 and YPT-65, the region in which the largest amount of particle distribution work was performed. From the data and figures presented in this section, several relationships were determined and are discussed in the following section.

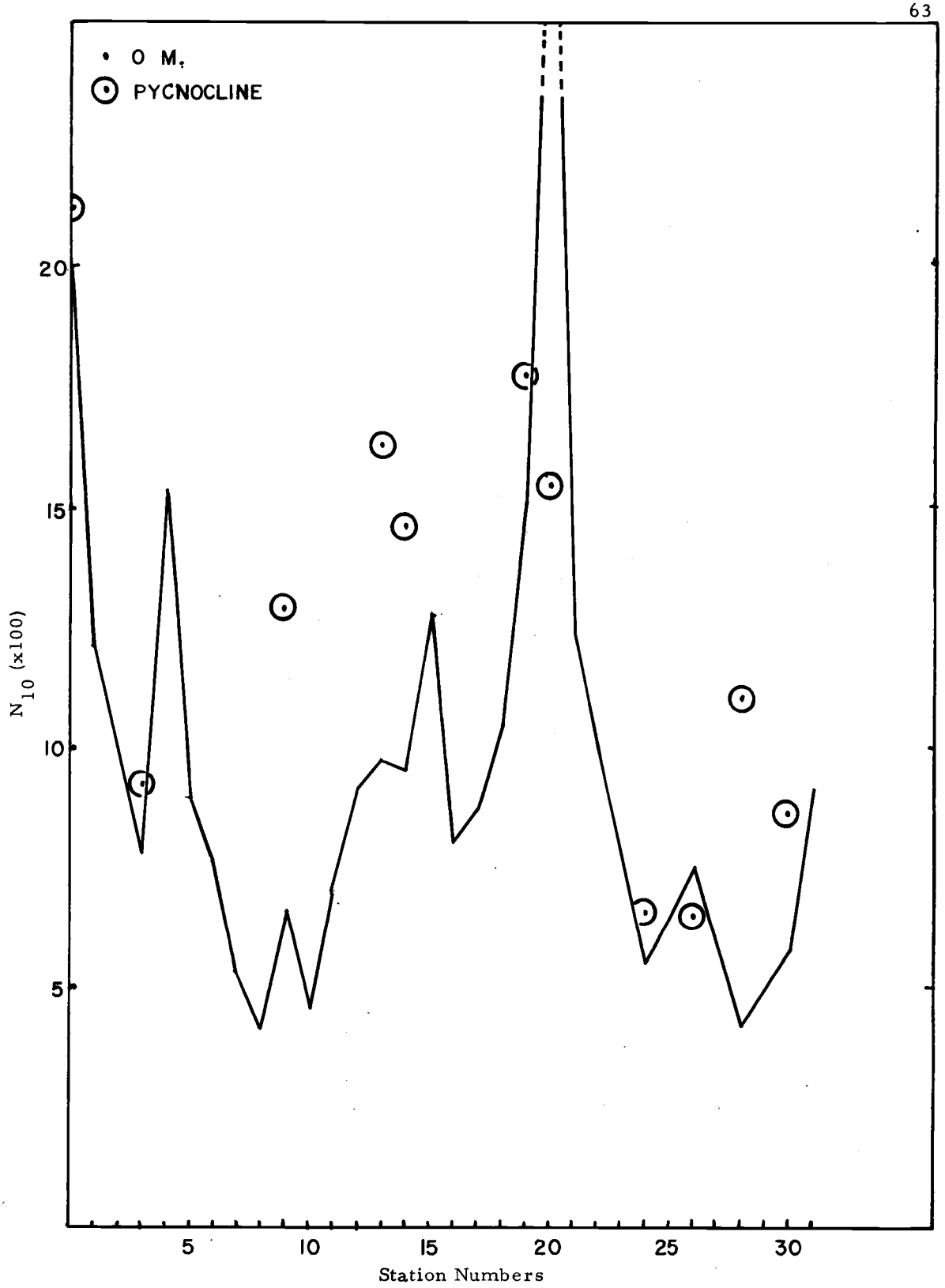

Figure 4.9. Surface and pycnocline particle content.

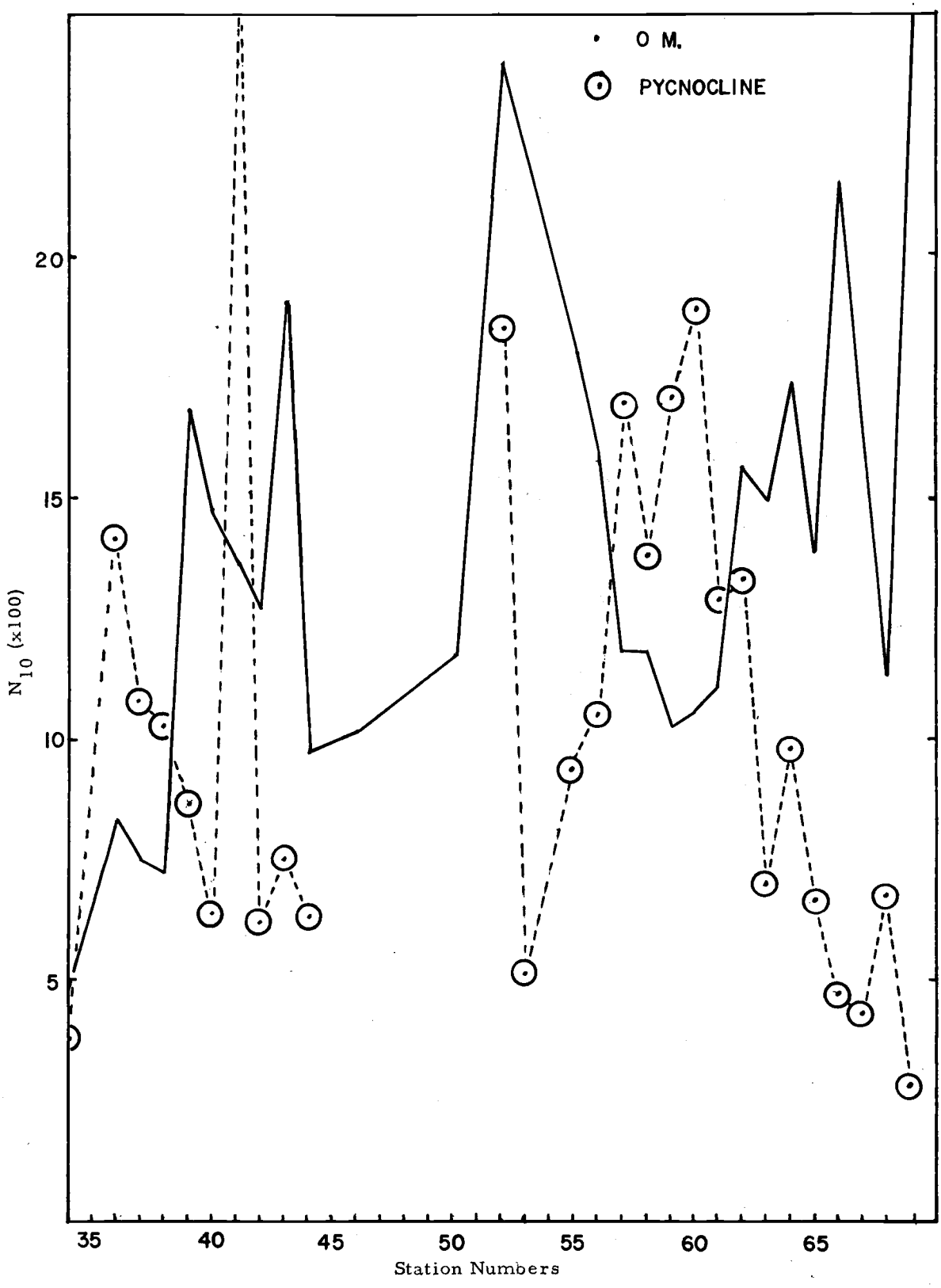

Figure 4.9. (cont.)

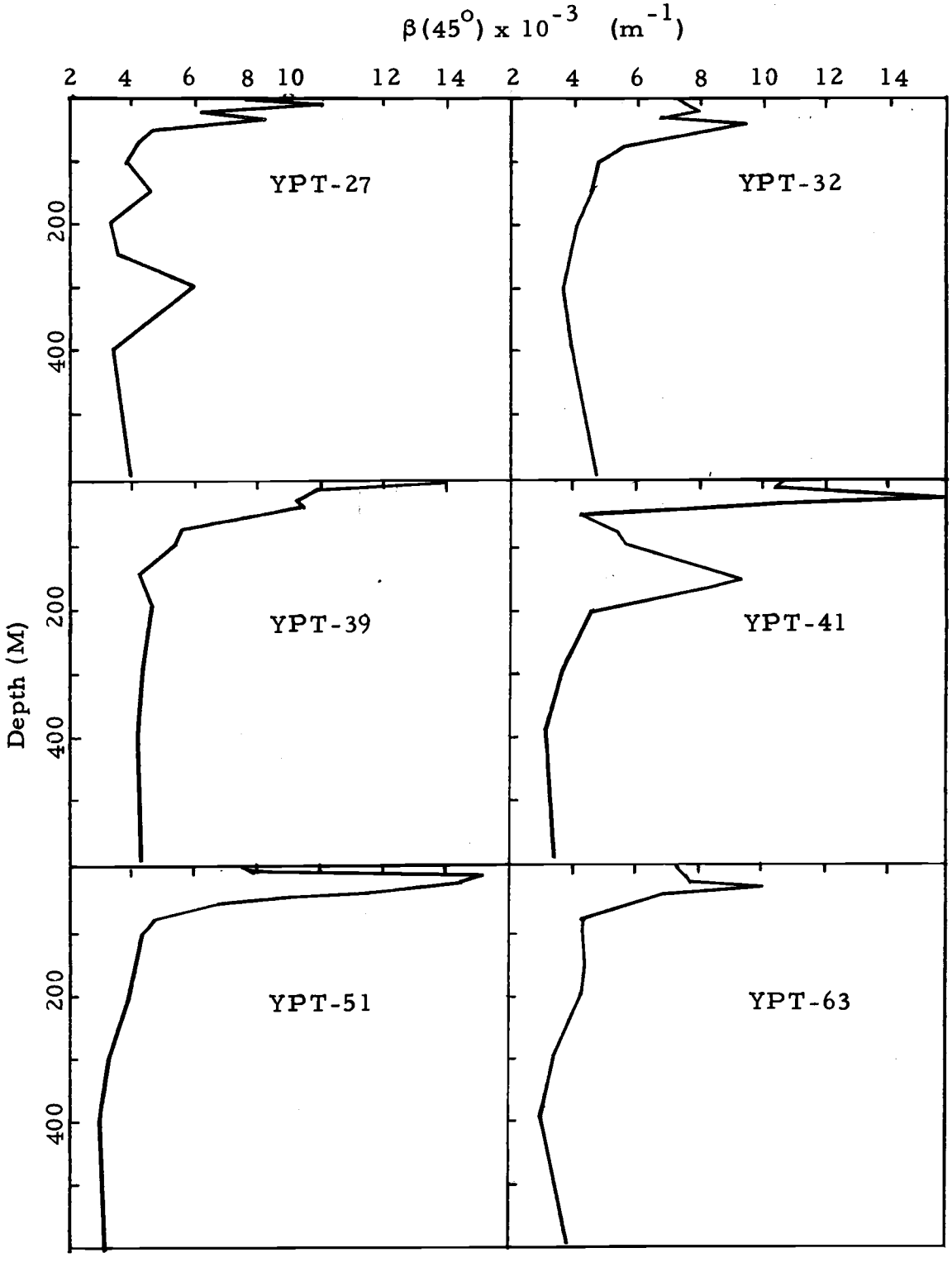

Figure 4. 10. $\beta(45^{\circ})$ profiles.

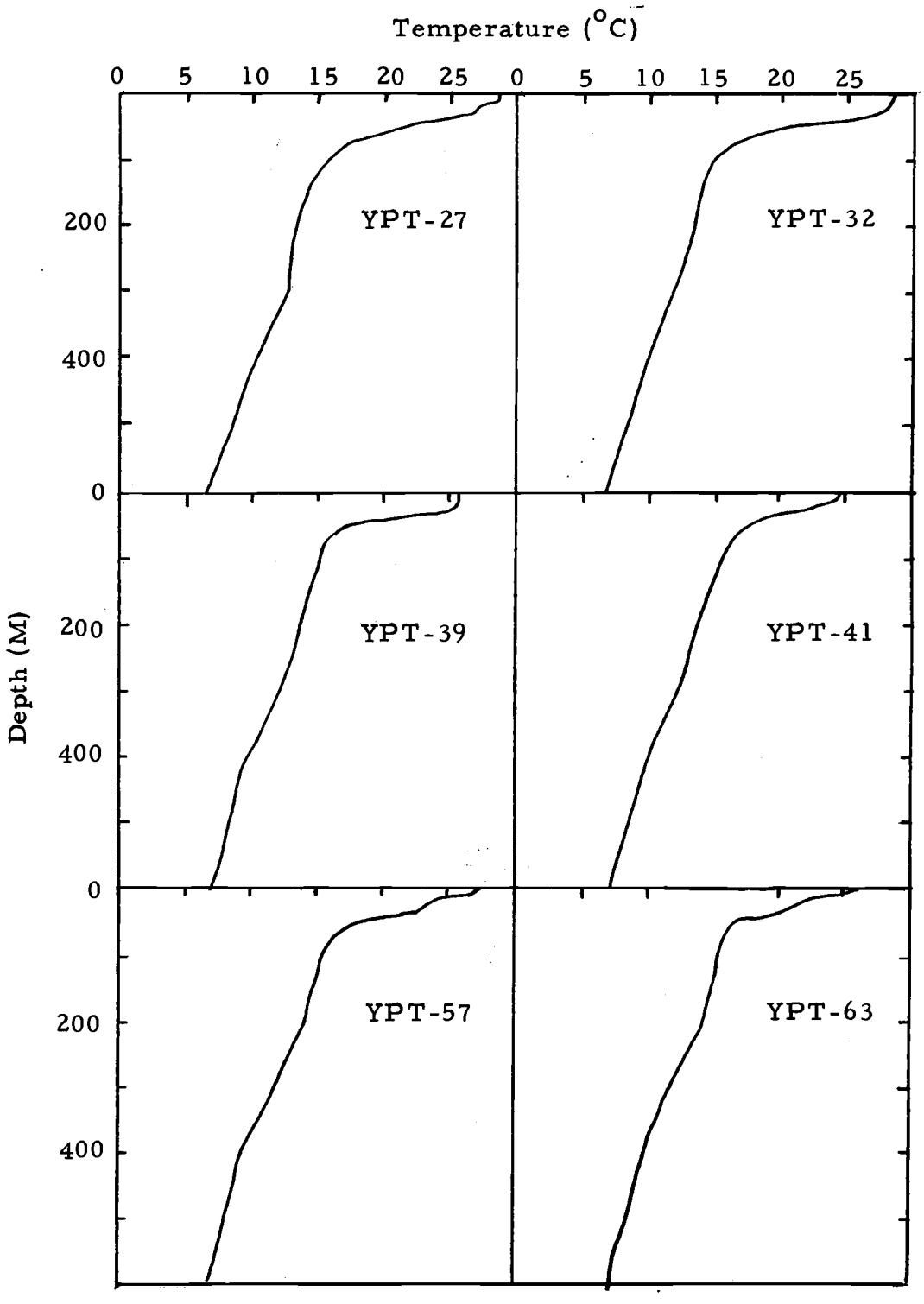

Figure 4.11. Temperature profiles.

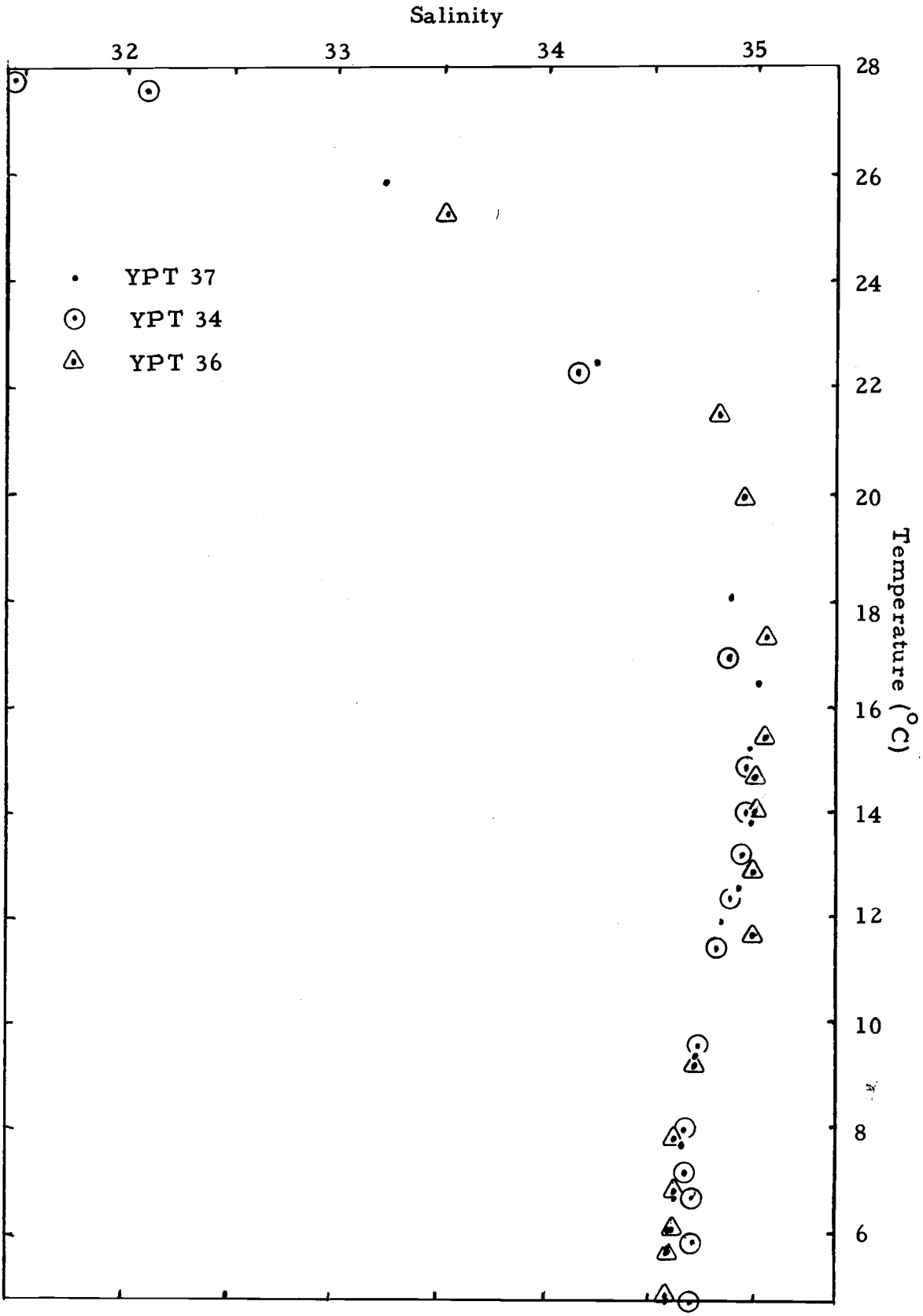

Figure 4.12. T-S diagrams for YPT-34, 36, 37.

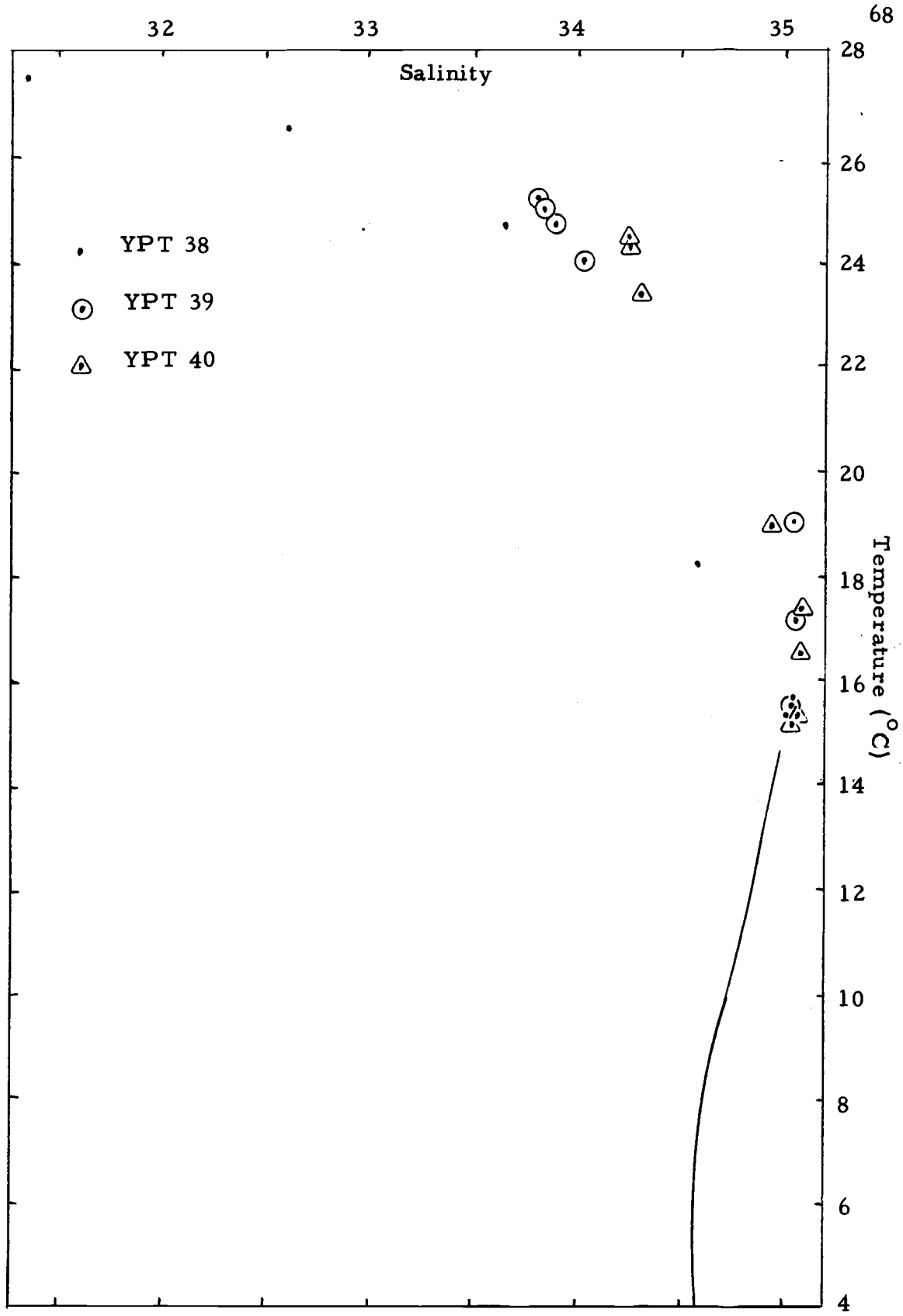

Figure 4.13. T-S diagrams for YPT 38, 39, 40.

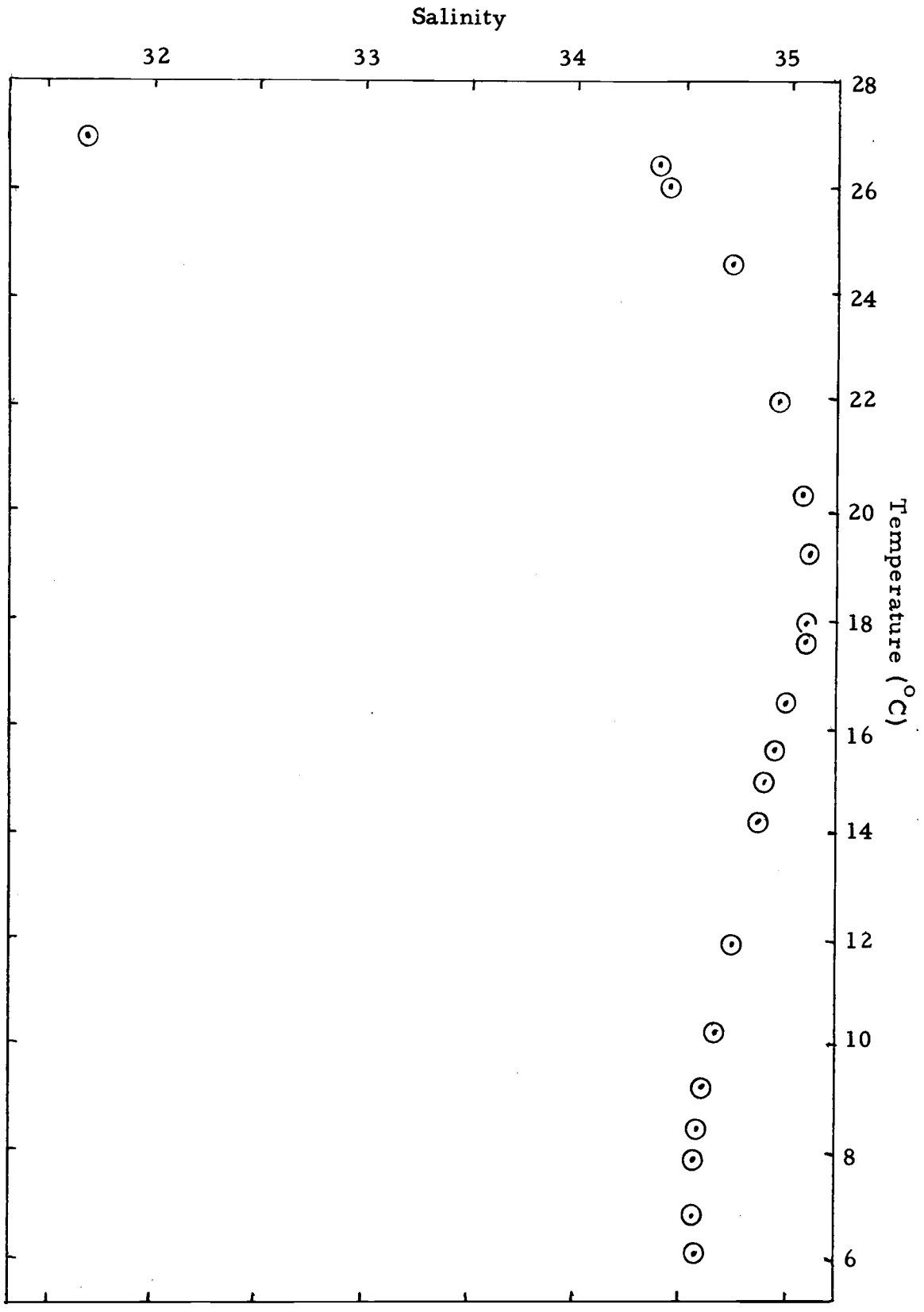

Figure 4. 14. T-S diagrams for YPT-41.

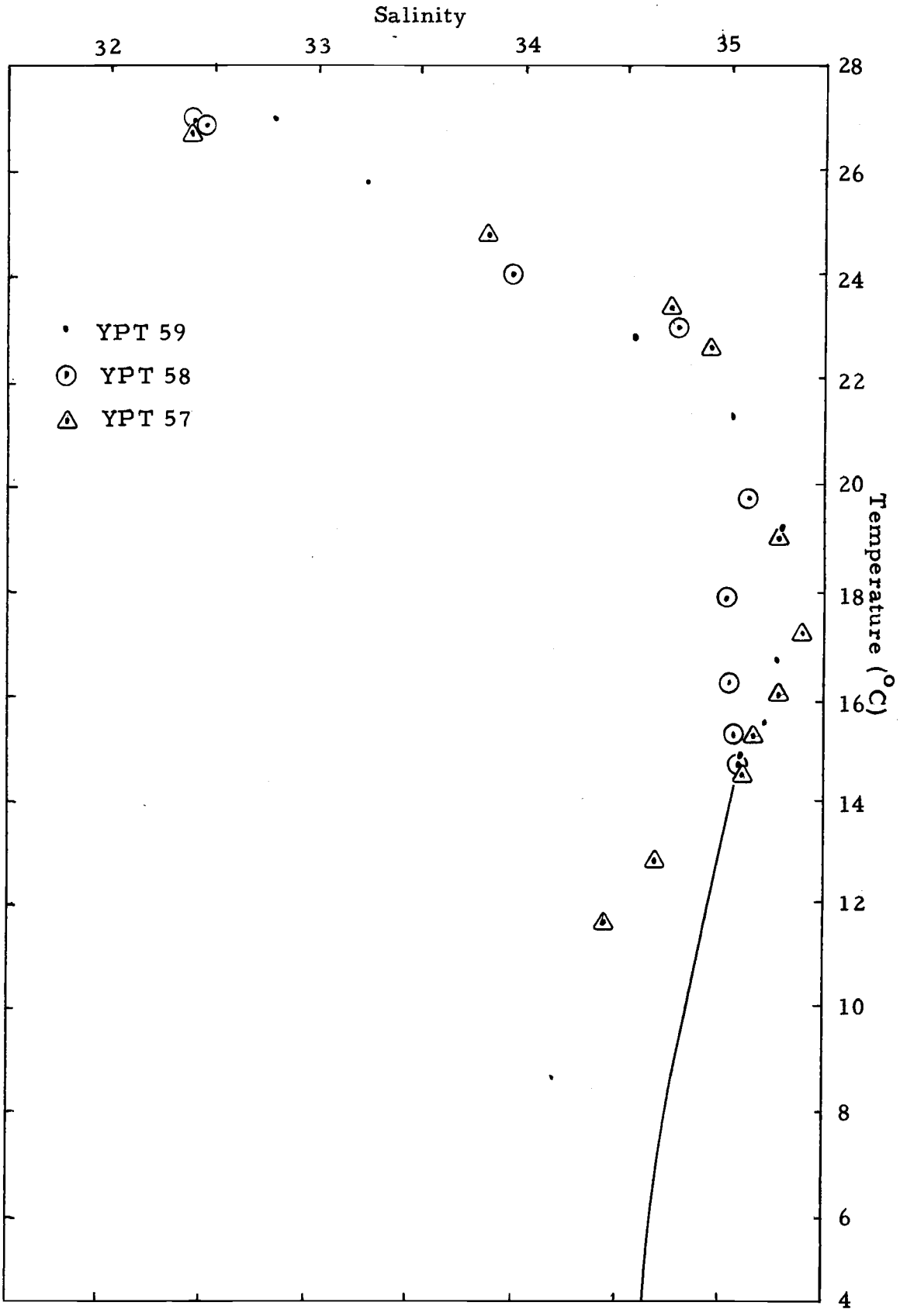

Figure 4.15. T-S diagrams for YPT 57, 58 59.

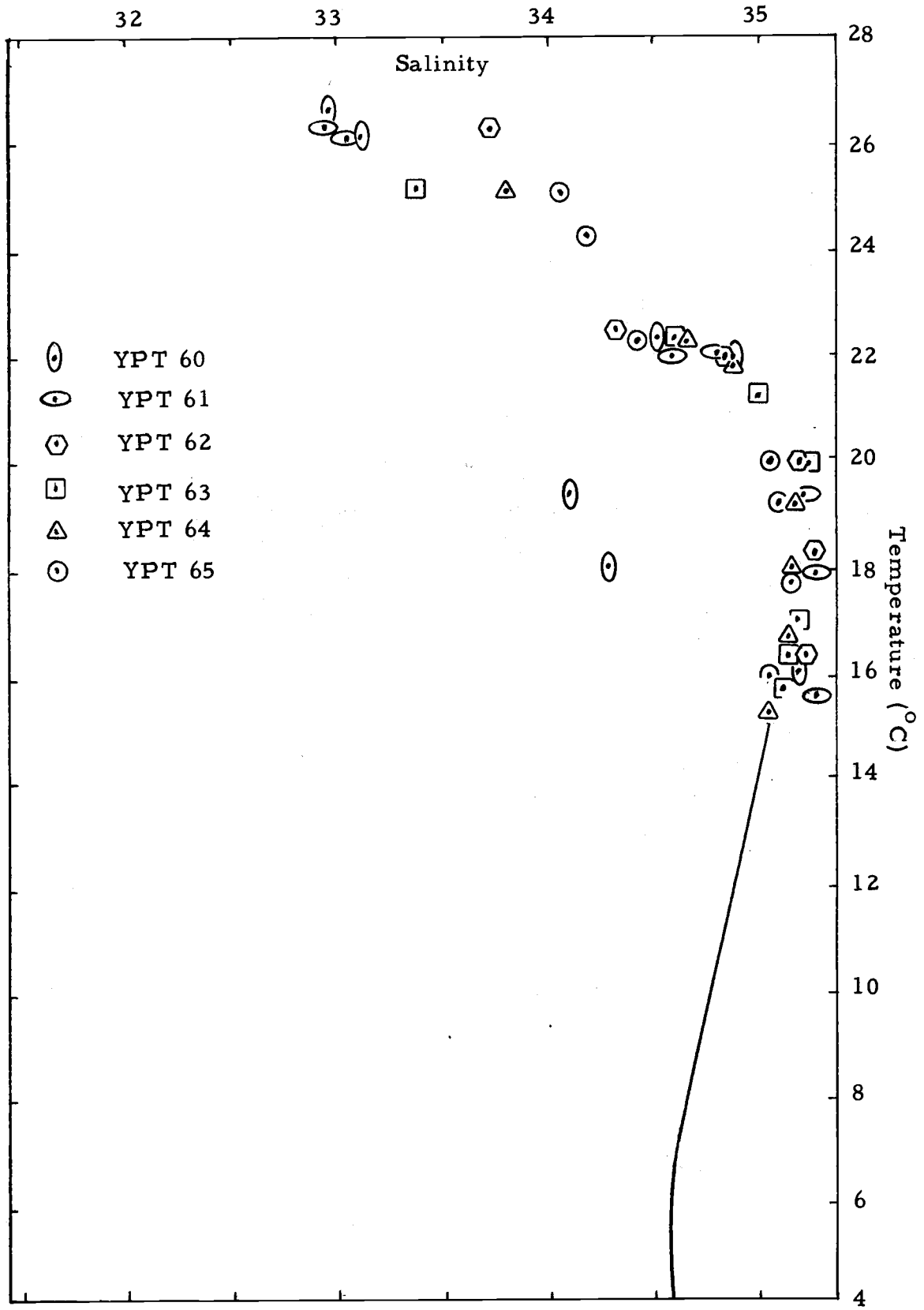

Figure 4.16. T-S diagram for YPT 60, 61, 62 63, 64, 65.

V. DISCUSSION

The apparent homogenity of the shapes of various particle distributions from different water samples is developed in this section. A certain degree of homogeneity in shape has already been demonstrated by the distributions of Figures 4. 3 and 4. 4, where all of the distributions in each figure have the same shape parameter α. It will be shown later that the particle distribution shape of each sample taken on YALOC-69 can be approximated by one of five characteristic shapes. These shape categories are each quite distinct, and only a few samples fail to fall in one of these domains. For easy reference these shapes are defined as Types I, II, III, IV, and V.

Since the particles counted in each water sample on YALOC-69 represent only those of diameter larger than 1. 13 μ, they make up only a part of the complete particle distribution. Consequently, they are represented by conditional or truncated distributions rather than complete distributions. This makes the task of typing or characterizing them much more difficult. The gamma distributions of Figures 4.3 and 4. 4 should actually be conditional distributions of the form.

$$f(x/x > 1.13\mu) = f(x)/[1-F(1.13\mu)], \tag{5.1}$$

where

$$f(x) = (x/\beta)^{\alpha-1} e^{-x/\beta} / \ (\alpha)\beta,$$

and

$$F(1.13\mu) = \int_0^{1.13\mu} f(x)\,dx$$

The problem is to approximate the relative size of $F(1.13\mu)$.

Since no direct measurements of $F(1.13\mu)$ have been taken, its value must be estimated. For this purpose another distribution the Weibull was used (see Appendix C) because of its similarity in shape to that of the gamma and its increased tractability when compared to the gamma.

The Weibull distribution function can be expressed as

(5.2) $$F(x) = 1-e^{-(x/b)^c},$$

where "b" is the scale parameter and "c" is the shape parameter. Since the particle distributions are actually conditional or truncated distributions an effort was made to determine the size of $F(1.13\mu)$ for the various samples. The Weibull distribution is linear on modified extreme value probability paper (see Appendix C). When the abscissa is in natural logarithmic units of the particle diameter, and values of N_i/N or $[1-F(x)]$ are plotted along the ordinate, the slope of the best Weibull fit to the data is a function of the shape parameter. For conditional distributions values of N_i/N_1 as

measured do not include measurements of the small particles. They must be modified by their multiplication with N_i/N. Here N_1 is the number of particles of diameter larger than 1.13μ, and N is the total number of particles in a given sample including those smaller than the detectable size limit of 1.13μ. This is illustrated as follows, where $\hat{F}(D_i)$ is an estimate of $F(x)$.

$$F(x) = 1-e^{-(x/b)^c} ,$$

so

$$1-\hat{F}(D_i) = N_i/N ,$$

and

(5.3) $$\hat{F}(D_i \mid D_i \geq 1.13\mu) = N_i/N_1 .$$

So,

$$(N_i/N_1) \cdot (N_1/N) = N_i/N = 1-\hat{F}(D_i) .$$

Since N is unknown it is determined by a trial and error process discussed in Appendix C.

Figures 5.1 and 5.2 show the best Weibull fit for YPT-64, 100m, a distribution with one of the highest shape parameters (c = 1.9) encountered on YALOC-69. The shape parameters for Figures 5.1 and 5.2 range from 0.85 to 1.08 and from 0.75 to 0.95 respectively. These ranges are used to define Types I and II. A distribution characterized by a Type I distribution must have a

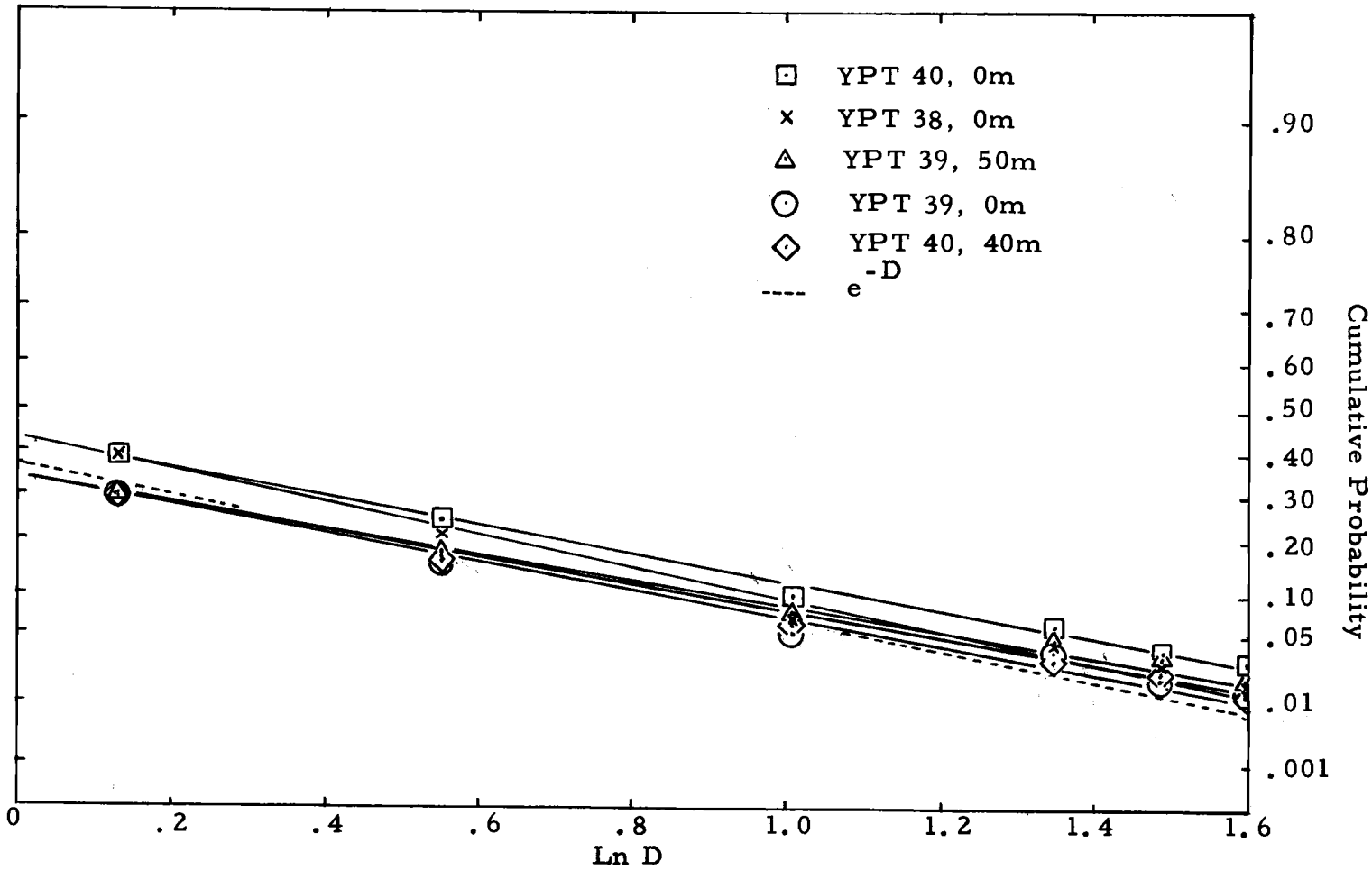

Figure 5.1. Weibull fit on extreme value paper for stations in region R_1.

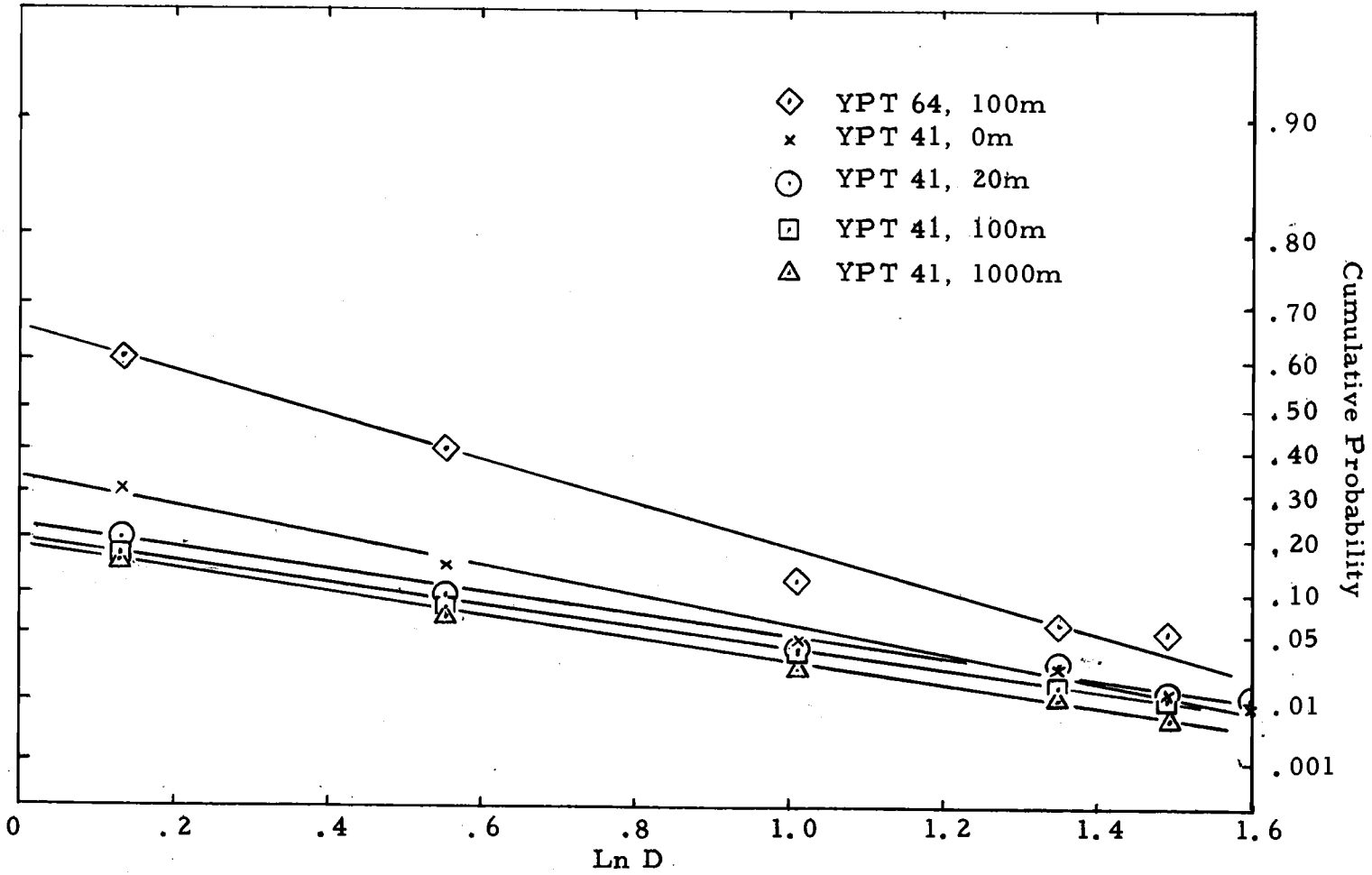

Figure 5.2. Weibull fit on extreme value paper for stations in region R_2.

shape parameter of about 1.0. One characterized by a Type II distribution must have a shape parameter of about 0.8. The curve of YPT-64, 100m typifies a distribution of Type V with the high valued shape parameter of about 1.9. The degree of difficulty involved in characterizing distributional curves in this manner dictated the necessity of finding a faster method. An optical technique was developed and is discussed later, at which time all of the particle distibutions are characterized.

The probabilities of at $x = 1.13$ or $\ln x = 0.122$ of Figures 5.1 and 5.2 represent that percentage of particles smaller than 1.13μ in diameter, assuming that these small particles also are Weibull in distribution. This assumption is, of course, ridiculous when molecular sizes are approached. On the other hand, if the uses to which the sample distribution characteristics are put involves only a small error, it would seem better to use the truncated or conditional distribution characteristics than to "correct" the data using assumptions that cannot be verified as in this case. The estimate of this error again involves some assumptions but a conservative estimate of this error can be made. For relative measurements, this error is in most cases greatly reduced. Since for optical applications the distributional second moment is of the greatest importance, as in the E.O.A., the small particle effect becomes less of a problem. Equation 2.12 showed that for an

exponential distribution with scale parameters of 2 and 1, the errors of truncation for the E. O. A. are respectively 4% and 8%. Due to distribution similarities, the relative errors between two different E. O. A.'s would be considerably smaller, so no "corrections" on the sample characteristics were made. From now on, when compared with optical measurements, the particle sample characteristics are used as if they were determined from a complete particle distribution. But, it must be borne in mind that they by themselves are truly conditional distribution sample statistics.

Since the particle distributions are well fit by the Weibull distribution function, and it is a two-parameter distribution, the first and second moments or estimates ($\overline{D}$ and $\overline{S}$) of these uniquely determine the basic shapes and scales of the particle distributions. Henceforth, they are used to identify the similarities and differences of the particle distributions.

Now, having discussed the distributions of particle sizes in the various regions of the ocean covered by YALOC-69, we turn our attention to the optical outputs due to the scattering of light by these particles.

Table 4. 2 lists the measured values of the volume scattering function at the angles 45° and 135°. It also lists the ratio of these two, called R. These are compared below with various particle distribution characteristics as outlined by Question 3 found

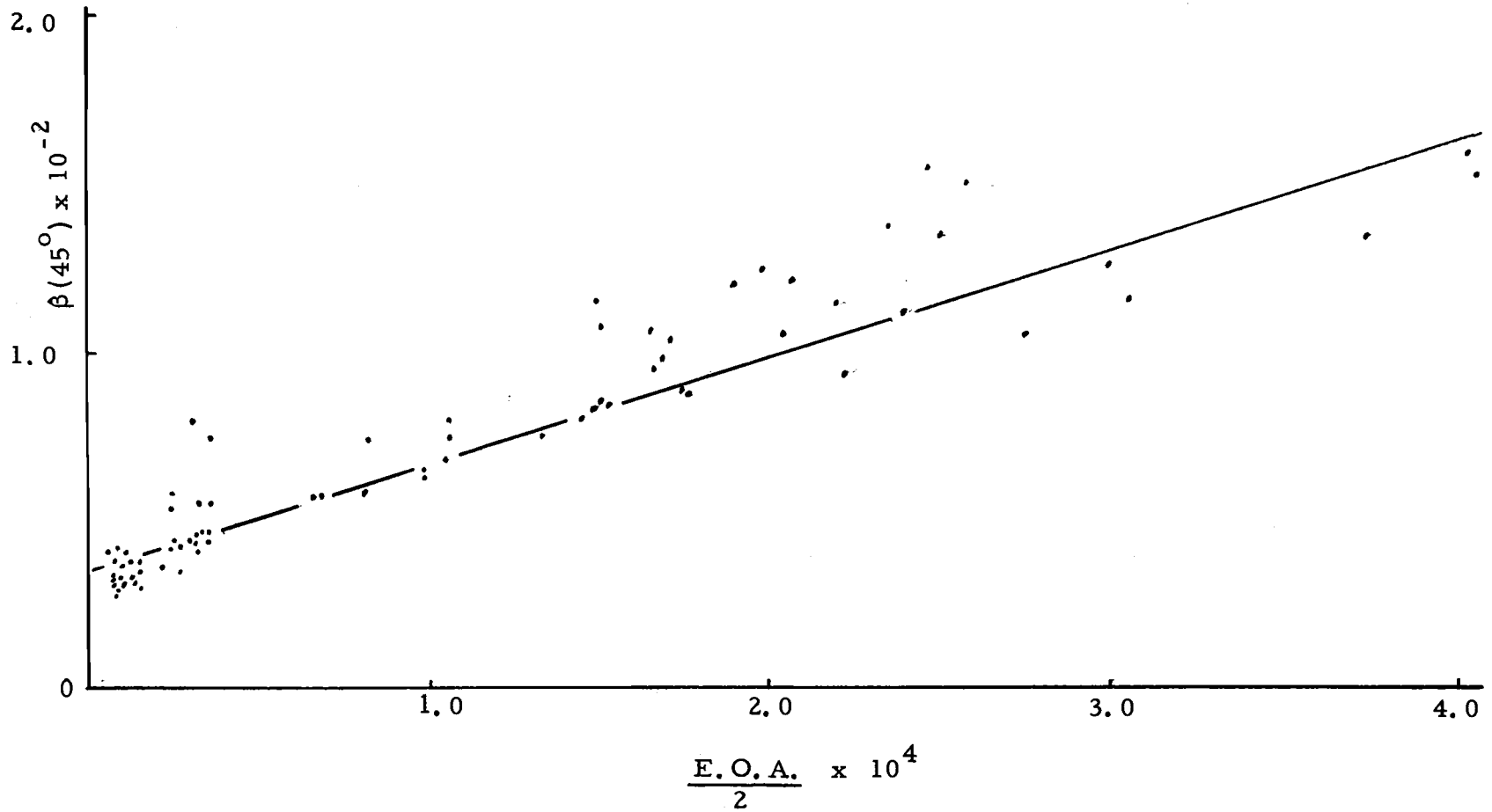

Figure 5.3. $\beta(45^{\circ})$ vs. the effective optical area for stations YPT 34 through YPT 69.

in the Introduction.

Figure 5.3 indicates the strong correlation between the volume scattering function at 45^{o} and the E.O.A./2 or the total particulate surface area/π, as expected in view of Equation 2.19. The scatter of these points could be due to small differences in the particulate indices of refraction, distributional differences and instrumental sampling variances. The distributional variations would not theoretically manifest themselves in an error if there were no small particle truncation assuming that the effective area coefficient K were 2. But, the truncation error varies with distributional changes as does K, so this is a possible cause for some of the correlative scatter.

According to Equation 2.19, the line on Figure 5.3 should pass through the origin. Instead, $\beta(45^{o})$ has a value of about $o.3x10^{-2}/m$ for an E.O.A. of zero. The prime factor contributing to this displacement is believed to be the small particle truncation. The particles smaller than 1.13μ are not counted by the Coulter Counter, but do scatter light. This gives $\beta(45^{o})$ an optical threshold only above which a comparison with the E.O.A. is made.

Since $\beta(45^{o})$ is a function of the total particulate surface area it is dependent upon both the number and size of the particles. It could also be expressed as a function of the total number N of

of particles, the mean surface area $\overline{S}$, and a distributional factor g(x) where x represents the particle diameters:

$$\beta(45^{o}) = g(x)\, N\, \overline{S} \tag{5.4}$$

If the distributional shapes vary little from sample to sample, g(x) would be constant. The question that remains is whether either N or $\overline{S}$ is dominant in their determination of $\beta(45^{o})$. Offhand, N would appear to be the more important factor since its range (150 to 6127 for N_5) is much wider than is that ($3.64\mu^2$ to $12\mu^2$) of $\overline{S}$. This assumption is verified by the scatter diagrams of Figure 5.4 in which $\beta(45^{o})$ is plotted separately against both N_5 and $\overline{S}$. Here N_5 is the better correlated of the two with $\beta(45^{o})$, but neither could be considered to be a dominant enough factor to allow the neglection of the effects of the other. The distributional factor g(x) becomes most important when distributional types are changed in going from sample to sample. These all play important roles in explaining the variations in $\beta(45^{o})$ when contouring or profiling the values of this parameter, so one cannot simply equate relative values of $\beta(45^{o})$ with those of the total number of particles or concentration of particles in a water sample as has been implied in the past. These factors are examined again at the end of this section.

In order to determine some of the relationships among the scattering ratio $\beta(45^{o})/\beta(135^{o})$, $\overline{D}$, and $\overline{S}/\overline{D}$, Figures 5.5 and 5.6

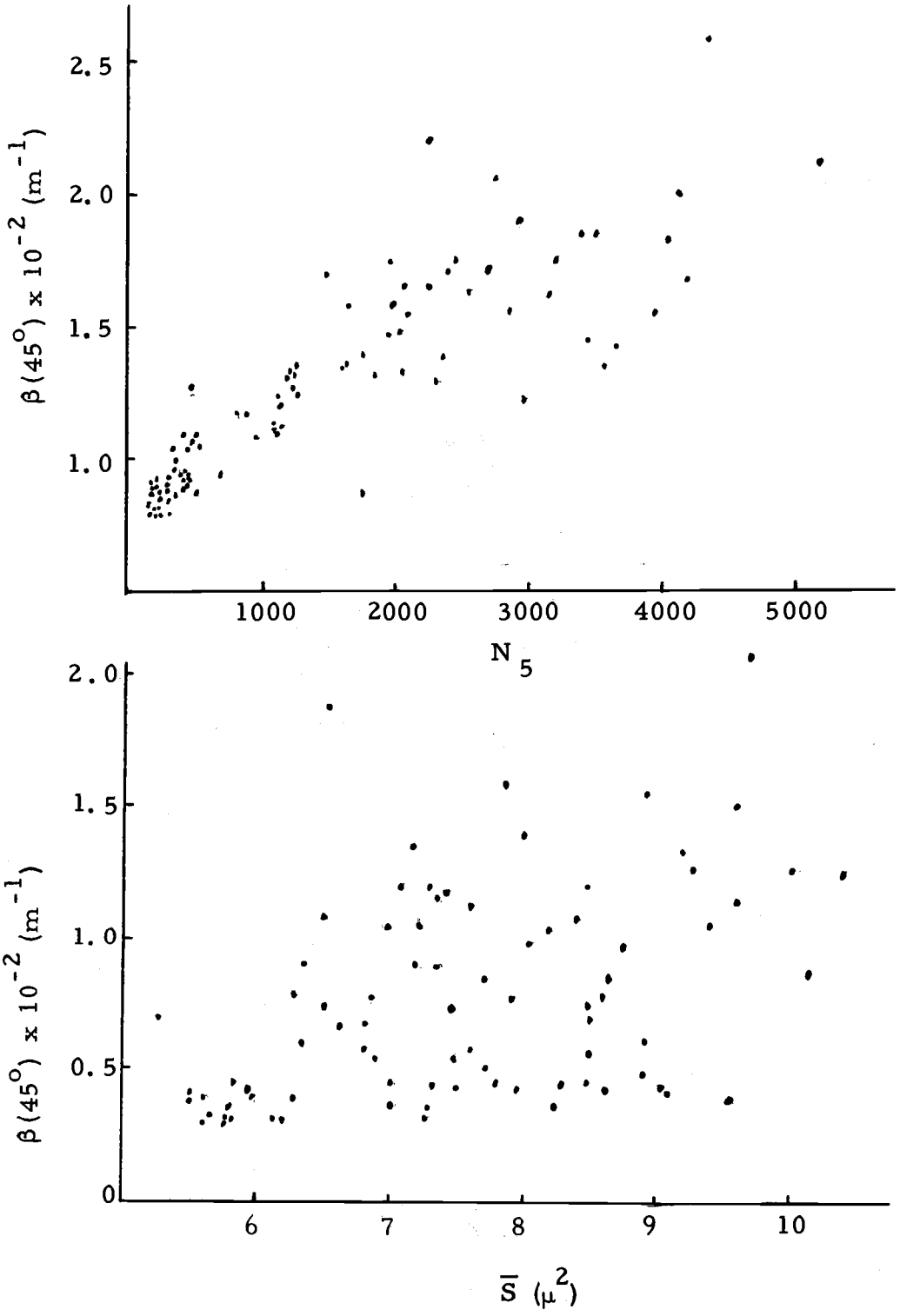

Figure 5.4. Scatter diagrams for $\beta(45^{\circ})$ versus N_5 and $\bar{S}$.

were drawn. Each figure shows generally linear relationships among these variables, which seem to vary with the distributional type. This was first noticed when $\overline{D}$ was plotted against the optical ratio for these types. So for distributions of Types I and II, the conditional mean particle sizes can be determined from the following equations respectively:

(5.5) $$\overline{D} = 1.804 + (0.1902)\,\beta(45^{\circ})/\beta(135^{\circ})$$

for Type I, and

(5.6) $$\overline{D} = 2.074 + 0.0585\,\beta(45^{\circ})/\beta(135^{\circ})$$

for Type II. Distributions of Type II have a fairly small range of mean diameters, while those of Type I have a larger range.

What causes the general linearity of Figure 5.5? This question can be partially answered by writing a general linear equation relating the scattering ratio, $\overline{S}/\overline{D}$, and $\overline{D}$:

(5.7) $$\beta(45^{\circ})/\beta(135^{\circ}) = K_1\overline{S}/\overline{D} + C_1 = K_2\overline{D} + C_2,$$

where K_1, K_2, C_1 and C_2 are linear coefficients. The expressions for the first and second moments of the gamma distribution are respectively $\alpha\beta$ and $(\alpha+1)\beta^2$. Substituting these moments for $\beta(45^{\circ})$ and $\beta(135^{\circ})$ in Equation 5.7, we have

(5.8) $$\alpha(\alpha+1)\beta^2/\alpha\beta = K_2\overline{D} + C_2$$

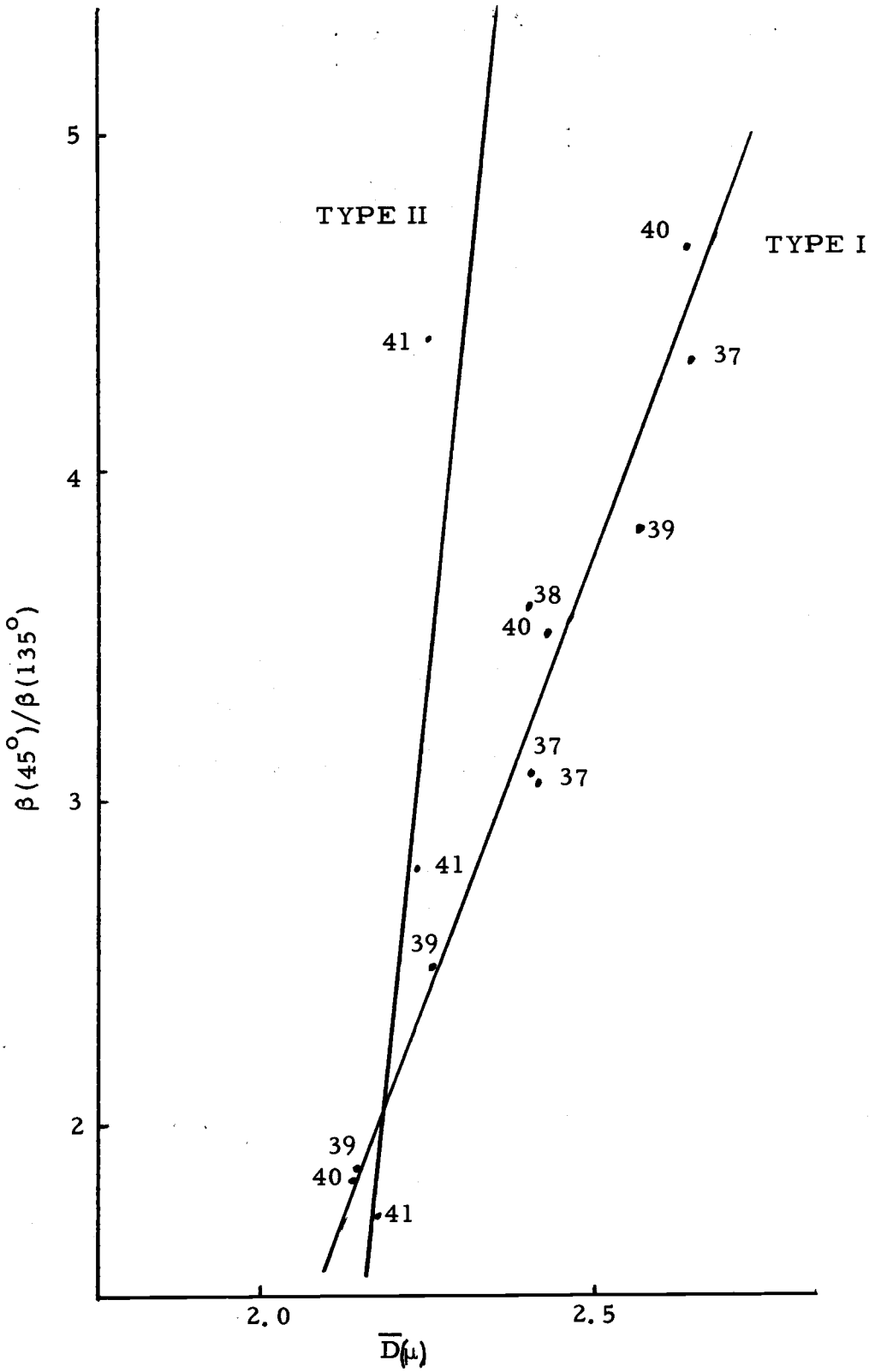

Figure 5.5. Mean diameter versus scattering ratio for distributions of Type I and Type II.

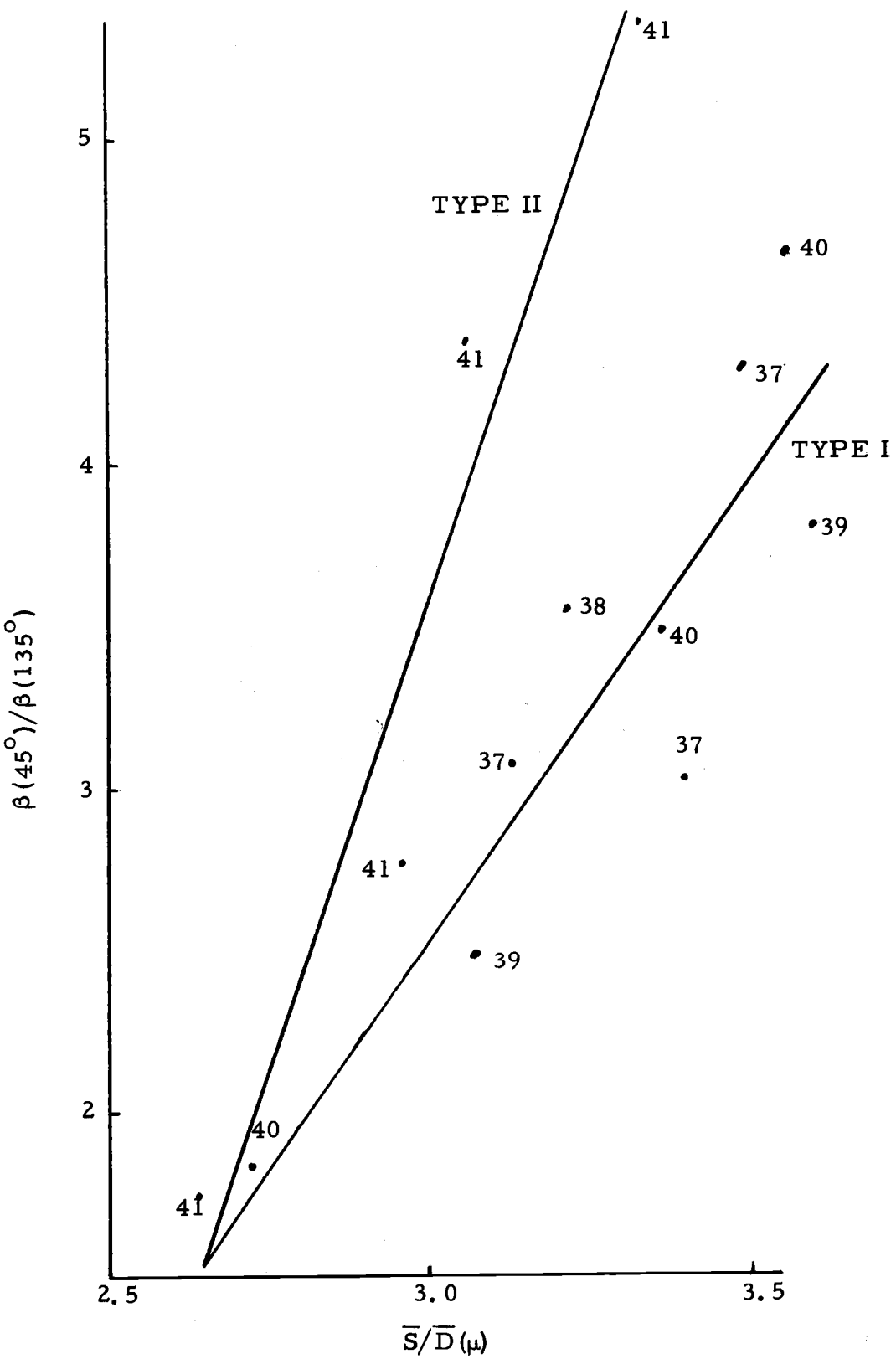

Figure 5.6. Scattering ratio versus moment ratio for distribution of TYPE I and TYPE II.

or

$$(\alpha + 1)\beta = K_2 \overline{D} + C_2 \tag{5.9}$$

For a constant shape parameter α, the scattering ratio is a linear function of $\overline{D}$. Intuitively the lines of Figure 5.5 would pass through the origin if particle truncation effects and instrumental intercalibration errors were not present. If this were the case, Equation 5.8 could be written as

$$(\alpha + 1)\beta^2/\alpha\beta = K_3 \alpha\beta,$$

or

$$K_3 = \frac{\alpha + 1}{\alpha} \tag{5.10}$$

In this case the slope K_3 is a function soley of the shape parameter. This means that the distributional shape is a very significant factor in the determination of the slopes in Figure 5.5, even though $\overline{D}$ includes small particle truncation effects. So, a homogeneity of shape parameters among various samples implies that their respective plots of the scattering ratio versus the mean diameter will for a linear graph, whose slope is highly dependent upon the value of the common shape parameter.

Since the second moment of a particle size distribution is less affected by small particle truncation than is the first moment, $(\overline{S})^{1/2}$ is less affected than is $\overline{D}$. For this reason $(\overline{S})^{1/2}$ is compared instead of $\overline{D}$ with the scattering ratio R. Figure 5.7 through 5.11 contain data from stations YPT-37 through YPT-68. Each of these lines has a different slope, and each slope is quite distinct. For this reason the stations and depths of the samples making up each of these lines of homogeneity are considered to be a separate group when referring to their common distributional shape. The sample points then are considered to be in one of the five regions of homogeneity of distributional shape defined by the five lines of Figure 5.7 through 5.11. These lines are used to define distributional Types I, II, III, IV, and V. A comparison of Figures 5.1 and 5.2 with Figures 5.7 and 5.8 indicates that an increase in the Weibull shape parameter corresponds to an increase in the linear slope of the $(\overline{S})^{1/2}$ vs. R relationship.

The generally linear grouping of the above five curves resulting from the homogeneity of the distributional shape parameters of each, suggests that a search be made for the cause or causes of these homogeneities. The first approach to answering this question was to investigate the water types involved by this T-S (temperature-salinity) diagrams. These are shown in Figures 4.13 through 4.17. The curves for distributional Types I and II of Figures 4.14 and 4.15 are practically identical below the

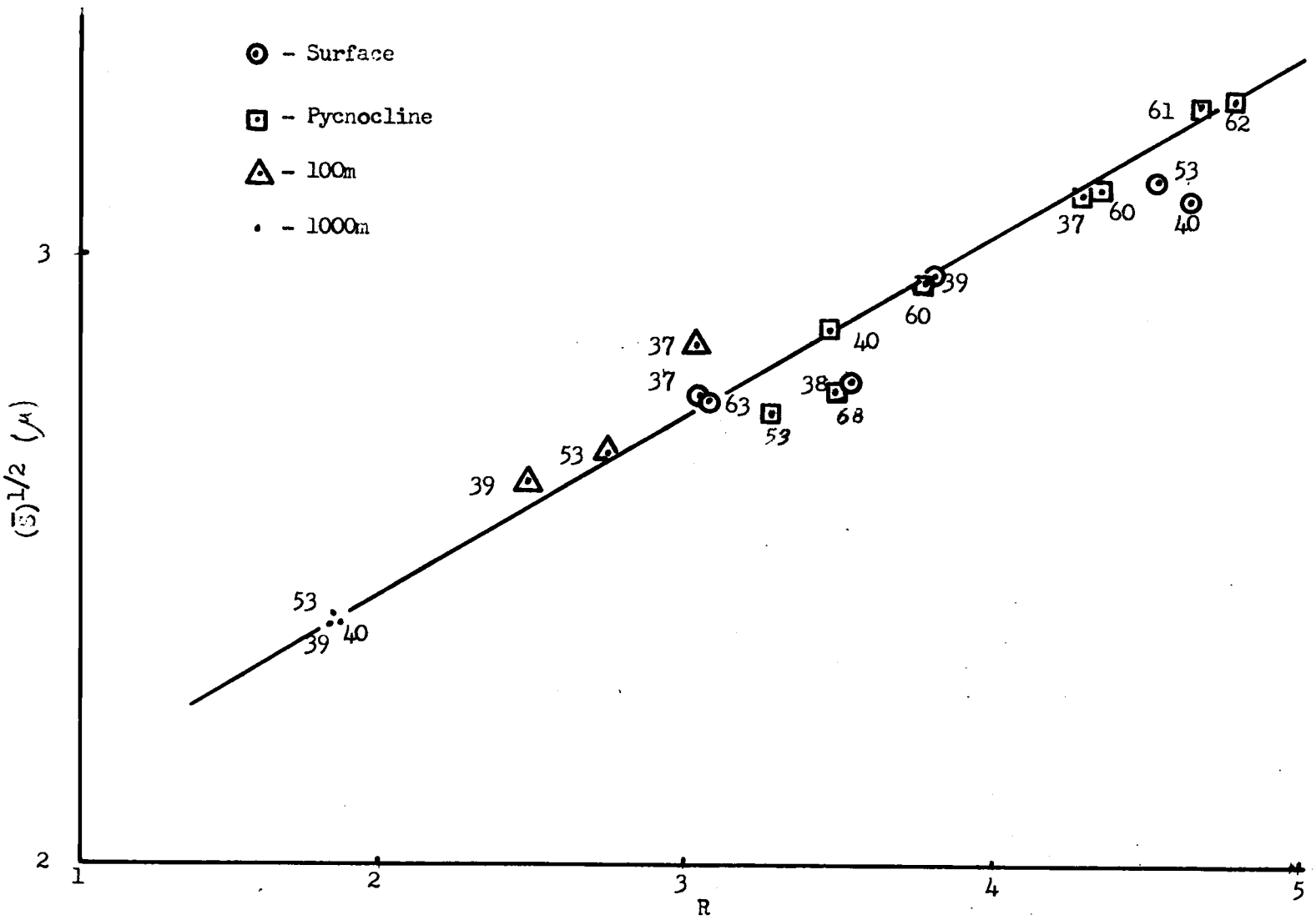

Figure 5.7. $(\bar{S})^{1/2}$ vs. the scattering ratio defining distributional Type I.

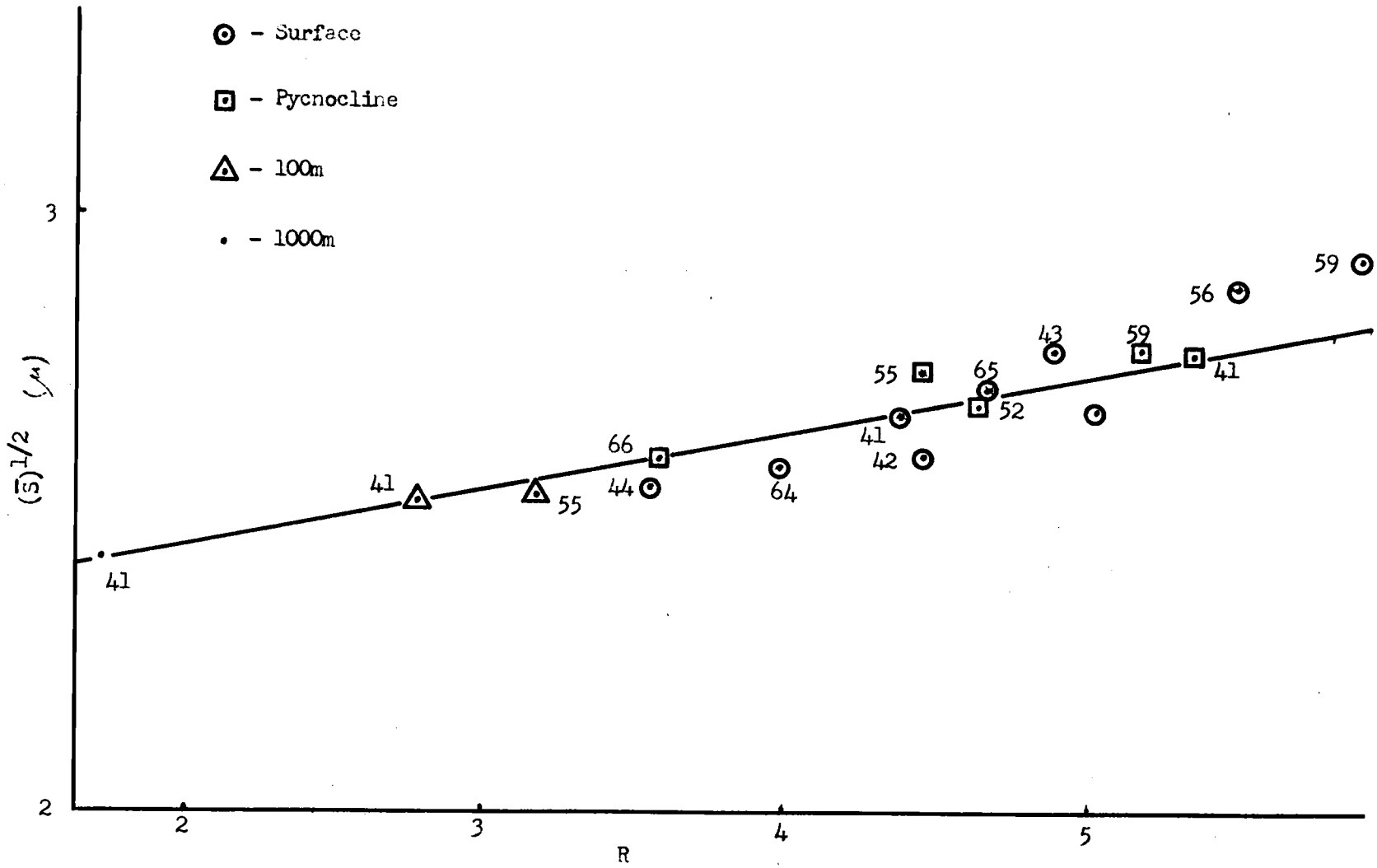

Figure 5.8. $(\overline{S})^{1/2}$ vs. the scattering ratio defining distributional Type II.

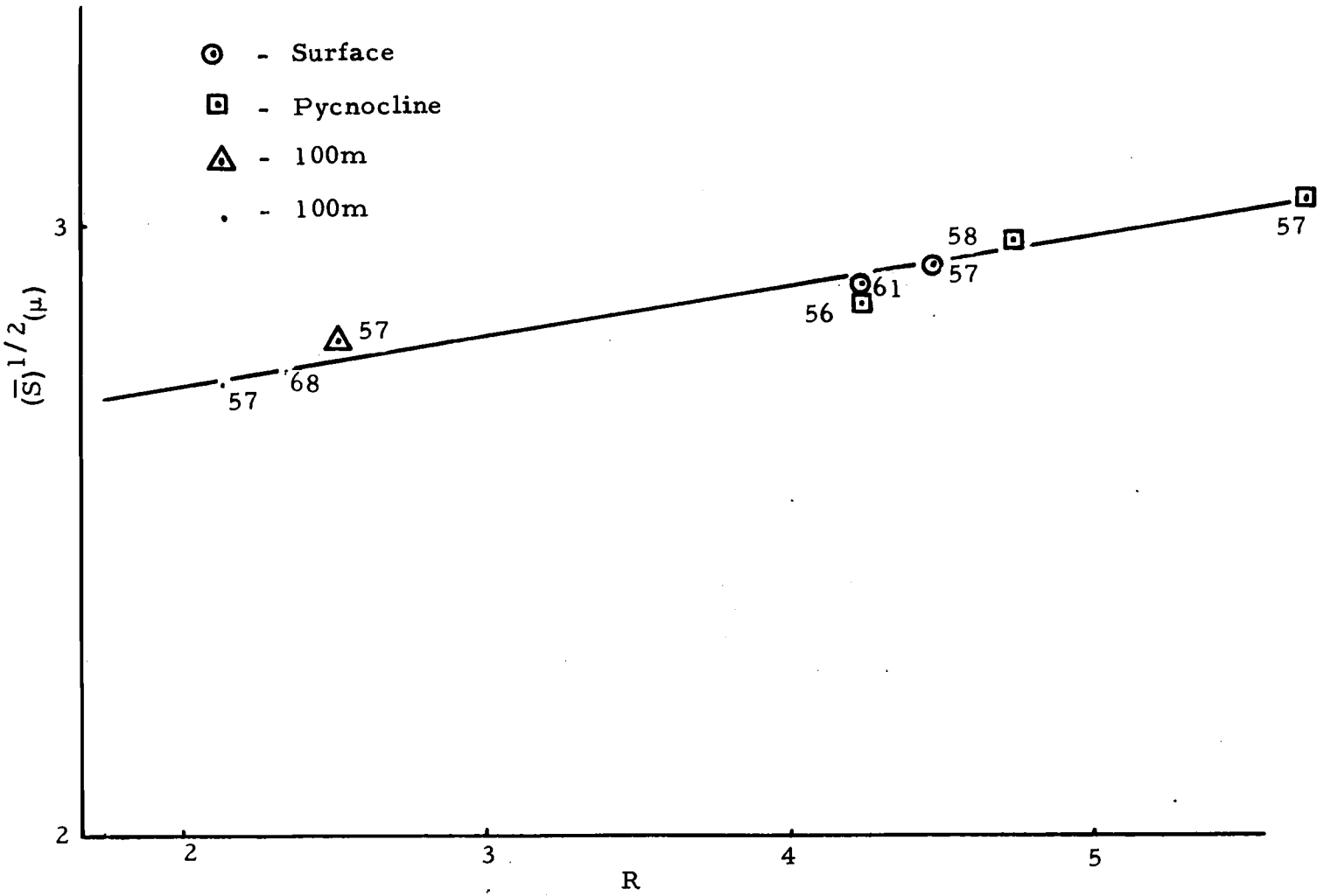

Figure 5.9. $(\bar{S})^{1/2}$ vs. the scattering ratio defining distributional Type II.

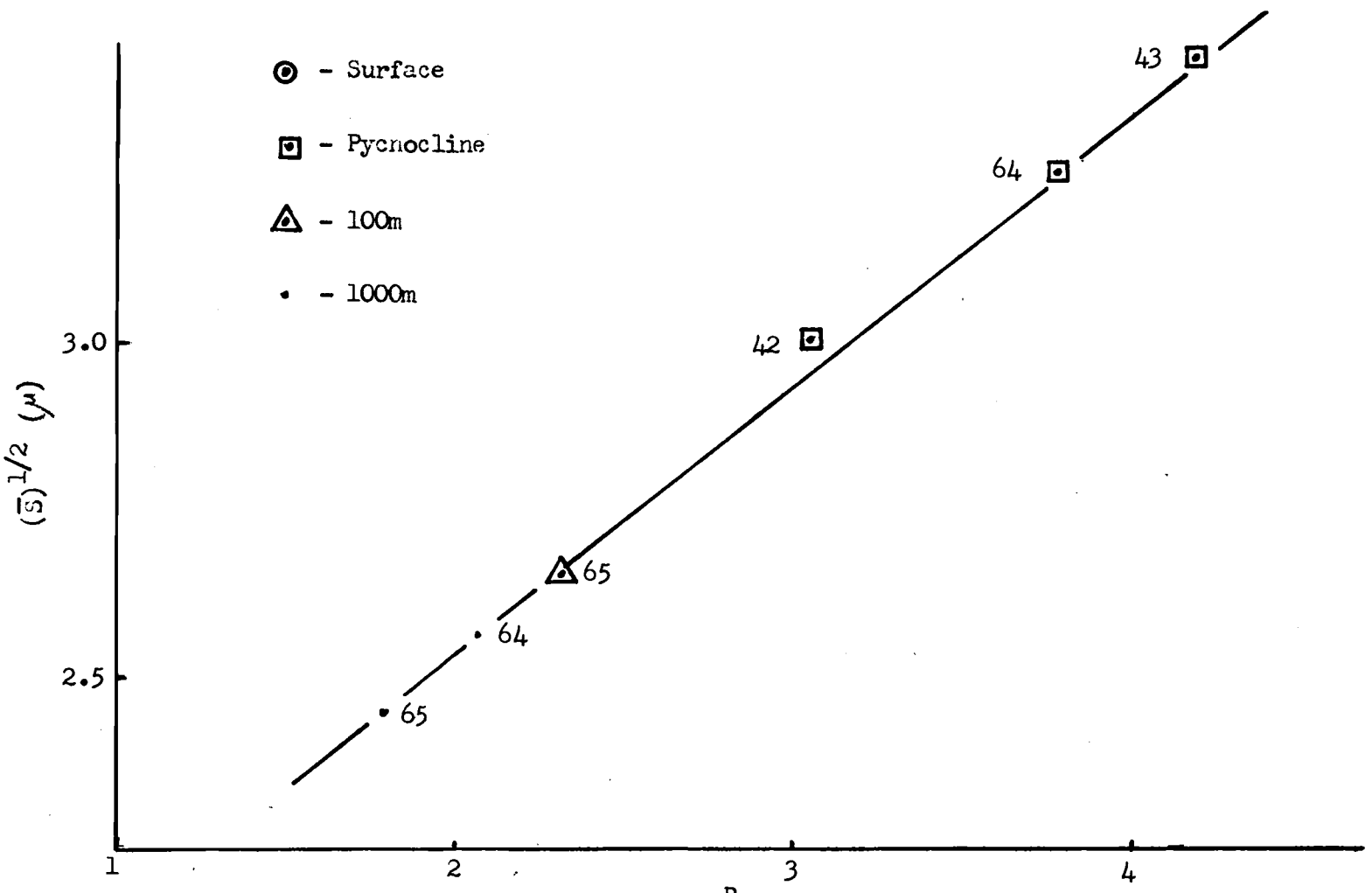

Figure 5.10. $(\bar{S})^{1/2}$ vs. the scattering ratio defining distributional Type IV.

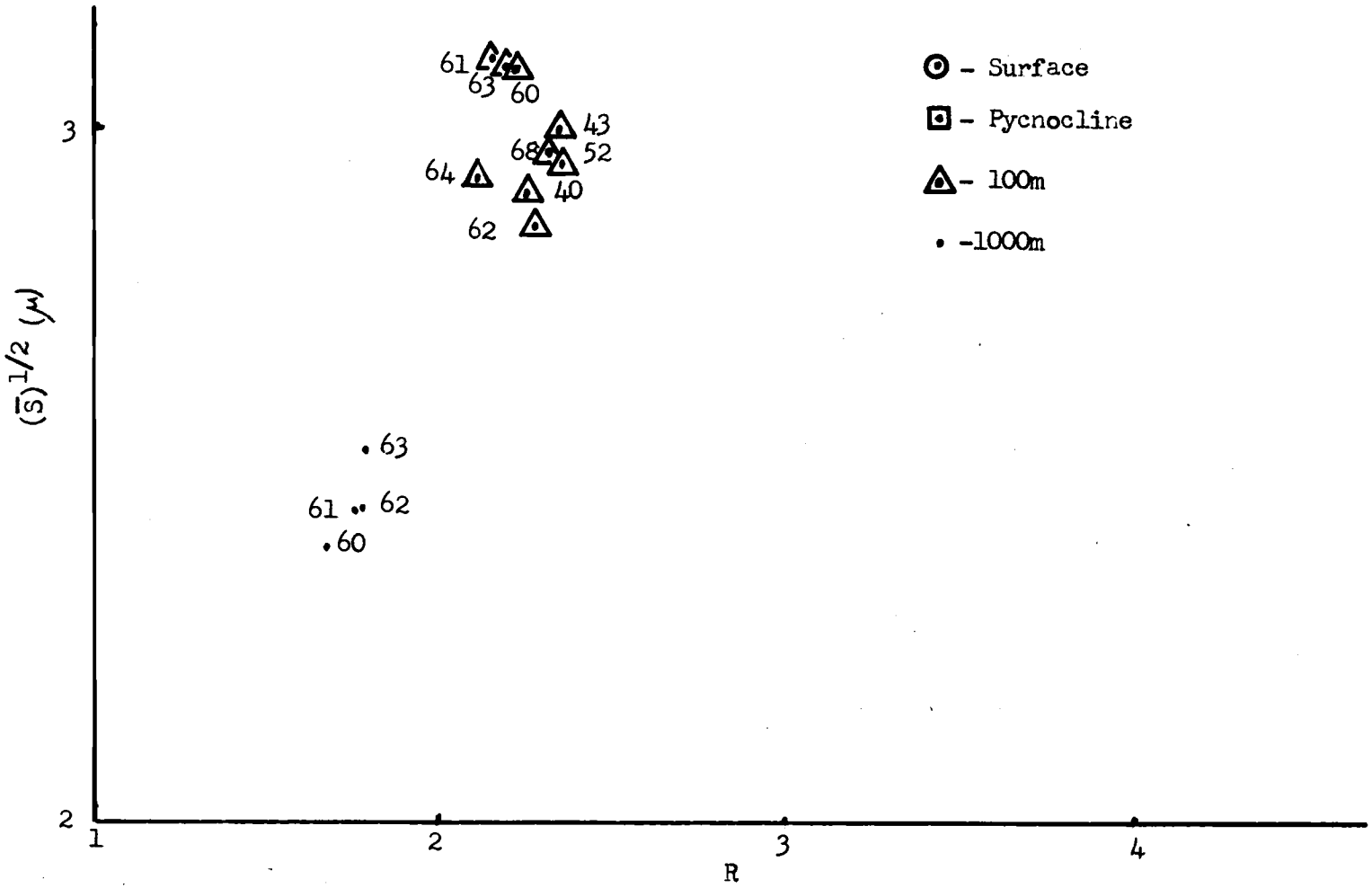

Figure 5.11. $(\bar{S})^{1/2}$ vs. the scattering ratio defining distributional Type V.

pycnoclines. Above the pycnoclines even the curves within Figure 4.14 are not homogeneous. This implies that there is no direct cause and effect relationship between water types and the shapes of particle size distributions; i.e. homogeneity of water type does not imply homogeneity of distributional shapes, and vice-versa. This is further emphasized by Table 5.1, which lists the distributions of YALOC-69 according to particle type.

Table 5.1 demonstrates the fact that the distribution types are quite mixed along the cruise track. Stations in the same geographical region sometimes have an intermixture of many different distribution types, while identical distribution types can be found hundreds of miles apart. Due to the possibility of a sudden change in distribution type from station to station or even with depth at a single station, optical oceanographers should take heed in contouring values of $\beta(45^{o})$ or other optical parameters.

Another possible cause for the homogeneity of the distribution shape parameters within given regions might be the particle sources dominant in each. In the equatorial waters far from land biological reproduction is probably the dominant particle source especially in the upwelling areas. Hence, within a location having a fairly uniform distribution of phytoplankton species, one might expect similar indices of refraction and shapes of particle distributions. Now, if currents carried these species and subsequent particle distributions away

Table 5.1. The particle distribution types encountered on YALOC 69.

Stations	37	38	39	40	41	42	43	44	46	50	52	53
Surface	I	I	I	I	II	II	II	II	bad	none	II	I
Pycnocline	I	I	I	I	II	IV	IV	II			II	I
100 m.	I		I	V	II	shallow	V	II			V	I
1000 m.			I	I	II	shallow	shallow	shallow			V	I

Stations	55	56	57	58	59	60	61	62	63	64	65	66
Surface	II	II	III	II	II	I	III	II	I	II	II	
Pycnocline	II	III	III	III	II	I	I	I	V	IV	II	II
100 m.	II		III or IV		I	V	V	V	V	V	IV	
1000 m.			III or IV		V	V	V	V	V	IV	IV	

Stations	67	68	69
Surface		II	
Pycnodine		I	
100 m.		V	
1000 m.		III	

from the source regions, certain fractions of the original characteristics would remain. Assuming that the sources were not too far away temporally, currents of differing origin would appear individually unique in particle content upon comparison.

Figure 5. 12 shows the temperature profile for the north-south transit of the equator from station YPT-34 to station YPT-43 and Figure 5. 13 is a current map (after Wyrtki, 1965) of the Galapagos region for the month of January. The isolines of Figure 5. 12 suggest the separation of the South Equatorial Pacific Current into two parts at station YPT-41 due to equatorial upwelling. Defant (1961) treated this circulation phenomenon in his chapter on tropospheric circulation and a hypothesis of current separation at YPT-41 seems consistent with the explanation of Defant and with the current patterns of Figure 5. 13. It shows the northern branch as having a Panama Basin origin, while the southern half has an extended Peruvian Current origin. If this is the case, the particle distribution characteristics of the northern branch could be expected to differ from those of the southern branch. This might explain the particle distribution differences that do exist between the stations YPT-38-40 of Type I and YPT-41 of Type II. Therefore, the hypothesis is made that the optical and particle distributional differences occurring between these two regions and Types result from a difference in current origin, assuming that the particle characteristics

Figure 5.12. Temperature contours with depth along the equatorial transit.

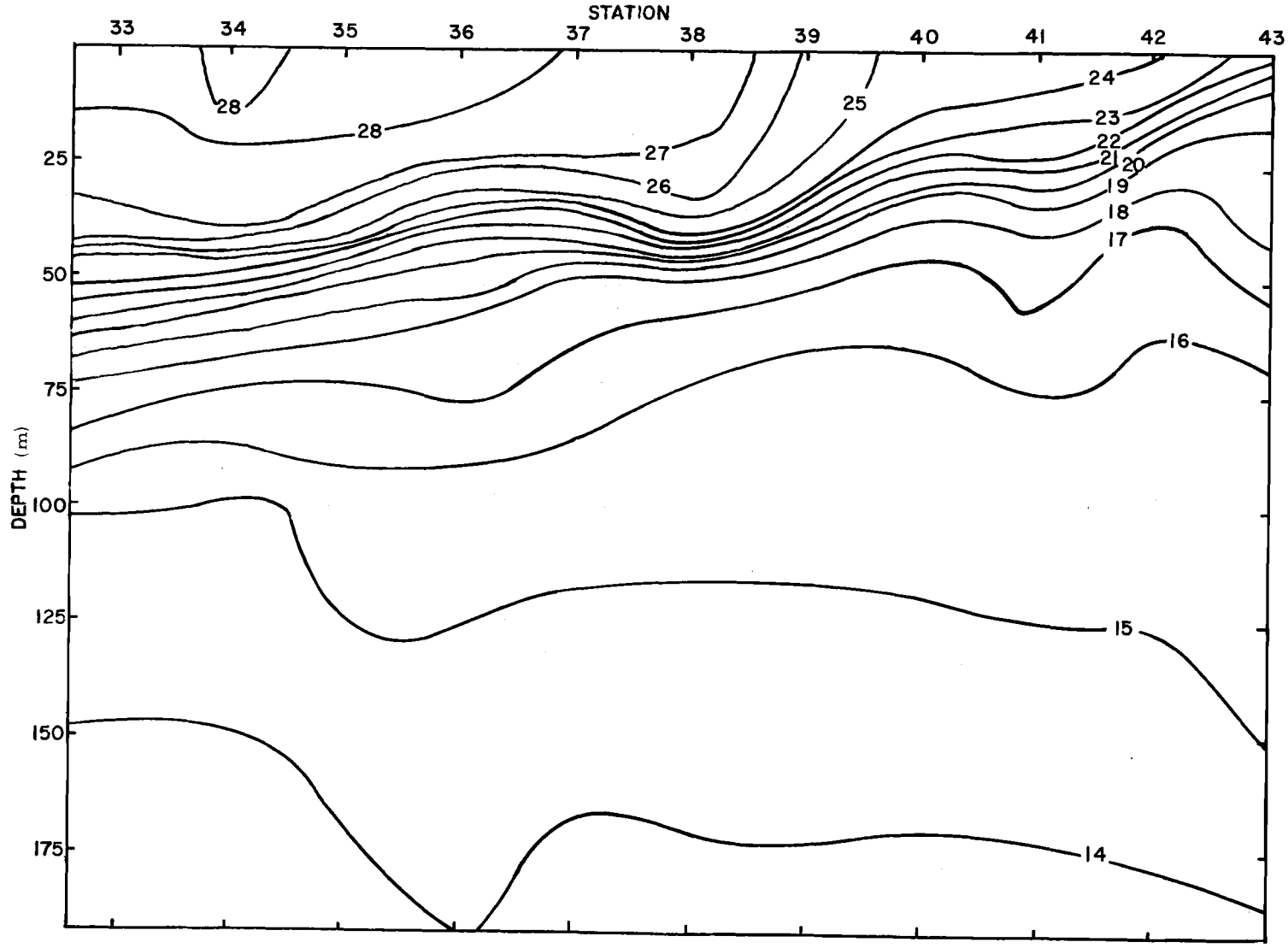
STATION
33
34
35
36
37
38
39
40
41
42
43
DEPTH (m)
25
50
75
100
125
150
175
28
28
27
26
25
24
23
22
21
20
19
18
17
16
15
14

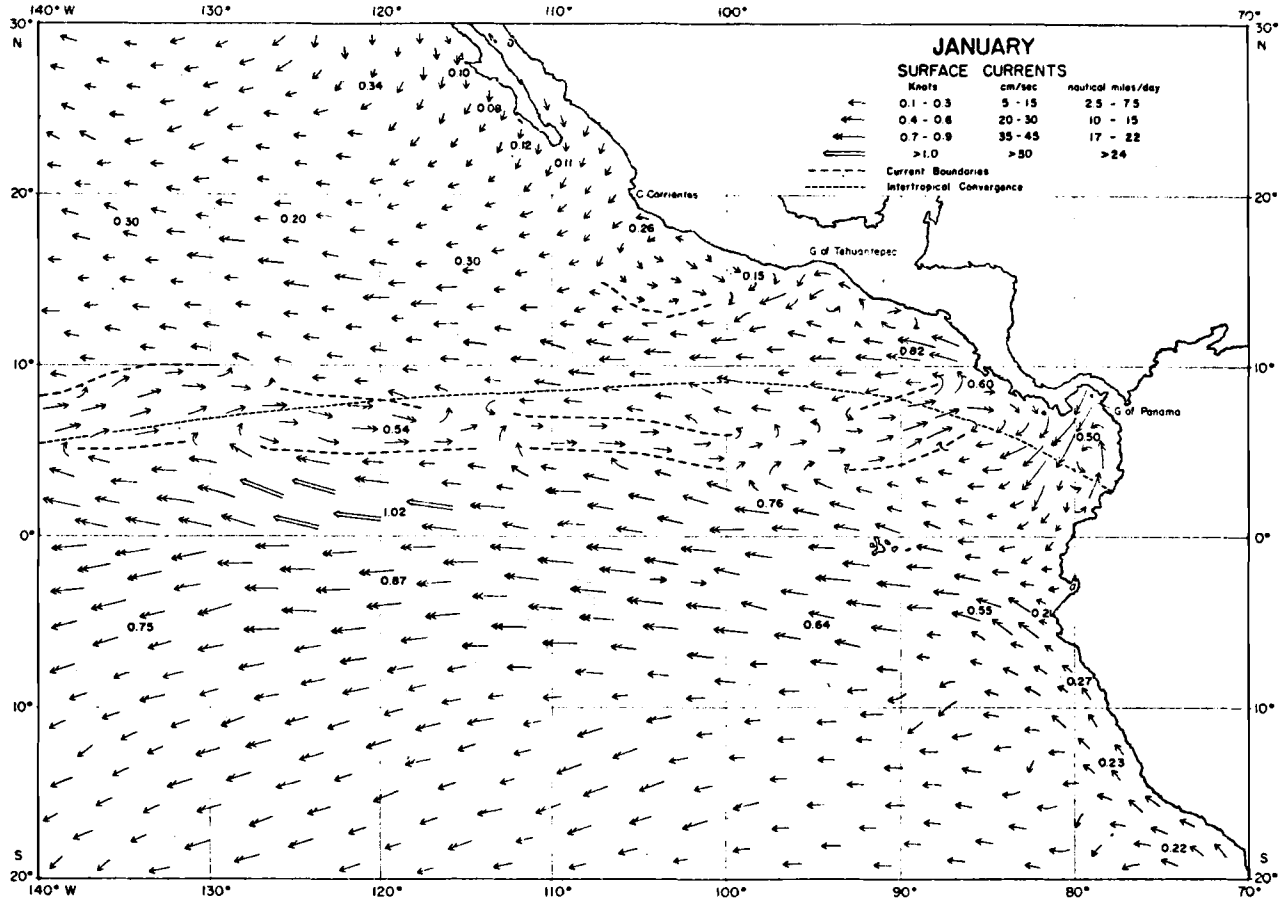

Figure 5.13. Monthly charts of the surface circulation of the Eastern Tropical Pacific Ocean (from Wyrtki, 1965, page 279).

of each source region are unique.

Since on YALOC-69 no particle distribution work was undertaken in the hypothesized particle source regions of the Panama basin and the Peruvian Current, no conclusions can be drawn at this time about the validity of this hypothesis. It would be an interesting problem to pursue on future Galopagos cruises as well as the determination of the optical and particulate characteristics of the Cromwell Current. The tracing of such currents by a distinguishable characteristic indicative of the current source region would be very important in those instances where the salinity, temperature, and oxygen contents of the current are similar to those of the surrounding waters, as is the case with the Cromwell undercurrent in the Galapagos region.

It is of interest to investigators in the field of hydrological optics to know the level of confidence that can be placed upon the agreement between the relative trends (increase or decrease) of certain optical parameters and particle sample characteristics.

Figure 5. 14 shows the excellent trend agreement (an increase in $\overline{D}$ accompanies an increase in $\overline{S}$ and etc.) between $\overline{S}$ and $\overline{D}$. The magnitudes of these trends differ in general, but an increase or decrease in the mean particle diameter is usually matched by an increase or decrease in the mean particle surface area.

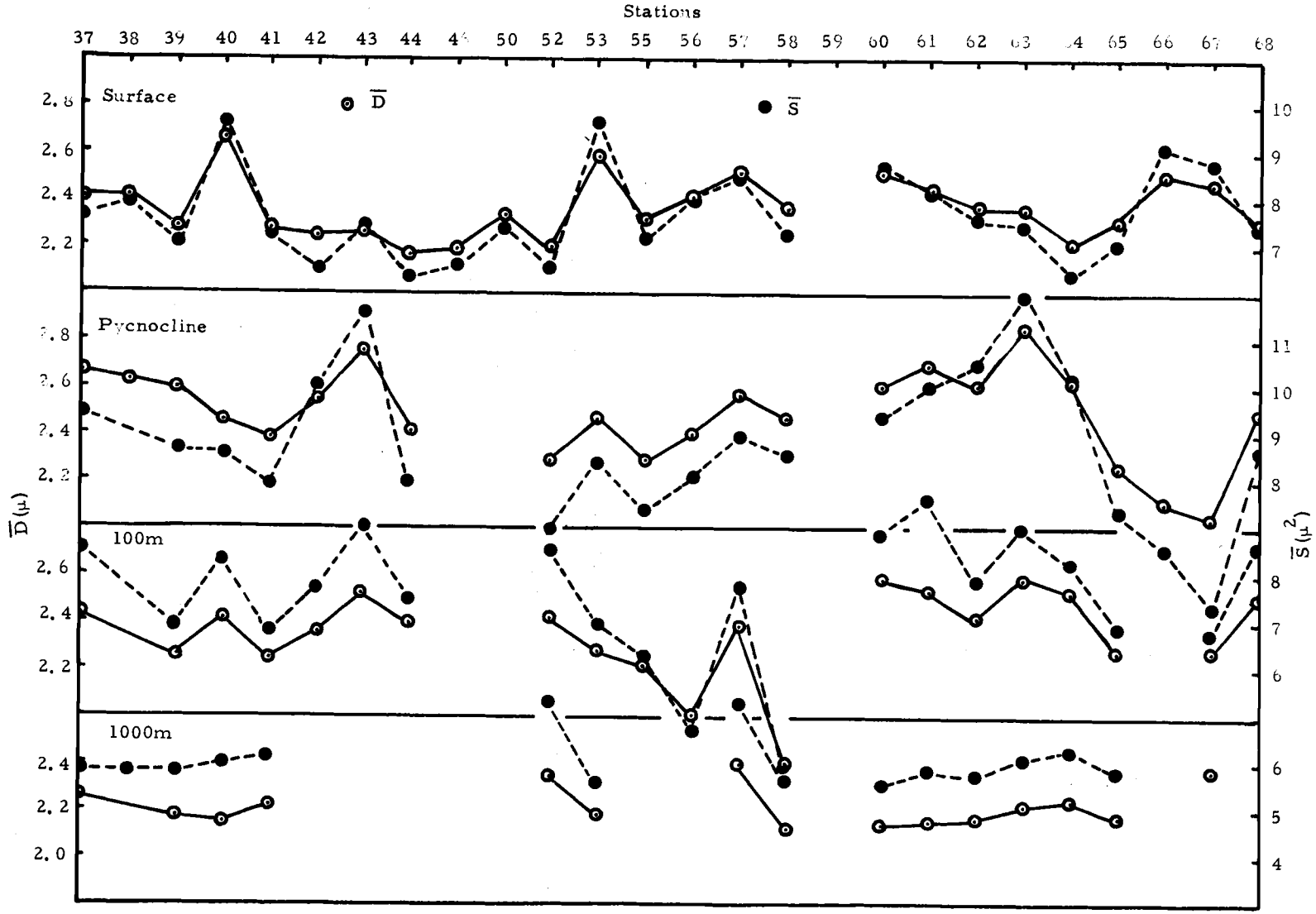

Figure 5.14. $\overline{D}$ and $\overline{S}$ at four depths along the cruise track.

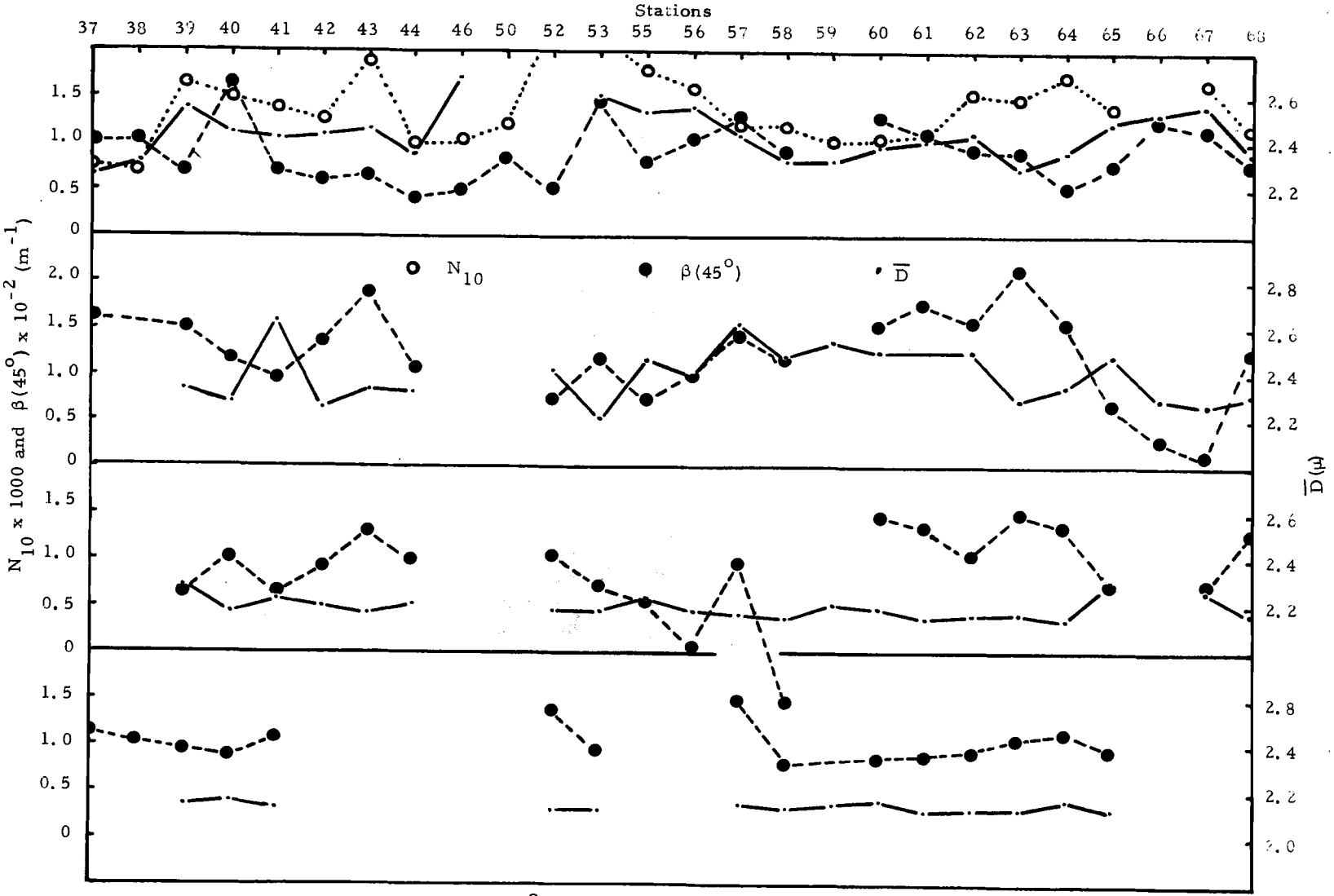

Figure 5.15. $\beta(45^{\circ})$, $\overline{D}$, and N_{10} at four depths along the cruise track.

$\beta(45^{o})$ is a function of the total surface area S of the particles in a sample, so it is roughly a function of N_{10} and $\overline{S}$. There is a poor trend agreement between N_{10} and $\overline{S}$ in Figure 5.15 so these two factors are in direct conflict much of the time in their joint determination of $\beta(45^{o})$. Since neither the trends of N_{10} nor those of $\overline{S}$ are consistently dominant, trends of $\beta(45^{o})$ can not be considered to be a measure of the relative trends of either the number of particles or the particle size separately in the horizontal plane. This is in agreement with the scatter diagrams of Figure 5.4.

In the verticle plane there is a general decrease in particle size and number with increasing depth, with the exception of regions having strong pycnoclines. Because of this profile trend agreement, vertical trends of $\beta(45^{o})$ are generally indicative of the relative vertical trends of both $\overline{D}$ and N_{10} as seen in Figures 4.4-4.7. For a direct comparison between the surface and pycnocline values of $\overline{S}$, N_{10}, and $\beta(45^{o})$, refer to Table 5.2. Here it can be observed that the average particle surface area is generally larger at the pycnocline than at the surface, while the surface values of $\beta(45^{o})$ and N_{10} are usually larger than are their respective values at the pycnocline.

Several aspects of the optical-particle interrelationships have been discussed. The separate development of each of these

as in this section detracts from their composite significance. For this reason several concluding remarks are made summarizing the developments of this dissertation.

TABLE 5. 2. Pycnocline versus surface particle characteristics.

Relations	Stations where relation holds
$\overline{D}_p < \overline{D}_s$:	40, 53, 65, 66, 67
$N_{10_p} < N_{10_s}$:	39, 40, 42, 43, 44, 46, 50, 52, 55, 56, 62, 63, 64, 65, 66, 67, 68, 69
$\overline{S}_p < \overline{S}_s$:	40, 53, 65, 66, 67
$N_{10_p} > N_{10_s}$:	37, 38, 41, 57, 58, 59, 60, 61
$\beta(45^o)_p > \beta(45^o)_s$:	41, 57, 58, 59, 60, 61, 62

VI. CONCLUSION

The cruise track of YALOC-69 crossed several different oceanographic regions: near-shore to open-ocean waters and temperate zone winter conditions to tropical zone summer conditions. The diverse temperatures and salinities encountered might suggest that a wide variety of particle size distributions would be expected. To the contrary, a high degree of similarity of distributional shapes and mean particle diameters was found. The mean diameter values ranged from 1.8 to 2.85 microns with the great majority of the distributional shapes being nearly that of the exponential distribution.

The relative frequency distributions along the track of YALOC-69 could be extremely well approximated by either of the two-parameter distributions, the Weibull or the gamma. The shape parameter of the Weibull distribution function ranged from 0.7 to 2.0 in fitting the YALOC data, with most parameters clustering around the value "1", the shape parameter of the exponential distribution. This means that the exponential (one-parameter) distribution is a first order approximation of the particle distributions of YALOC-69, while the Weibull is a good second order approximation.

Extreme value probability paper was found to be very effective in the fitting of the truncated particle diameter relative frequency data by a straight line (Weibull line). Since these truncated relative

frequency distributions were actually representative of conditional probability distributions, a technique was developed to estimate the percentage of particles too small to be measured.

Since a large number of the particle distribution shape parameters were clustered around the value "1", the exponential distribution was used to approximate the error expected in the effective optical area (E. O. A.) due to the use of statistics from conditional rather than complete particle size distributions. The error was estimated to be about 8%. The error in relative measurements would be reduced from this value. This means that the truncated particles were mostly below the optically active size.

The volume scattering function $\beta(\theta)$ at $\theta = 45^{\circ}$ was compared with N_5 and $\overline{S}$. The resultant scatter diagrams indicated that N_5 was better correlated with $\beta(45^{\circ})$ than $\overline{S}$ was. Even so, the correlation was not high enough to warrant the expression of $\beta(45^{\circ})$ as being a linear relationship with N_5 for the water samples studied on YALOC-69. In comparing $\beta(45^{\circ})$ to the total particulate surface area, the resultant scatter diagram was generally linear in shape. This means that $\beta(45^{\circ})$ might be used effectively in particle surface adsorption studies.

The graphical comparison of $\beta(45^{\circ})/\beta(135^{\circ})$ with $(\overline{S})^{1/2}$ resulted in five different linear plots each having a unique slope. The samples falling on each of these lines had particle size

distributions with very similar values of the distributional shape parameter c, which was found to be linearly related to the slope of the respective line. In this manner five distribution shapes or types characterized all but a few of the particle distributions encountered on YALOC-69.

The investigation as to the cause or causes of the division of the particle distributions into five characteristic types determined that the water type (temperature and salinity) was not related to distribution type. Identical distribution types were measured in oceanic regions of quite varied water types, whereas dissimilar distribution types could be found in the same water type.

The typically exponential shape of the small particle ends of the distributions suggested that the decay or decomposition of detritus was a dominant shaping factor in the oceanic regions investigated. If this were the case, differences in the kinds of organisms (i.e. species of phytoplankton) could be expected to influence the rates of detrital decay. For this reason it was hypothesized that the distribution shapes found in the area of the Galapagos were dependent upon the organisms dominant in the regions acting as the particle sources of these waters. The source of the Type I particle distribution was hypothesized as being the Panama Basin region, while that of the Type II distribution was considered to be the Peruvian Current. Since no measurements were taken in these hypothesized

source regions substantiation of these claims could not be made.

The optical ratio $\beta(45^{\circ})/\beta(135^{\circ})$ became an estimate of the particle size $(\overline{S})^{1/2}$ or $\overline{D}$ when the distribution type of a sample was known such as for stations YPT-38, 39, and 40, where the samples were homogeneously of Type I distributions.

A general increase in particles was found in the near-shore and equatorial upwelling region, while the relatively stable subtropical waters contained the fewest particles. Excellent trend agreement was found between $\overline{D}$ and $\overline{S}$. The trends of $\overline{D}$, $\overline{S}$, and N_5 compared quite unfavorably with $\beta(45^{\circ})$ in the horizontal plane, but they all showed a general decrease with depth except at the depths of occasional turbidity maxima found near the tops of the respective thermoclines in waters of high stability. In these areas, their pycnocline values exceeded their surface ones.

It would be of interest to return to the Galapagos region of the Pacific equipped with a smaller orifice for the Coulter Counter in order to study the distribution of particles smaller in diameter than 1μ. If the generally exponential trend of the truncated distributions continues into the smaller range of sizes, that would be strong evidence that a particle decay mechanism is dominant in the determination of the shape of the small particle distributions. If measurements of particle size distribution and the scattering ratio were made upstream from the Galapagos region, the testing of

optical-particulate current tracing techniques could be carried out. A more thorough knowledge of the phytoplankton crop in each sample would be invaluable in terms of estimating relative indices of refraction and detrital rates of decay. It would also be of interest to locate and optically tag the characteristics of the Cromwell undercurrent west of the Galapagos in order to attempt the tracing of this elusive current.

BIBLIOGRAPHY

Ashley, L. E. and C. M. Cobb. 1958. Single particle scattering functions for latex speres in water. Journal of the Optical Society of America 48: 261-268.

Beardsley, G. F., Jr. 1966. The polarization of the near asymptotic light field in sea water. Ph. D. thesis. Cambride, Massachusetts Institute of Technology. 119 numb. leaves.

Burt, W. V. 1955. Distribution of suspended materials in Chesapeake Bay, Journal of Marine Research 14: 47-62.

Coulter Electronics. 1965. Industrial model "A", Coulter Counter instruction manual. Chicago. 69 p.

Defant, A. 1961. Physical oceanography. Vol. I. New York, Macmillan. 729 p.

Deirmendjan, D. 1963. Scattering and polarization properties of polydispersed suspensions with partial absorption. I. C. E. S. Electromagnetic Scattering 5: 171-189.

Eppley, R. W., R. W. Holmes and J. D. H. Strickland. 1967. Sinking rates of marine phytoplankton measured with a fluorometer. Journal of Experimental Marine Biology and Ecology 1: 191-208.

Hinzpeter, H. 1962. Messungen der Streunfunktion und der Polarisation des Meerwassers. Kieler Meeresforsch 18: 36-41.

Hodkinson, J. R. 1963. Light scattering and extinction by irregular particles larger than the wavelength. I. C. E. S. Electromagnetic Scattering 5: 87-100.

Hogg, R. V. and A. T. Craig. 1965. Introduction to mathematical statistics 2d ed. New York, Macmillan. 383p.

Jerlov, N. G. 1953. Influences of suspended and dissolved matter on transparency of sea water. Tellus 5: 306-307.

_____ 1955. The particulate matter in the sea as determined by means of a Tyndall meter. Tellus 7: 218-225.

Jerlov, N. G. 1961. Optical measurements in the eastern North Atlantic. Meddelande fran Oceanografiska Institute i Goteborg 30: 1-40.

_____1968. Optical oceanography. Amsterdam, Elsevior. 194 p.

Jerlov, N. G. and B. Kullenberg. 1953. The Tyndall effect of uniform minerogenic suspensions. Tellus 5: 306-307.

Johnson, N. L. and F. C. Leone. 1964. Statistics and experimental design in engineering and the physical sciences. New York, Wiley. 523 p.

Kullenberg B. 1969. Light scattering in the central Baltic. (Abstract) In: Program of the 1969 spring meeting of the Optical Society of America, San Diego. p. 9.

Lisitsyn, A. P. 1961. Raspredelemie i sostav vzvchennogo materiale v moryakh. sovremennye osadki morei i okeanov, Moskya, p. 175-232.

Mattern, C., F. Brackett and B. Olson. 1957. Determination of number and size of particles by electrical gating: blood cells. Journal of Applied Physiology 10: 56-70.

Mie, G. 1908. Beitrage zur optic truber medien, speziall kolloidalen mettallosugen. Annalen der Physik 25: 377.

Mulligan, H. F. and J. M. Kingsbury. 1968. Applications of an electronic particle counter in analyzing natural populations of phytoplankton. Limnology and Oceanography 13: 499-506.

Ochakovsky, Yu. E. 1966. On the dependence of the total attenuation coefficient upon suspensions in the sea. U. S. Department of Commerce, Joint Publication Series, Report 36: 16-24.

Pak, H. 1969. The columbia River as a source of marine light scattering particles. Ph. D. thesis. Corvallis, Oregon State University, 110 numb. leaves.

Sasaki, T. N. Okami, G. Oshiba and S. Watanabe. 1962. Studies on suspended particles in deep sea water. Scientific Papers of the Institute of Physical and Chemical Research (Tokyo) 56: 77-83.

Sheldon, R. W. and T. R. Parsons. 1967a. A continuous spectrum for particulate matter in the sea. Journal of the Fisheries Research Board of Canada 24(5): 909-915.

_____1967b. A practical manual on the use of the Coulter Counter in marine research. Toronto, Coulter Electroncs. 66p.

Van de Hulst, H. C. 1957. Light scattering by small particles. New York, Wiley. 470 p.

Wyrtki, K. 1965. Surface currents of the Eastern Tropical Pacific Ocean. Bulletin of the Inter-American Tropical Tuna Commission 9(5): 269-304.

APPENDICES

APPENDIX A

THE COULTER COUNTER MODEL A

a. Introduction

The basic principle behind the Coulter Counter method is that of passing a conducting fluid through a small orifice (100μ) in a dielectric orifice jacket (pyrex) and counting the number of particles (dielectric with respect to the conductivity of the fluid) carried along with this fluid. An electrode plate is placed on either side of the orifice, with a potential difference set up between them. When a particle passes through the orifice, it acts as a momentary resistor whose resistance is proportional to the particle volume (manual, 1965). These resistors cause voltage pulses whose sizes are also proportional to particle volume. By envolking a decade scaler counting mechanism which counts only pulses larger than the level of a variable threshold bias voltage, a cumulative particle size distribution can be generated by varying the bias level and repeating the counting operation several times. See Figure A-1.

The diameter that corresponds to a given threshold bias depends upon the voltage between the two electrodes and the conductivity of the fluid relative to that of the particles involved. By calibrating the electrical threshold biases against the known mean

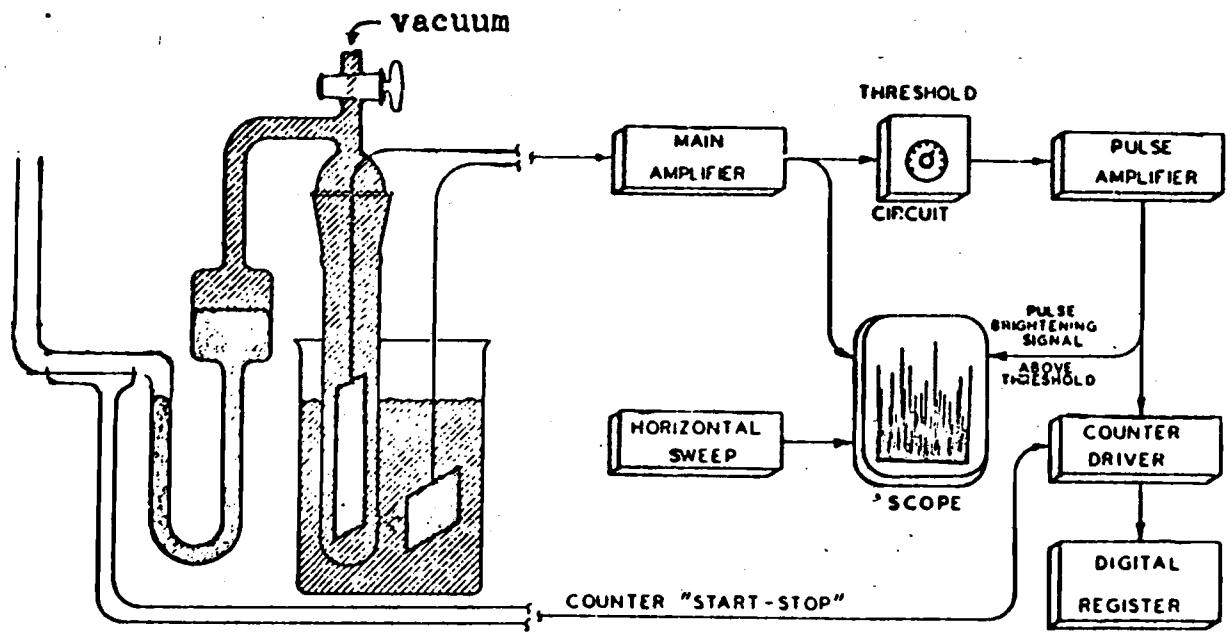

Figure A. 1. Coulter Counter Schematic.

diameters of uniformly sized particles (latex spheres), one can accurately attribute the number of counts at a given threshold level to being the number of particles of diameter greater in size than that corresponding to the threshold bias level.

b. Calibration

Assuming that the instrument is properly zeroed, the relationship between the threshold at some given gain, current setting, and conductivity of fluid is (manual, 1965)

(A. 1) $$K = d/t^{1/3} .$$

Here "k" is the calibration constant and slope, and "d" is a particle diamter. "t" is equal to a given threshold setting "t" times a factor "F" determined by the current setting (gain control) and fluid conductivity (supplied by the manufacturer). Obviously for a small particle, "t" will be small, so a graph of Equation A. 1 is Figure A. 2.

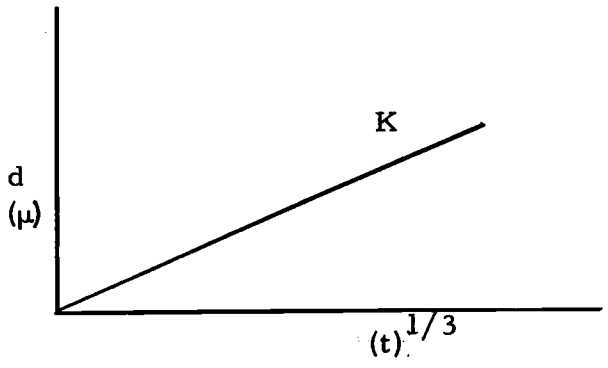

Figure A. 2. Graph of calibration equation.

One can see that a precise zeroing of the threshold is critical when only one point (some monosized concentration of particles) is used to determine the calibration slope "k". If the particles that one is interested in measuring are themselves quite small, the larger the zeroing error, the greater is the error in the reported particle sizes. Consequently, if a slope calibration is determined by using two systems of monosized particles which are quite different in size, an intercept-independent method can be used. Figure A. 3 helps to illustrate the concept.

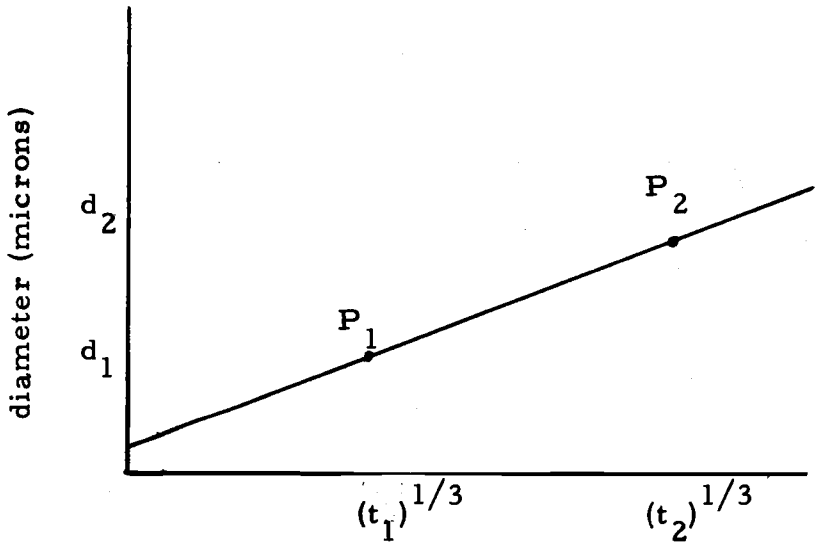

Figure A. 3. Intercept-independent calibration slope.

If P_1 and P_2 represent the points on the above graph defined by particles of known sizes d_1 and d_2 which result in threshold values t'_1 and t'_2, then the calibration slope is determined by the equation

(A. 2) $$k = (d_1 - d_2)/[(t_1)^{1/3} - (t_2)^{1/3}] .$$

In general, the above curve represents the overlapping of curve segments derived from several different current settings. For best results it is important to use calibration particles whose sizes are close to those within the expected range of sizes of unknown particles to be measured. In this way extrapolation errors will be minimized. The calibration of the instrument used in this experiment serves as an example of the method and accuracy attainable.

To calibrate the Coulter Counter, particles of average diameters 1.099μ, 10.5μ and 21.0μ were used as particle size standards. Table A. 1 lists the particle sizes and corresponding gain, current, and electrical threshold bias settings, as well as the calibration F_i factors determined by conductivity measurements and a correlation table supplied by the manufacturer (refer to manual, 1965).

TABLE A. 1. Calibration Values

Known Diameter	Gain	Current	F	t'	t	$(t)^{1/3}$
1.099 ± .001μ	3	10	.00301	4.74	.0143	.243
10.5 ± 0.5μ	3	6	.0325	51.77	1.68	1.19
21.0 ± 1.0μ	3	3	.252	50.48	12.7	2.33

Using Equation A. 2 for each of the three combinations of slopes possible from the data in Table A. 1, slope values of 9. 21, 9. 52, and 9. 90 were obtained for the lines between 10. 5μ and 21. 0μ 1. 099μ and 21. 0μ, and 1. 099μ and 10. 5μ particles respectively. The value 9. 52 was chosen as most representative since it encompassed the widest range of particle diameters and thus contained the smallest amount of propagated error. It also was the median as well as being nearly the average of the three slope values. The average and standard deviation of these three slopes are 9. 54 ± 0. 27. This standard deviation is used to represent the most probable calibration error in the error analysis part of this section.

Since most of the particles in the oceans occur in a particle range near 1. 099μ as compared with the other standard particle sizes, extrapolation about this value introduces smaller error than the corresponding use of 10. 5μ or 21. 0μ. Also, the accuracy of the mean diameter (supplied by the manufacturer) is much better for the smaller spheres (see Table A. 1). So, rearranging Equation A. 2, we have

(A. 3) $$d = 9.52\ (\sqrt[3]{t_2} - 0.243) + 1.099\mu$$

where $k = 9.52$, $t = 0.243$, and $d_2 = 1.099\mu$. Table A. 2 lists the diameters corresponding to various threshold and current settings for gain = 3 as derived from Equation A. 3.

Table A.2. Diameters corresponding to current and threshold settings.

Current	10	10	10	10	10	10	7	7	7	7	7	7
Threshold	5	10	30	50	70	90	20	30	40	50	60	70
Diameter (μ)	1.13	1.75	3.05	3.84	4.44	4.93	5.40	6.36	7.12	7.76	8.32	8.83
Current	7	7	7	5	5	5	5					
Threshold	89	90	100	40	60	80	100					
Diameter (μ)	9.28	9.70	10.08	11.73	13.62	15.11	16.37					

c. Instrument operation

The step by step instructions for the Coulter Counter operation are thoroughly covered in the manual (1965). In addition, Parsons (1967) has published a useful manual on the use of this instrument for vaious applications. For this reason these operations are not duplicated at this time. So sample collection and treatment for Coulter processing are immediately detailed.

The samples of sea water to be Coulter counted were gathered by plastic NIO bottles from various depths and locations at sea. The water was carefully drained into a clean beaker from the NIO bottles by pouting it slowly down the side of the beaker in order to prevent the formation of bubbles. A stirrer was used throughout the entire

Coulter analysis to insure homogeneity of the distribution of particles within the beaker.

d. Data Reduction

Three replicate measurements were performed on each sample, counting the particles in a 0.5c.c. volume of sea water each time. Only the particles of size greater than that of the voltage bias threshold value used were counted. In this way, by varying the threshold setting, the cumulative frequency distribution can be obtained. Then the frequency of particles falling between any two threshold settings is determinable. Table A.2 lists the thresholds and corresponding diameter sizes used for these measurements.

Let N_i be the number of particles larger in diameter than D_i. Then $N_i - N_{i+1}$ represents the number of particles whose diameters fall between D_i and D_{i+1}. The diameter increments $D_{i+1} - D_i$ are unequal in length, so since the area under a histogram and within some size increment $D_{i+1} - D_i$ is equal to the frequency $(N_i - N_{i+1})$ of the particles within that interval, the height of the histogram above this increment must be

$$h_i = (\text{area})_i/(D_{i+1} - D_i) = (N_i - N_{i+1})/(D_{i+1} - D_i)$$

This is illustrated in Figure A-4.

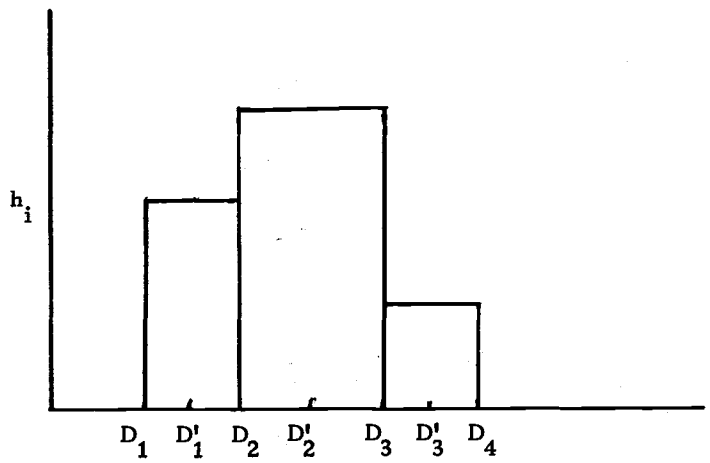

Figure A-4. Frequency histogram.

Dividing h_i by $\sum_{i=1}^{n-1} h_i$ makes relative frequencies out of the areas of the histogram blocks, where n is the number of diameters D_i defining the increments. Now, if the center points D'_i of each class interval $(D_{i+1} - D_i)$ are connected by straight lines, a relative frequency polygon can be generated. It is this polygon that is often approximated by a statistical probability density function in order to obtain a model that can be used to treat a given problem theoretically (see Appendix C).

The relative frequencies generated by the Coulter Counter can be expressed as

$$\frac{N_i - N_{i+1}}{N_i}$$

where N_i is the total number of particles larger than D_i. This

equation is not quite exact since the total number of particles N_{1i}, drawn through the orifice when N_i particles greater than D_i are counted, is unknown. N_i can be expressed as $\mu_1 \pm \sigma_{N_1}$, where μ_1 is the expected value of N_1 and σ_{N_1} is the standard deviation of N_1 about μ_1. Since the expected value and standard deviation of N_{1i} are identical to those of N_1, N_1 is used as an estimate for N_i. For samples containing a large number of particles the approximation is quite good.

The expected value of the relative frequency of particles in the i^{th} increment can be expressed as

$$E\left(\frac{N_i - N_{i+1}}{N_i}\right) = E(N_1 - N_{i+1})\, E\left(\frac{1}{N_i}\right)$$

since each of these counts is independent. By using a Taylor's expansion of N_1 about μ_1, we can write

$$E\left(\frac{1}{N_1}\right) = E\left[\frac{1}{\mu_1} - \frac{(N_1 - \mu_1)}{\mu_1^2} + \frac{(N_1 - \mu_1)^2}{\mu_1^3} - \ldots\right]$$

$$= \frac{1}{\mu_1} + \frac{\sigma_{N_1}^2}{\mu_1^3} + E[\ldots]$$

$$\doteq \frac{1}{\mu_1} + \frac{\sigma_{N_1}^2}{\mu_1^3}$$

$$\doteq \frac{1 + (\sigma_{N_1} / \mu_1)^2}{\mu_1} .$$

So for $(\sigma_{N_1} / \mu_1)^2 << 1$,

$$E\left(\frac{1}{N_1}\right) \doteq \frac{1}{\mu_1} .$$

Thus,

$$E\left(\frac{N_i - N_{i+1}}{N_1}\right) \doteq \frac{E(N_i) - E(N_{i+1})}{\mu_1} = \frac{\mu_i - \mu_{i+1}}{\mu_1}$$

Since the median of three values of N_i was used throughout YALOC-69 in the data reduction, it symbolized μ_i, and reduced the variance of N_i from $\sigma^2_{N_i}$ to $\sigma^2_{N_i} / 3$.

In order to estimate some of the particle sample characteristics such as the sample mean diameter, surface area, and volume certain assumptions were made:

1. The center $\overline{D}_i$ of the i^{th} diameter increment or size class is most representative of the size distribution of particles within that class if the probability density function of the particle class as a whole is unknown; i.e. given N_i particles of a size between D_i and D_{i+1} with an unknown particle distribution within that increment, a uniform probability density function is assumed within each size class, meaning the expected diameter within each class is the incremental midpoint, D'_i.

2. The sample characteristics are assumed to come from truncated distributions. Only the higher moments of the truncated distribution can be used to represent those of the complete distribution without appreciable error.

Using the above assumptions, we can express the particle sample mean as

$$\text{(A. 4.)} \qquad \overline{D} = \sum_{i=1}^{n-1} \frac{(N_i - N_{i+1})}{N_1} \quad (D_i + D_{i+1})$$

where n is the number of thresholds used, and N_i is the number of particles larger in size than the diameter corresponding to threshold "i". In a similar fashion, the expected surface area of the particles in a sample can be written as

$$\text{(A. 5)} \qquad \overline{S} = \pi \sum_{i=1}^{n-1} \frac{(N_i \quad N_{i+1})}{N_1} \frac{(D_i + D_{i+1})^2}{2}$$

and the expected particle volume as

$$\text{(A. 6)} \qquad \overline{V} = \frac{\pi}{6} \sum_{i=1}^{n-1} \frac{(N_i - N_{i+1})}{N_1} \quad \frac{(D_i + D_{i+1})^3}{2}$$

Any additional sample characteristics discussed in the text can be derived from these statistics.

d. Error Analysis

The errors involved in the particle analysis part of this

dissertation can be separated into three basic groups: coincidence errors, counting variances, and calibration errors. Each of these catagories is discussed below. There exists a paradox in designing a Coulter Counter experiment: increasing the size of the sample size decreases the sampling variances, but increases the size of the coincidence errors. Coincidence error occurs when two or more particles pass through the critical volume (small volume surrounding the orifice) at the same time. They appear as a single particle of a larger size. A theoretical treatment correcting for coincidence in a monodisperse-system of particles is given by Mattern et. al. (1957). This treatment is not readily applicable to the oceanic situation when the diameter spectrum is quite wide. Coincidence was neglected in this investigation because the total particle counts were always below 6000 and usually below 2000. In some work with an algal culture, the calculated coincidence error in this count range was found by dilution techniques to be about 5%. It will be shown later that the errors resulting from sample variances are the more significant.

The error in the calibration slope is assumed to be that of the standard deviation of the three slopes of the lines in Section A. b. This value was found to be 0. 27. Using Equation A-3, with a threshold setting error of 0. 1, a slope error of 0. 27, and a reference particle diameter error of 0. 001, the fractional error in the

diameter of particles of diameter 5.40μ, say, is

$$\frac{d}{D} = \pm \frac{\sqrt{\left(\frac{.27}{9.52}\right)^2 + \frac{.1^2 + .1^2}{(35.43)^2 (3)^2} \quad (9.52)^2 (.404)^2 + (.001)^2}}{(9.52)(.404) + 1.099}$$

$$= \pm \quad 2.21\%$$

Since for all samples measured on YALOC-69, $\overline{D}$, $(\overline{S}/\pi)^{1/2}$, and $(\overline{V}6/\pi)^{1/3}$, are each much smaller than 5.40 μ, the diameter used above for error propagation, a 2% calibration error is assumed as an outside limit for the particle sample characteristics involved in this dissertation. This is assuming that the particles are sphere-like when dealing with non-volumetric measurements. For diameters and areas, a non-sphericity factor would be involved, since these characteristics were determined from particle volume measurements using a spherical particle shape assumption. No information can be given about the size of this term for the waters encountered on YALOC-69, since no particle shape determinations were made. It is expected that non-spericity increases with decreases in particle size, due to the increased irregularity of detritus over that of phytoplankton such as pieces cell walls and etc.

The variances of N_i for the different samples can be attributed primarily to two different causes: small inhomogeneities in the distribution of particles within the sampling beaker (sampling error)

and a certain amount of electrical noise. The first one is considered to be dominant, since the sampling variance increased for the small counts at the large particle end of the distribution, and electrical noise decreases with increased particle size.

Since three replicates of N_i were made at each threshold setting on the entire cruise, estimates of sampling variance are easily attainable from the replicate variance. The % standard errors in N_i for stations in regions R_1 and R_2 are determined by the expression $(\sum_{i=1}^{3} N_{ij}/2)^{1/2}(100\%)$ and are listed in Table A-3. These are representative of the % standard error present throughout the cruise. Generally the error increased as the number of particles counted decreased. So, reliability is greatest for the first few cumulative counts for samples in the isothermal surface layer.

Realistic estimates of the variances in the sample mean diameters $\overline{D}_i$ by the variances in the counts N_i can be generated by the following shceme:

1. The data for a given sample can be listed as below:

Replicates	D_1	D_2	D_3	D_4 .... D_n
1	N_{11}	N_{21}	N_{31}	N_{41}.... N_{n1}
2	N_{12}	N_{22}	N_{32}	N_{42}.... N_{n2}
3	N_{13}	N_{23}	N_{33}	N_{43}.... N_{n3}

Here, the data is treated as if each run "j" of N_{ij} for

Table A. 3. Percent standard errors in N_i for regions R_1 and R_2.

Station	Diameter (μ)											
Depth	1.13	1.75	3.05	3.84	4.44	4.93	5.40	6.36	7.12	7.76	8.32	8.83
YPT-37												
0 m.	1.01	1.72	8.96	11.33	2.81	6.74	2.09	21.66	16.46	45.50	17.32	31.22
40 m.	2.13	3.24	5.49	5.76	7.12	6.13	10.91	14.97	13.93	6.40	13.86	31.13
100 m.	2.69	10.82	4.74	10.91	15.17	22.43	25.12	11.44	51.62	62.98		
1000 m.	9.90	4.66	23.90	35.20	50.80	90.10						
YPT-38												
0 m.	2.95	4.49	8.12	3.44	8.36	16.17	7.26	22.36	24.33	17.66	25.75	28.64
YPT-39												
0 m.	1.15	2.63	3.11	8.53	3.24	5.83	4.25	8.69	10.86	18.28	2.18	13.86
50 m.	4.00	2.42	3.22	5.56	7.92	4.51	16.40	17.69	28.35	10.90	12.45	24.02
100 m.	6.24	9.81	10.72	6.77	18.12	30.74	31.35	41.30	22.22	54.13		
1000 m.	1.30	4.45	16.67	11.91	48.44	34.47						
YPT-41												
0 m.	3.18	4.20	4.91	6.86	1.07	3.14	8.64	11.34	12.89	14.28	17.44	19.52
20 m.	1.98	4.17	4.02	2.58	3.61	4.17	4.85	8.92	3.26	9.88	21.30	8.31
100 m.	3.33	5.44	11.26	15.02	4.98	34.64	21.21	24.78	42.86	40.00		
1000 m.	1.91	13.43	9.84	28.20	24.74	5.97						

$j = 1, 2, 3$ is considered independently from the other two runs. The mean diameter $\overline{D}_i$ of each run is found as in Equation A-4. These are listed in Table A-4.

2. The % standard error, % $\sigma_{\overline{D}}$, among these mean diameters $\overline{D}_i$ can be determined by the following formula:

$$\% \ \sigma_{\overline{D}} = \sqrt{\frac{\sum_{i=1}^{3} (\overline{D}_i - \overline{D})^2}{2}} \quad x \quad (100\%)$$

These results are found in Table A-4 also.

The standard errors of the mean diameters are generally much smaller than those of the particle counts N_i. Standard error, similar to that of the mean diameters could be generated for the mean surface areas, but they are expected to be in the same range as those in Table A-4.

TABLE A-4. % standard errors in $\overline{D}$ for stations YPT-39 and YPT-41.

Station/Depth	$\overline{D}_1$	$\overline{D}_2$	$\overline{D}_3$		% $\sigma_{\overline{D}}$
YPT-39 0m	2.303	2.271	2.281	2.280	.67%
50m	2.542	2.646	2.413	2.534	4.6%
100m	2.243	2.262	2.219	2.241	0.965%
1000m	2.190	2.131	2.126	2.149	1.66%
YPT-41 0m	2.250	2.233	2.327	2.270	2.34%
20m	2.377	2.370	2.389	2.379	0.403%
100m	2.264	2.211	2.220	2.232	0.126%
1000m	2.076	2.226	2.242	2.18	4.17%

APPENDIX B

. THE BRICE PHOENIX LIGHT SCATTERING PHOTOMETER

a. Introduction

The Brice Phoenix light scattering photometer is essentially the same type of instrument as a laboratory nephalometer. It is designed to measure the radiant intensity $I(\theta)$ scattered by a water sample volume V at some angle θ from the path of the incident irradiance E. If $I(\theta)$ is measured at angles 45^{o}, 90^{o}, and 135^{o}, then the relationships between the incident and scattered light is expressed as follows:

(B. 1) $$\beta(\theta) = I(\theta)/EV$$

The volume V is held by a semi-octagonal pyrex glass scattering cell centered in the light beam. The light source is an 85 watt mercury arc lamp which by means of lenses and apertures is rendered plane-parallel. Several different interference filters are available for the selection of the wavelengths of interest. The photomultiplier tube detector would be exposed to a wide range of intensities if a set of neutral density filters were not available to limit this range to less than two decades in width. This allows the detector to operate in the same small range from sample to sample as well as permitting a chart recorder to register the detector ouput voltages.

This instrument is described in detail by Beardsley (1966) and Spilhaus (1965), so additional instrumental explanations are felt to be repetative.

b. Calibration

A complete description of the calibration process for the Brice Phoenix light scattering photmeter used in this experiment has been derived by Pak (1969). It is sufficient to say that in agreement with his work, the absolute volume scattering function $\beta(\theta)$ can be determined by the ratio R_v of the detector signal voltage for angle θ to that for angle 0^o. At angle 0^o for the Brice Phoenix, a working-standard diffusor (Lambert's law diffusor) plate is automatically introduced into the incident beam. Since the transmissivity and radiant output field of this diffusor are known, and since its output passes through the scattering cell before it hits the detector, R_v is independent of the incident radiance, detector sensitivity, glass and water path attenuations, and the detector-scattering cell solid angle. Therefore, the volume scattering function $\beta(\theta)$ can be written

$$\beta(\theta) = KR_v \sin\theta \qquad \text{(B. 2)}$$

where K is a calibration constant expressed by

$$K = V_w T_o / V_{op} t$$

where "t" is the beam width, and V_w/V_{op} is the ratio of the detector voltages when the working standard diffusor and the opal standard diffusor respectively are placed in the incident beam. The transmissivity T_o of the opal standard (used only for calibration) is supplied by the manufacturer and used to periodically to check or re-calibrate the working standard.

c. Instrument Operations

The operational procedures for the determination of the volume scattering function $\beta(\theta)$ include the water sampling, the Brice Phoenix operation, and the generation of $\beta(\theta)$ from the raw data.

Before any samples could be processed optically, a one-half hour warmup period was required for the lamp and detector unit of the Brice Phoenix. Once it was installed for a cruise, the Brice Phoenix was allowed to run continuously. A voltage regulator was used with it in order to prevent large voltage fluctuations in the line voltage.

Water samples were collected with plastic NIO sampling bottles by lowering them open on a hydro-wire, and closing them at the desired depth. Once back on the surface, the bottles were drained into the scattering cell after two rinsings. Care was taken to prevent the generation of bubbles in pouring the samples into the scattering cell. The cell was a semi-octagonal cylinder, allowing measurements to

be made at 0, 45, 90, and 135 degree angles with respect to the beam direction of propagation. This scattering cell was thoroughly cleaned at the beginning of the cruise and was rinsed with and stored containing distilled de-ionized water between each station.

After the sample was drawn, the cell was placed on the cell base or stand within the Brice Phoenix and adjusted for orthogonal alignment with the light beam by insuring that the reflected beam was superimposed over the source slit. A switch in the photomultiplier detector circuit opened and closed with the lid to the light-tight scattering photometer to prevent serious damage to the photomultilier tube due to the relatively high photon flux of the room lights.

At the beginning of the measurements of each station, the position, time, date, and other pertinent information was logged onto the recorder chart paper. Then before each bottle sample was processed, the depth, time, bottle number, and incident light wavelength were logged.

A series of measurements at four angles, 0, 45, 90, and 135 degrees, were made for each of three incident wavelengths (436, 546, and 577 millimicrons) of light. In order to allow the detector to operate in a relatively small range of radiant flux, four neutral density filters with respective transmissivities of about 50%, 25%, 12.5% and 6.25% were insertable into the incident light beam. So, the measurement angle θ and the neutral density filters being used

were also logged on the chart paper as the respective measurements for $\beta(\theta)$ were being taken.

For each measurement a certain amount of detector output voltage fluctuation occurred due to large particles passing into and out of the light beam. For this reason the record was made long enough to determine some fairly stable base voltage upon which the fluctuations were assumed to be superimposed. This essentially eliminated the relatively few large particle motes from the measurements, which would be difficult to treat uniformly.

The data was read from the chart paper and processed by a CDC 3300 computor to determine the volume scattering function for each measurement. The program used was identical to that used by Pak (1969).

d. Error Analysis

For several samples Spilhaus (1965) sequentially measured the scattering from both halves of a divided sample and compared the two measurements. The standard error of $J(\theta)$ was $\pm$ 0.034 due to the deviations of θ about its average value.

Beardsley (1966) also studied the errors involved in using this same instrument. He took the time average of several readings, one second each in duration, to ascertain a standard error due to electri-optical drift of 4%. This figure can be reduced by

the rapid transition from the 0^{o} measurement (calibration sub-standard measurement) to that at θ, the angle of interest. Using only three angles θ_i, these measurements can be taken easily in less than one minute. This eliminates appreciable drift effects of longer than one minute duration. Beardsley also determined the repeatability of the calibration to have an error of 2%.

Pak (1969) tested the repeatability of the instrument as a whole. He added 10.5 micron latex spheres to seawater, filtered several times through 0.8 micron Millipore filters. Measurements were taken two days apart by two different individuals on separate latex samples. These sample measurements were normalized by dividing each $\beta(\theta)$ by its respective concentration of spheres as determined by a Coulter Counter. The standard errors of his measurements for blue and green light at 45, 90, and 135 degrees were less than 5.1% with the error increasing with the angle.

Since Pak's repeatability standard errors included all of the operational errors as well as some Coulter Counter error, they are representative of the total errors to be expected in making relative measurements with the Brice Phoenix. Beardsley's calibration standard error of 2% would be an additional consideration when making absolute measurements. Since only absolute measurements are shown in this dissertation, a maximum optical most probable error ϵ_{op} can be determined:

$$\epsilon_{op} = [(2\%)^2 + (5\%)^2]^{1/2} = 5.4\%$$

Most of the operational errors were much less than 5% including some Coulter Counting error, so ϵ_{op} was considered as a maximum error for the Brice Phoenix light scattering photometer measurements of $\beta(\theta)$ in this dissertation.

APPENDIX C

THE GAMMA AND WEIBULL DISTRIBUTIONS

a. Introduction

In order to attempt to estimate the complete dsitribution of particle diameters from truncated sample distribution data, theoretical models must be assumed which allow one to extrapolate for the probabilities of particles smaller than those large enough to be measured. The decision designating a particular model as being representative of the distribution of particles can only be based upon that part of the particle distribution curve which is measureable. If a particular model fits the larger particle end of the curve reasonably well, then it is used to estimate the proportion of the particles which could not be measured. This method also allows one to correct sample characteristics such as sample means for errors due to distribution truncation of small particle frequencies. Of course the validity of this method depends for the most part upon how well the unmeasured particle frequencies continue to follow the hypothesized model. This can only be determined by a later, more thorough examination of the particle size spectrum. Two candidates for particle distribution models are the gamma and the Weibull distributions, discussed below.

The gamma probability density function as defined by Hogg and Craig (1965) is

$$(A\text{-}3.1) \qquad f(x) = (x/\beta)^{\alpha-1} e^{x/\beta} / \Gamma(\alpha)\beta, \quad 0 < x < \infty$$

$$= 0 \text{ elsewhere,}$$

for $\alpha > 0$, $\beta > 0$, and $\Gamma(\alpha) > 0$. These are respectively the shape and scale parameters, and the gamma function. The gamma function is defined as

$$\Gamma(\alpha) = \int_0^\infty y^{\alpha-1} e^{-y} dy ,$$

or

$$\Gamma(\alpha) = (\alpha-1)\,\Gamma(\alpha-1) \qquad \text{for } \alpha > 1 .$$

For α a positive integer greater than one,

$$\Gamma(\alpha) = (\alpha-1)!$$

Since the cumulative distribution function for the gamma is not expressible in closed form, it is quite a tedious distribution to work with. If $\alpha = \nu/2$ and $\beta = 2$, then a special form of the gamma probability function emerges, the chi-square distribution

$$f(x) = [(x)/2]^{\nu/2-1} e^{-(x)/2} / 2\Gamma(\nu/2), \qquad \text{for } x > 0,$$

where ν is called the degrees of freedom. Since the only cumulative distribution function of the gamma type used in this dissertation was a chi-square with 2 d.f., it is the only one considered here.

It has the following c. d. f.

$$F(x) = 1-e^{-x/2} \qquad \text{for } x>0 .$$

This c. d. f. is easily tabulated, and graph paper of the form

$$\ln(1/(1-F(x))) = x/\beta$$

is available. If $F(x)$ is plotted against x directly, then β is an inverse slope parameter, and 0 is the abscissa intercept. This type of paper is available only for integer values of $\alpha/2$ (chi-square), so its applicability is quite limited for our purposes.

The Weibull probability density function can be expressed as

$$f(x) = c/b(x/b)^{c-1}\ e^{-(x/b)^c}$$

for $x> 0$, $b > 0$, $c > 0$, according to Johnson and Leone (1964). The cumulative distribution function is

$$F(x) = 1-e^{-(x/b)^c}.$$

Weibull distribution paper is available, or extreme value probability paper can be adapted to Weibull use. To make a linear expression for (x/b), one can perform the following operations

$$\ln[\,1-F(x)] = -(x/b)^c,$$

$$\text{Ln}1/[\,1-F(x)] = (x/b)^c,$$

or

$$\ln[\,\ln(1/1-F(x)))] = c\ln(x/b).$$

For Weibull paper, the ordinate $F(x)$ is plotted directly against x. For extreme value probability paper, one must first calculate

$\ln(x/b)$ and then plot it against the ordinate $1 - F(x)$.

The plotting of $F(x)$ against the particle diameters on gamma or Weibull probability paper offers a quick method of determining the similarity of the particle distribution to one of these distributions. A linear plot is proof positive that the distribution of particles is a gamma or Weibull, depending upon which paper is used. There is a minor problem encountered when one attempts to plot a truncated particle distribution on the above probability papers. This problem is dealt with in the following section.

Use of Weibull and Gamma Distribution Paper with Truncated Data

When dealing with truncated distributions, probability paper can not be used directly. One must approximate by a trial and error recursion technique the portion of the distribution which is truncated in order to obtain a linear plot. The problem is that the relative cumulative frequency of the first order statistic x', where x' is the smallest measured diameter, should represent the truncated proportion of the curve rather than to start with a value of about 1.0. The following steps outline the technique of plotting truncated distribution data on probability paper;

1. Plot $[1-F(D_i)] = N_i/N_1$, where $D_1 = 1.13\mu$, on the extreme value probability paper versus the abscissa values of $\ln D_i$.

2. Draw a line tangent to the large-particle end of the graph and extrpolate this line out to the first order statistic. For our purposes we call the first order statistic 1.13μ. This probability $N_1/N' = [\,1\text{-}F'(1.13)]$ will be some positive decimal > 0.

Dividing $[\,1\text{-}F'(1.13)]$ into the cumulative frequency N_1 gives an approximation N' of the total number of particles in the untruncated sample.

3. Plot N_i/N' versus $\ln x_i$ where x_i represents the particle diameters. This new plot should be closer to a straight line. If it is still concave or convex repeat steps 2 and 3 until a straight line is as closely approximated as is possible with the data given. See Figure C-1.

The small-particle distribution values have a smaller measurement variance than have the larger ones but they are more highly influenced by truncation correction errors.

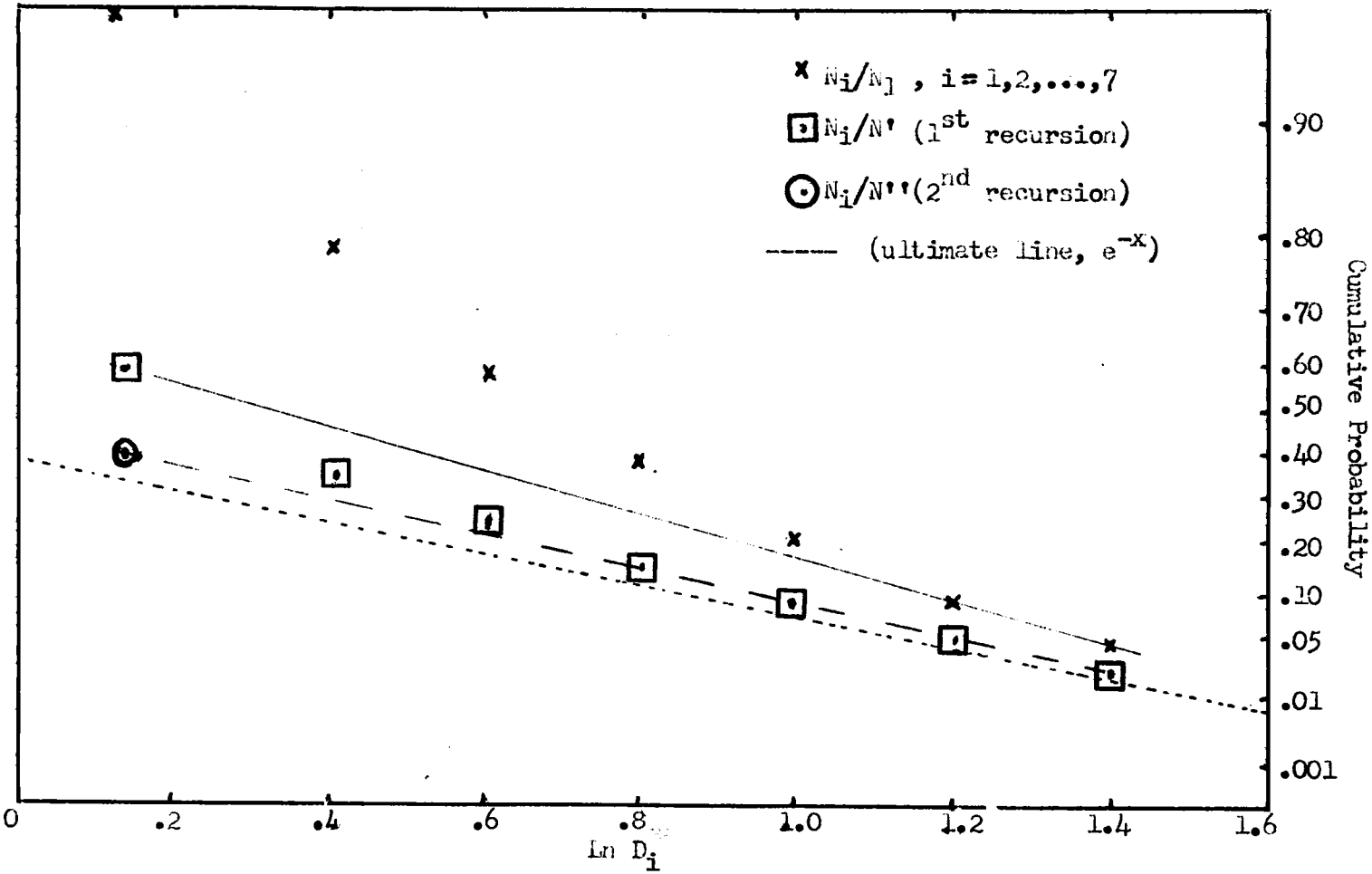

Fig. C-1. Illustration of recursive scheme for truncation correction of an exponential distribution on extreme value probability paper